

SEISMIC PERFORMANCE EVALUATION OF A FIRE-DAMAGED HIGH-RISE BUILDING

MD. ABDUL MOMIN

M.Sc. ENGINEERING THESIS



**DEPARTMENT OF CIVIL ENGINEERING
MILITARY INSTITUTE OF SCIENCE AND TECHNOLOGY
DHAKA, BANGLADESH**

MARCH 2023

MOMIN

M.Sc. Engg. THESIS

MIST • CE • 2023

SEISMIC PERFORMANCE EVALUATION OF A FIRE-DAMAGED HIGH-RISE BUILDING

MD. ABDUL MOMIN (SN. 1016110012)

A Thesis Submitted in Partial Fulfillment of the Requirements for
the Degree of Master of Science in Civil Engineering



DEPARTMENT OF CIVIL ENGINEERING
MILITARY INSTITUTE OF SCIENCE AND TECHNOLOGY
DHAKA, BANGLADESH

MARCH 2023

SEISMIC PERFORMANCE EVALUATION OF A FIRE-DAMAGED HIGH-RISE BUILDING

M.Sc. Engineering Thesis
By
MD. ABDUL MOMIN (SN. 1016110012)

Approved as to style and content by the Board of Examination on March 2023:

Lt Col Khondaker Sakil Ahmed, PhD, PEng, CEng Associate Professor Department of Civil Engineering MIST, Dhaka	Chairman (Supervisor)
------------------------------------------------------------------------------------------------------------------------	-----------------------

Dr. Raquib Ahsan Professor Department of Civil Engineering BUET, Dhaka	Member (External)
---------------------------------------------------------------------------------	-------------------

Dr. Tanvir Mustafy Associate Professor Department of Civil Engineering MIST, Dhaka	Member (Internal)
---------------------------------------------------------------------------------------------	-------------------

Brig Gen Md Wahidul Islam, SUP, ndc, psc Dean & Head Department of Civil Engineering MIST, Dhaka	Member (Ex-officio)
-----------------------------------------------------------------------------------------------------------	---------------------

Department of Civil Engineering MIST, Dhaka

SEISMIC PERFORMANCE EVALUATION OF A FIRE-DAMAGED HIGH-RISE BUILDING

DECLARATION

I hereby declare that the study reported in this thesis entitled as above is my/our own original work and has not been submitted before anywhere for any degree or other purposes. Further, I certify that the intellectual content of this thesis is the product of my own work and that all the assistance received in preparing this thesis and sources have been acknowledged and or cited in the reference section.

MD. ABDUL MOMIN

Department of Civil Engineering MIST, Dhaka

ACKNOWLEDGEMENT

First and foremost, all praise and profound gratitude go to the almighty Allah, who is the most beneficent and the most merciful, for allowing the author a great opportunity and the ability to bring this effort to fruition safely and peacefully.

The author conveys his heartiest gratitude to his supervisor, Lt Col Khondaker Sakil Ahmed, Ph.D., PEng., CEng. Associate Professor, CE Dept, MIST, for his systematic support and supervision in the dissertation. His guidance and suggestions worked as inspiration to unlock different new avenues for research.

The author is grateful for the technical support provided by the Center for Advisory & Testing Services of the Civil Engineering Department (CATS-CE) and the financial support of MIST, Dhaka, Bangladesh. The author would also like to acknowledge the contribution of lab technicians of concrete and SM lab of the Civil Engineering Department of MIST.

ABSTRACT

Seismic Performance Evaluation of a Fire-Damaged High-Rise Building

Concrete is widely used all over the world for the construction of buildings and infrastructures that may remain stable under fire. It shows some damage and deformations that requires maintenance. Although rehabilitation and restoration procedures of fire-damaged buildings are usually time-consuming and costly, the post-fire resilience of the structure is very important to understand the structure's capacity and situations. In the seismic zone, the buildings must satisfy the seismic demand after the potential repair and retrofitting of the fire-damaged building. A simple verified simulation procedure for the post-fire seismic analysis is necessary to advance the understanding of the post-fire seismic performance of RC structures. However, individual computer programs which can perform well in the both thermal and seismic analysis may help structural engineers taking decisions. Damage identification is the first step to predict the resilience of RC structures after fire events. This study investigates the performance assessment of different structural elements (column, beam, shear wall) within a code-designed RC frame building and thus compares pre and post-fire structural strength and serviceability parameters. Fire occurred at the 7th, 8th and 9th floors of a twenty-three-storied reinforced concrete building with two basements. The building can be categorized as a dual framing system which is located in Dhaka. Primarily, a damage assessment has been performed following some field investigation and testing techniques. A series of non-destructive tests such as UPV, carbonation concrete core, and rebar tensile strength tests have been carried out in the field and at the laboratory on the collected samples for damage classification and identification. Damage intensity of eighth-floor roof was found (8%) to be more than the other two (Seventh and ninth) floors (5%) whereas concrete strength reduction of vertical elements was found up to 33% (in the columns and shear wall) and 23% in the horizontal elements (beams and slab). Based on the maximum gas temperature, a parametric fire curve has been constructed to simulate the thermal stress of fire-affected (seventh, eighth, and ninth) floors that influence the capacity of the materials by FIN EC software. The simulated material strength is compared with the equivalent concrete compressive strength obtained from the test data. The entire building is then modeled using finite element based computer program to assess the structural performance at pre and post-fire conditions. Initially, linear static analysis has been performed to obtain the force-based structural capacity of the building at

different performance levels such as maximum considered earthquake (MCE), design basis earthquake (DBE), and service level earthquake (SLE) and the capacity was compared between pre and post-fire conditions. The mechanical properties of concrete after fire exposure, such as residual compressive strength, stiffness, and constitutive responses were reviewed. Finally, a nonlinear dynamic time history analysis using ten different ground motions is performed to observe the actual response of the structure. The results are presented in terms of storey drift and displacement, stiffness, and column demand /capacity ratios and they are compared for pre and post-fire exposure at different performance levels, i.e. SLE, DBE & MCE. The results showed that the inter-storey drifts and demand /capacity ratio in the few cases particularly at the fire-damaged floors exceeds the allowable limit. The displacement increases and storey stiffness decreases considerably due to stability loss by elevated temperature. In most of the cases, it fulfills the requirement of strength and serviceability of structure in terms of strength, displacement, and drifts. The maximum concrete and rebar strain developed in the RC elements is found within the allowable limit of performance criteria for all service levels. The proposed assessment procedure is capable of capturing the actual scenario of a fire-damaged building at different performance levels that may help the stakeholders to take further strategic decisions on the damaged structure.

NOTATION

A_o	opening area [m ²]
A_{tot}	total compartment boundary area, including the openings [m ²]
c	specific heat capacity [J/kgK]
c_p	specific heat capacity at constant pressure [J/kgK]
d	thickness [m]
h	heat transfer coefficient [W/m ² K]
h_c	convection heat transfer coefficient [W/m ² K]
h_r	radiation heat transfer coefficient [W/m ² K]
H_o	opening height [m]
H_c	compartment height [m]
k	thermal conductivity [W/mK]
L_c	compartment length [m]
m_a	mass flow of air [kg/s]
m_o	mass flow of air out from compartment [kg/s]
m_i	mass flow of air in to the compartment [kg/s]
Θ	temperature difference ($T_T - T_i$) [°C]
O	opening factor for the compartment [m ^{1/2}]
t	time [s]
t_d	critical time for treating a solids as semi-infinite [s]
R	thermal resistance [m ² K/W]
T_{core}	core temperature [°C]
T_f	fire temperature [°C]
T_g	gas temperature [°C]
T_i	initial temperature [°C]

V_c	compartment volume [m^3]
W_c	compartment width [m]
q	heat flow rate [W]
q_b	rate of heat being stored as gas [W]
q_c	rate of heat released by combustion [W]
q_l	rate of heat loss by convection through openings [W]
q_r	rate of heat loss by radiation through openings [W]
q_w	rate of heat loss conducted through the walls, ceiling and floor [W]
q''	heat flux per unit area [W/m^2]
α_1	flow factor [$kg/m^{5/2}s$]
α_2	combustion yield [J/kg]
ε	emissivity [-]
σ	Stefan Boltzman's constant [W/m^2K^4]
ρ	density [kg/m^3]
τ	time constant [s]

LIST OF TABLES

Table 2-1: Structural hazard level definition (Pekelnicky et al., 2012).....	22
Table 2-2: Structural performance level definition (Pekelnicky et al., 2012)	23
Table 3-1: Post-fire Damage Ratings and descriptions (FIB 2008).....	29
Table 4-1: Effect of temperature on common materials (Concrete Society, 2008)	42
.Table 4-2: Summary of visual inspection	49
Table 4-3: Location & Picture of Carbonation for column shear wall and slab	52
Table 4-4: Summary of inspection and test results	53
Table 4-5: Fire Unaffected Column/Shear wall Concrete Equivalent Comp. Strength as per ACI 562.....	55
Table 4-6: Fire Affected Column/Shearwall Concrete Equivalent Compressive Strength as per ACI 562	55
Table 4-7: Fire Unaffected Beam/Slab Concrete Equivalent Compressive Strength as per ACI 562.....	57
Table 4-8: Fire Affected Beam/Slab Concrete Equivalent Compressive Strength as per ACI 562.....	57
Table 4-9: Tensile strength test for rebar of used and new samples	58
Table 4-10: Fire Zone Properties	61
Table 4-11: Material Combustion Properties.....	61
Table 4-12: Considered Fire Parameters.....	61
Table 4-13: Results of Parametric Fire Curve	62
Table 4-14: Constitutive relationships of high-temperature properties for concrete of column (EN, 2002)	65
Table 5-1: Property of fire-affected and unaffected concrete (<i>Pekelnicky et al., 2012</i>)....	70
Table 5-2: Load Consideration	73
Table 5-3: Load Combination.....	73
Table 5-4: Seismic parameters.....	73
Table 5-5: Fundamental period and frequency	75
Table 5-6: Drift and deflection increase for fire effect	78
Table 5-7: Stiffness loss due to fire effect	80
Table 5-8: Variation of column PMM ratio due to fire effect	83
Table 5-9: Reference ground motions data used in the analysis.....	86
Table 5-10: Fiber stress and status of hinge-W8H19 (7F).....	108
Table 5-11: Hinge state and status of 7 th floor wall	109

LIST OF FIGURES

Fig 1.1: Fire at World Trade Center (Klersfeld and Nordenson, 2003).....	2
Fig 1.2: Total fire incident in Bangladesh.	4
Fig 1.3: Total casualties due to fire incident in Bangladesh.	4
Fig 2.1: Variation of residual strength of rebar and concrete as a function of maximum temperature (EN, 2004).	14
Fig 2.2: Temperature development of a real fire and a standard fire (Bisby and Stratford, 2013).....	17
Fig 2.3: Temperature time curves.	18
Fig 2.4: Temperature time curves for various opening factors and fire load (Van Coile et al., 2015).	19
Fig 2.5: Assumed force-deformation relationship (Varela et al., 2004).	20
Fig 2.6: Illustration of performance level (Pekelnicky et al., 2012).	23
Fig 2.7: Structural performance criteria (Pekelnicky et al., 2012).....	24
Fig 3.1: Flow chart for assessment of fire-damaged RC building.	28
Fig 3.2: Principle and method of wave transmission used in UPV.	30
Fig 3.3: UPV data collection from the concrete core sample.	30
Fig 3.4: Onsite carbonation test and depth measurement.	31
Fig 3.5: Concrete Core Test, sample collection and preparation.	32
Fig 3.6: Rebar tensile strength test.....	33
Fig 4.1: General view of the building under fire.	38
Fig 4.2: Rescuing operation during the fire incident.	39
Fig 4.3: The external appearance of the building after the fire.....	40
Fig 4.4: Floor damages inside the building.....	41
Fig 4.5: Some pictorial evidence of structural concrete damage.	45
Fig 4.6: Typical floor subdivided into 900 mm X 900 mm grid.....	46
Fig 4.7: Column and slab subdivided into 900mm X 900mm.	47
Fig 4.8: Damage Intensity layout with color code.....	49
Fig 4.9: Compressive strength vs. ultrasonic pulse velocity plot for RC columns and slab.	50
Fig 4.10: 3D View of FR Tower (Fire Affected 7th, 8th & 9th Floor).....	59
Fig 4.11: Fire zone walls.....	60
Fig 4.12: Time vs. gas temperature curve for parametric fire.	62
Fig 4.13: Time vs. concrete temperature at different concrete depths.....	63
Fig 4.14: Time vs. Rebar Temp at a different location.	63
Fig 4.15: Heat Transfer analysis by FIN software for C2 on the 8th floor.....	64

Fig 4.16: Heat transfer analysis by FIN software for periphery beam on the 8th floor.....	65
Fig 4.17: Concrete compressive strength reduction with temperature.	66
Fig 5.1: Typical floor plan & 3D view of the building.....	69
Fig 5.2: Cross-section of columns and beam with rebar arrangements.....	70
Fig 5.3: Material nonlinearity.....	71
Fig 5.4: Beam & Column Hinge Properties.....	72
Fig 5.5: Spectral acceleration curve at different earthquake levels.....	74
Fig 5.6: First four-mode shape.....	75
Fig 5.7: Column Moment Curvature.....	76
Fig 5.8: Column Interaction Diagram.....	77
Fig 5.9: Maximum Deflection.....	78
Fig 5.10: Storey drift.....	79
Fig 5.11: Storey Stiffness.....	80
Fig 5.12: Column PMM ratio.....	82
Fig 5.13: Shearwall demand capacity ratio.....	85
Fig 5.14: Time history functions of ten different ground motions.....	87
Fig 5.15: Scaled Time history function- 2475 Years.....	88
Fig 5.16: Scaled Response Spectrum- 2475 Years.....	88
Fig 5.17: Scaled Time history function- 475 Years.....	89
Fig 5.18: Scaled Response Spectrum- 475 Years.....	89
Fig 5.19: Scaled Time History Function- 43 Years.....	90
Fig 5.20: Scaled Response Spectrum- 43 Years.....	90
Fig 5.21: Base shear at different GMs for pre-fire MCE condition.....	91
Fig 5.22: Base shear at different GMs for post-fire MCE condition.....	92
Fig 5.23: Base shear at different GMs for pre-fire DBE condition.....	92
Fig 5.24: Base shear at different GMs for post-fire DBE condition.....	93
Fig 5.25: Base shear at different GMs for pre-fire SLE condition.....	93
Fig 5.26: Base shear at different GMs for post-fire SLE condition.....	94
Fig 5.27: Storey drift ratio for different GMs (post-fire MCE condition).....	95
Fig 5.28: Maximum storey drift ratio in the X direction for MCE, DBE & SLE condition (for Trinidad GMs).....	96
Fig 5.29: Maximum storey drift ratio in the Y direction for MCE, DBE & SLE condition (for Trinidad GMs).....	97
Fig 5.30: Rebar stress-strain curve for hinge W8H19 (7F), fiber-19.....	98
Fig 5.31: Concrete stress-strain curve for hinge W8H19 (8F), fiber-17.....	98

Fig 5.32: Rebar stress-strain curve for hinge W2H18 (8F), fiber-19 for MCE, DBE & SLE condition.....	99
Fig 5.33: Concrete stress-strain curve for hinge W8H19 (7F), fiber-4 for MCE, DBE & SLE condition.....	100
Fig 5.34: Concrete stress-strain curve for hinge W2H18 (8F), fiber-17 for MCE, DBE & SLE condition.....	101
Fig 5.35: Concrete stress-strain curve for hinge W278H16 (9F), fiber-1 for MCE, DBE & SLE condition.....	102
Fig 5.36: Hysteretic Response of Hinge for different GMs.....	103
Fig 5.37: Shear wall moment rotation curve for hinge W8H19 (7F), for MCE, DBE & SLE condition.....	104
Fig 5.38: Shear wall moment rotation curve for hinge W2H18 (8F), for MCE, DBE & SLE condition.....	105
Fig 5.39: Shear wall moment rotation curve for hinge W278H16 (9F), for MCE, DBE & SLE condition.....	106
Fig 5.40: Comparative strain for various fibers of concrete and rebar for W8H19 (7F) hinge at MCE & DBE condition.	107
Fig 5.41: Comparative rotation of various wall hinges of 7th floor at MCE & DBE condition.	107
Fig 5.42: Comparatives of column hinge (W8H19-8F) rotation for MCE & DBE condition.	110
Fig 5.43: Comparatives of beam (8F) hinge rotation for MCE & DBE condition.	110

TABLE OF CONTENTS

ACKNOWLEDGEMENT	I
ABSTRACT.....	II
NOTATION.....	IV
LIST OF TABLES.....	VI
LIST OF FIGURES	VII
TABLE OF CONTENTS.....	X
CHAPTER 1 : INTRODUCTION.....	1
1.1 Introduction	1
1.2 Background and Motivation.....	6
1.3 Research Objectives	7
1.4 Scope of the Thesis.....	7
1.5 Organization of the Thesis	8
CHAPTER 2 : LITERATURE REVIEW	9
2.1 Introduction	9
2.2 Damage Assesment	9
2.3 Materials Properties Assesment	12
2.4 Thermal Stress Analysis.....	16
2.5 Seismic Analysis	19
2.6 Summary	24
CHAPTER 3 : METHODOLOGY	26
3.1 Introduction	26
3.2 Damage Evaluation Methods	26
3.3.1 Visual Inspection	27
3.3.2 Damage Classification.....	27
3.3.3 Ultrasonic Pulse Velocity Test	29
3.3.4 Carbonation Depth Test.....	31
3.3.5 Concrete Core Test.....	32
3.3.6 Rebar Tensile Strength Test	33
3.3 FEM Analysis Methods.....	34
3.4.1 Fire Analysis by FEM	34
3.4.2 Structural Analysis by FEM	35
3.4.3 Summary.....	37
CHAPTER 4 : DAMAGE ASSESMENT AND FIRE ANALYSIS	38

4.1	Introduction	38
4.2	Fire Information	38
4.3	Fire Damages to the Structural and Non-structural Components.....	42
4.4	Damage Classification.....	45
4.5	Evaluation of the Material Properties.....	49
	4.5.1 Ultrasonic Pulse Velocity Test	50
	4.5.2 Depth of Carbonation Test	51
	4.5.3 Concrete Core Test	54
	4.5.4 Rebar Test.....	58
4.6	Evolution of Material by Fire Temperature	59
	4.6.1 Development of Parametric Fire Curve.....	60
	4.6.2 Calculation of Concrete and Rebar Temperature	62
	4.6.3 Heat Transfer Analysis of Column at FIN Software	64
	4.6.4 Residual Concrete Compressive Strength Based on Heat Analysis	65
4.7	Summary	66
CHAPTER 5 : FINITE ELEMENT ANALYSIS OF DAMAGED BUILDING		68
5.1	Information	68
5.2	General Properties of the case Studies	68
5.3	Material Properties (Linear)	70
5.4	Material Properties (Nonlinear).....	71
5.5	Nonlinear Hinge Properties	71
5.6	Load Consideration	72
5.7	Seismic Parameters for Different Earthquake Level.....	73
5.8	Linear Static Analysis	74
	5.8.1 Modal Analysis.....	74
	5.8.2 Column Moment Curvature.....	76
	5.8.3 Column Interaction Diagram.....	76
	5.8.4 Deflection	77
	5.8.5 Drift	79
	5.8.6 Stiffness	80
	5.8.7 Column PMM Ratio	81
	5.8.8 Capacity of Shearwall.....	84
5.9	Nonlinear Time History Analysis (NLTHA)	86

5.10	Interpretation of Result for Performance-Based Analysis	91
5.10.1	Base Shear	91
5.10.2	Drift Ratio.....	94
5.10.3	Concrete and Rebar Stress-Strain Curve	98
5.10.4	Moment Rotation Curve of Hinges	103
5.11	Summary	111
CHAPTER 6 : CONCLUSIONS AND RECOMMENDATIONS.....		112
6.1	Conclusions	112
6.2	Limitation	115
6.3	Recommendations for Future Research	116
REFERENCES		117

CHAPTER 1

INTRODUCCION

1.1 Introduction

The fire discovered to help early hominids has evolved into an integral component of modern society. It sometimes triggers an unanticipated phenomenon in any structure, resulting in significant structural damage that causes severe loss of lives and property. Despite pessimistic fire effects on structural elements, building construction can not be completed without fire effects due to specific difficulties (Poliakova and Grigoryan, 2018; and Wang et al., 2011). The performance of structural systems under fire exposure had previously given considerable attention, it wasn't until the terrible World Trade Center collapse on September 11, 2001 that more emphasis was placed on creating effective fire safety regulations (Gulvanessian et al., 2002) for buildings (Fig 1.1). Some precautionary steps should be taken during design to overcome these challenges. The structural design against fire can be performed following the fire design codes for building (IBC, 2012a; ISO, 1999b; EN, 2002; and EN, 2010). Life safety protection has been a primary consideration in the development of current rules and provisions for fire design of building structures (Spinardi et al., 2017). As a result, the main goals of performance standards are to guarantee that building occupants have enough time to evacuate and to keep the fire brigade safe while conducting search and rescue operations. On the other hand, little thought is given to protecting property or rebuilding structures after a fire (Mostafaei et al., 2014).

However, the issue of preserving functionality and enabling quick recovery for structures and other infrastructures harmed by an unplanned incident like a fire has recently drawn more attention. This change is the result of a widespread realization that the built environment must be resilient, or able to quickly recover from setbacks and disruptions (Bocchini et al., 2014). Resilience is particularly crucial in an era of rapid urbanization, where municipal infrastructure systems are under pressure and any disturbance could have significant socioeconomic effects. For instance, closing down of a school, a hospital or a bridge after a fire event would result in significant indirect economic cost. As a result, property protection needs to be included in performance requirements for structures under

fire. New techniques must be created in the meantime to be able to evaluate the degree of destruction or the level of remaining safety of structures following a fire. These techniques are necessary to facilitate and expedite the decision-making process after a disaster by offering reliable information regarding the state of the structure.



Fig 1.1: Fire at World Trade Center (Klersfeld and Nordenson, 2003).

Indeed, decision makers need to know whether a building can be re-used as is, needs structural repair, or should be demolished and rebuilt. Any delay in the decision process translates into a longer loss of functionality.

However, evaluating a building's condition after a fire is a challenging task. In fact, engineers fundamentally lack of knowledge regarding the following components:

- a) The fire event: Very little knowledge about exposure to different temperatures over time and space of the structure. Therefore, engineers must rely on expert judgment or utilize models and indirect measurements to assess the intensity of the fire.
- b) The features of the building before the incident: as-built drawings might not be available. Additionally, the structure can have undergone modifications or deterioration throughout the course of its lifetime.

- c) The effect of the fire on the structure and the residual material properties: estimations can be made through models and calculations, but this inevitably introduces simplifying assumptions and modelling uncertainties.

Many variables can contribute to a fire becoming out of control. A large fire can inflict significant damage to buildings and infrastructure. The spread of fire is aided by hot, dry, and windy weather. At the same time, inadequate communication and transportation networks hinder access to firefighting in disaster areas, and a shortage of water delivery systems limits fire control efforts. In that instance, more effort and extinguisher material, such as water, will be required to extinguish the fire. As a result, setting fire safety objectives for buildings and urban architecture is critical. It's also vital to ensure the structural integrity of the damaged structures for a particular period during a fire so that emergency resources can be used. These considerations should be considered while designing new buildings and retrofitting old ones.

Bangladesh is a densely populated country with high risk of natural disaster. It is considered as fifth most disaster prone country in the world (Schwab and Sala-I-Martin, 2010). In addition, the area is specially vulnerable to fire and earthquake disaster due to the density of ancient, unreinforced brick structures and the small, winding streets in the area. With the recent occurrence of numerous notable fires in Bangladesh, including the Nimtoli Fire, Bashundhara City Complex Fire, Bangladesh Steel and Engineering Corporation (BSEC) Bhaban Fire, Tazreen Garments Fire, Tampaco Foils Ltd Factory Fire, Fire at Rohingya camp, FR Tower Fire, Hashem Food and Beverage factory Fire, Chottogram Container Fire, and Sitakundu Fire , among others, fire hazard has emerged as a significant issue of concern alongside earthquake risk.

The frequency of fire occurrences in Bangladesh is on the rise, according to a study report from the Bangladesh Fire Service and Civil Defense (BFSCD). Fig 1.2 has been reproduced based on the report of Bangladesh Fire Service and Civil Defense and (Sahebi et al., 2020) indicates that a total of 262814 fire incident occurs in the period of 2006 to 2021.

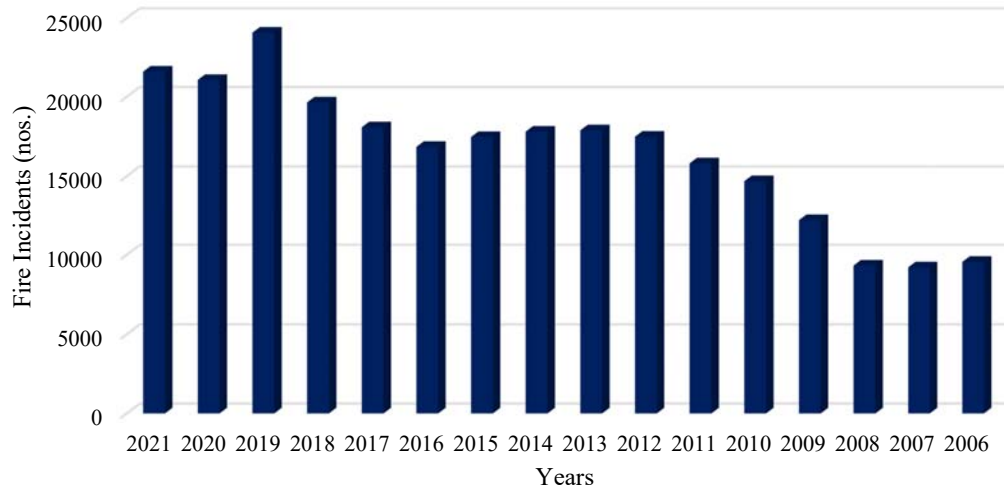


Fig 1.2: Total fire incident in Bangladesh.

Moreover, Fig 1.3 has also been reproduced using (Naoshin et al., 2020) and BFSCD that shows the the death and injurious of 2527 and 12141 people respectively. Due to its dense concentrations of buildings, narrow roads, flammable building materials, outdated water and electrical infrastructure, chemical factories in residential areas, and lack of preparedness and response capabilities among locals and the fire authority, Dhaka the capital of Bangladesh frequently faces fire hazards.

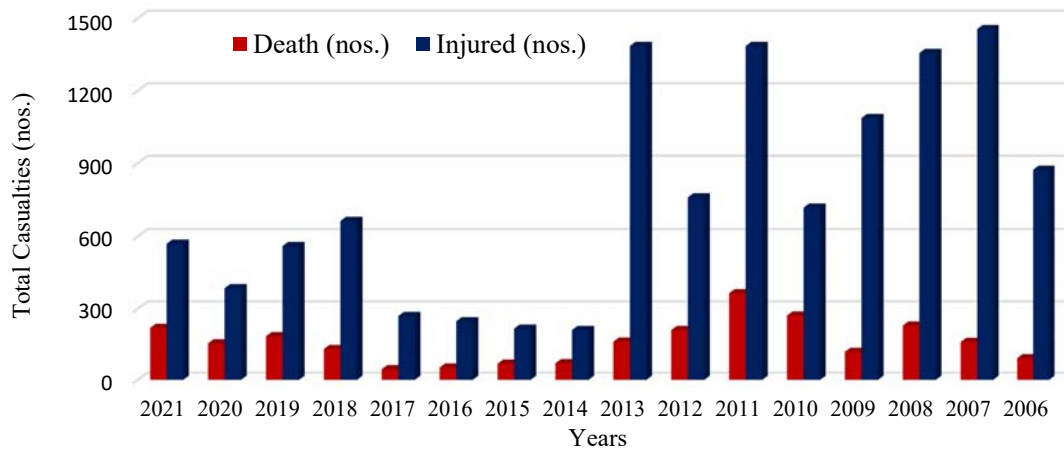


Fig 1.3: Total casualties due to fire incident in Bangladesh.

Given the many uncertainties mentioned above, the assessment of the post-fire condition of a structure needs to rely on a rigorous methodology. The objective of this research is to propose such a methodology. Emphasis is put on the post-fire load bearing capacity of

concrete structures, but the methodology could easily be applied to other types of structures. The work adopts a reliability-based approach to quantify the residual load bearing capacity of a concrete structural element after a fire. This approach allows making the link with the reliability-based philosophy of the initial design by providing a clear understanding of the residual safety after the event. For practicality, the result is expressed in terms of maximum allowable imposed load for a given target safety level for the post-fire assessment (for instance, equal to the safety level of the initial design).

The presented work focuses on a reinforced concrete structure, which is one of the most common structural elements in buildings and infrastructure. Recent efforts directed to improve (the understanding of) the resilience of concrete structure with respect to fire include amongst others fragility assessments through expert-judgment (Ioannou et al., 2017), detailed reliability assessments (Van Coile, 2015) and an application of the PEER framework (Lange et al., 2014). In this work a more direct approach is followed where the residual capacity is directly assessed after a specific fire event. The considered structure is typically a multi-storied commercial building. Damage classification by color contouring and material assessment by nondestructive and destructive testing has been done to estimate the fire effects. In function of the assessed case, influences of degradation should be taken into account in the methodology through the characteristics of the fire-exposed structural element (e.g. reinforcement strength, concrete compressive strength).

The proposed methodology starts from the observation of a fire event and the collection of data and goes through the different steps up to the estimation of the maximum allowable imposed fire loads. It makes use of a combination of forensic investigation (e.g. on-site measurements, discussion with firefighters and building designers), simplified fire temperature methods, advanced numerical modelling (e.g. by finite element method), reliability-based methods, and engineering judgment. Throughout the study, the method is illustrated by a real case study.

The application of reliability concepts allows to make a post-fire seismic performance assessment which is in agreement with the safety philosophy.

1.2 Background and Motivation

The structure's design should enable enough time for residents to evacuate in the event of an earthquake or fire and the safety of any emergency-services professionals who may be required to enter during or after such catastrophes (Mousavi et al., 2008). However, most of the past studies on the behavior of structures exposed to such risks have focused on either fire or earthquakes separately. As a result, the current research intends to improve the engineering community's understanding of structural behavior under consecutive fire-earthquake stresses, including both post-earthquake fires and post-fire earthquakes.

A major earthquake can result in destructive post-event flames and aftershocks (Dahal and Mullen, 2021). In this case, an RC structure that has survived a post-earthquake fire may be vulnerable to significant damage or collapse in future earthquakes (Kam et al., 2011), which raises another safety issue: the performance of RC structures after a fire. Post-fire earthquake scenarios may potentially occur in the event of a huge fire preceding a future earthquake. As a result, knowing structural performance under such threats is required for resilient design and evaluation of existing infrastructure (Naser and Kodur, 2018).

Due to the high expense of tests under consecutive fire-seismic loads, numerical analysis is essential in evaluating the post-fire earthquake performance of structural components. An effective and efficient simulation approach is required to capture the reaction to both fire and earthquake loads (Ni, 2018). A comprehensive parametric study is also required to fully understand the post-fire seismic performance of structural components to identify critical situations where the impact of fire damage is significant (Qin et al., 2021). Furthermore, engineers should develop simplified modeling tools to aid them in capturing the effects of fire within the context of models and software widely used for seismic research.

Currently, there are two major study subjects in the realm of fire and structures:

- the residual condition of structures after fire
- design for fire resistance

The strength and serviceability loss of a structure following a fire occurrence and the structure's long-term health are the key concerns of the residual condition of structures after

the fire. Fire resistance, on the other hand, is defined as "the ability of a building element to fulfill its planned function for a length of time in the case of a fire," which is more relevant to the design and retrofit of concrete structures.

1.3 Research Objectives

The main objectives of the present research are

- a) To evaluate the damage states of different structural components for a high-rise building after the fire incident.
- b) To investigate the post-fire seismic capacity of the building using a performance-based seismic design (PBSD) approach by finite element simulation.

The combination of different methods or tools used for each analysis stage is needed to ease the simulation and the analysis procedure faster. It also intends to capture the fundamental behavior for post fire seismic performance.

1.4 Scope of the Thesis

To achieve the goals of the study, the material properties and different techniques for seismic assesment of fire damaged structures were obtained from the literature review. The study presents the damage state as well as finite element analysis to calculate the residual strength of fire damaged structure. The suitability for the use of performance based analysis to calculate the actual residual strength of structural elements (Shearwall, column and beam) can be determined. In this study, a 23 storied building with 2 basement located at the heart of Dhaka city has been selected for the evaluation. Initial visual inspection was performed to collect the information about the damage. Further inspection helps to prepare the drawing of the structure. Damage classification by color contour helps to detect damage severity with locations. Some destructive testing has been performed based on the damage severity. Moreover some non-destructive testing has been performed to correlate the test results. Residual strength of material has been calculated. Development of parametric fire curve helps to perform heat transfer analysis of structural members by FIN software. A full-scale three dimensional finite element model will be developed using structural analysis software. Floor plan and section properties were exactly followed as per project data.

Material properties has used as per the laboratory and heat transfer analysis data. Primarily, FBD analysis will be performed to check the adequacy for the considered equivalent static load at different service period i.e. MCE, DBE, and SLE. Design of the building using BNBC (2020) has been performed to assess the capacity of the column. Finally, non-linear time history analysis will be conducted for ten sets of ground motions to observe the actual response of building beam, column and shear wall and hence the performance at 43, 475 and 2475 years return period.

1.5 Organization of the Thesis

The thesis has been organized into six chapters. The objectives of the thesis with some introductory materials are presented in the current chapter, i.e., Chapter 1. A review of previous works and ongoing work on this topic is incorporated in Chapter 2. The methodology of the research are presented in Chapter 3. Chapter 4 depicts about the damage assessment and heat transfer analysis. Material Properties at elevated temperatures are also described in this chapter. Finite element analysis and explanation of results has been described in chapter 5. The summary of the thesis, including the conclusions and recommendations, are presented in Chapters 6. A list of references is arranged at the end of the thesis.

CHAPTER 2

LITERATURE REVIEW

2.1 Introduction

The structural response of buildings to fire conditions has been the focus of intensive research activity in recent years. For composite steel / concrete buildings, this has been driven by the motivation to achieve more cost-effective designs and, more generally, by the need to attain a greater understanding of the underlying behavioral mechanisms that occur in fire. As a result, there has been an increasing recognition of the benefits of employing performance-based fire design, in comparison with prescriptive approaches which are based on unrealistic idealizations. This chapter summarizes on the literature review on thermal analysis and mechanical properties of materials (i.e concrete and rebar) under fire. This section also focuses on past research performed on the seismic performance of reinforced concrete by performance based analysis.

2.2 Damage Assessment

RC buildings have high natural fire resistance and high temperatures may not always result in destruction. A post-fire assessment is essential because of the concrete construction state of the building. Buildings with concrete that has been subjected to fire does not have the same cross-sectional characteristics. The concrete layer closest to the surface deteriorated the most severely (Wróblewska and Kowalski, 2020) In spite of the damage and ongoing deformations, RC constructions often stay stable after a fire (Ni and Gernay, 2020). The effectiveness of concrete constructions damaged by fire has been extensively studied by academics (Ryu, Shin and Kim, 2018). Compared to wood and stainless steel structures, reinforced concrete buildings have superior natural fire resistance (Kodur, 2014). The reinforcement is protected from the heat as the concrete coating seeps further into the cross-section of the member. This enables a building's load-bearing capacity to stay relatively high during and after a fire. Conversely, lightweight concrete has greater fire resistance than high-strength concrete, which has less fire resistance than regular concrete. Despite this, concrete is rarely destroyed totally in a fire, in contrast to steel and wood. When

concrete is exposed to high temperatures, its mechanical properties are weakened by thermal, physical, and chemical processes (Bažant, Kaplan and Bazant, 1996). Normal concrete, high-strength concrete, lightweight concrete, shotcrete, and mortars all have equivalent severe heat characteristics (Bamonte and Gambarova, 2014). In the early stages of a fire, RC beams and slabs close to the ceiling that are exposed to rising convective currents are more susceptible (Kodur and Agrawal, 2016). Due to concrete's higher fire resistance, RC structures that have been exposed to fire maintenance have a significant amount of residual capability, and it is frequently possible to reuse the structure in the future. On the other side, thermal deterioration may result in a permanent loss of strength and use. To make precise judgments concerning future usage and the necessity of repairs in fire-damaged structures, a detailed assessment of the residual capacity is required (Agrawal and Kodur, 2020).

The ability to evaluate the impact of a fire on the structural load-bearing capacity and safety generally requires measuring the concrete residual strength. This can be used to determine if the structure is fit for current usage, what sort and how extensive repairs are needed, or even to demolish the damaged building. If the structural components have been significantly damaged by fire, damages and areas of concrete deterioration are readily apparent and recognisable (Knyziak, Kowalski and Krentowski, 2019). Concrete changes in appearance cannot be seen during the initial visual inspection of less damaged parts. Testing in the lab and on-site can provide more detailed information on the state and internal structure of the concrete. The most crucial aspect to take into account following fire damage is concrete compressive strength. It is crucial to measure the thickness of the concrete's exterior layer in the area where damage to the concrete has occurred before it has to be taken into consideration (Felicetti, 2014). All three types of fire standard, parametric, and natural are utilized to analyze RC structures without cooling. The parametric and natural fires, as opposed to conventional flames, often replicate real fires more accurately (Huang, 2010). In assessing structures after a fire, the thickness of the external crossings, in which the concrete is sufficiently damaged to be regarded as destructed is very important (Wróblewska and Kowalski, 2020).

According to the textbook, the low-slender RC components in normal constructions have a fire resistance of 50–60%. To build RC members with a 4-hour fire-resistance, the Euro code specifications for cross-sectional dimensions and axial reinforcement distance from

the concrete surface can be employed (Felicetti, 2014). On the other hand, these codes believed that the temperature of the steel reinforcement was a substantial contributor to the degradation of strength. Based on the fire strength class for the load-bearing requirements of 30 or 60 min in normal fire exposure, the Eurocode (EN 2004) provides profiles for the temperature distribution across the slab thickness for slabs, cross-sections for beams, and columns. It teaches how to compute mechanical behavior using fundamental methods like the zone and 500 °C isotherm procedures (Al-Rousan, 2020). The National Fire Protection Association (NFPA) 101 states that modernizing a building would make its occupants safer. The Nigeria National NBC evaluates the safety of buildings and takes into account fire safety measures such as structural fire resistance, detection, alarm, and extinguishing systems. Examples of general safety are evacuation procedures and fire safety regulations (Wakelyn, Thompson and Nevius, 2006).

Researcher performed fire tests and low-frequency cyclic loading tests after fire on three conventional high strength concrete (HSC) shear walls and a superimposed HSC shear wall with precast recycled aggregate concrete (RAC) panel. They investigated the spalling of concrete, temperature distribution and deformation of specimens for 45 min, 90 min, and 135 min separately as a indicators of fire response. They found that the HSC suffer severe spalling than conventional wall during fire. Use of RAC panel can alleviate spalling more than 60% compared to conventional wall (Xiao et al., 2017). The health assessment of fire damaged structure has been performed (Aseem et al., 2019). They estimated the residual durability and mechanical properties by performing some non-destructive and destructive testing. Moreover, they have developed a framework to estimate the exposure temperatures of various structural units with the help of microstructural and thermal analysis. In the paper (Elghazouli, Cashell and Izzuddin, 2009) describes an experimental investigation into the influence of elevated temperatures on the mechanical properties of steel reinforcement. They examined the residual post-cooling properties of reinforcing bars. They also assessed the performance of reinforcement of 6mm, 8mm and 10mm diameter and the influence of temperature for enhancing the ductility of reinforcement. Some researcher performed damage assessment of a RC factory building. To evaluate the effects of the fire on the concrete, spectrophotometer and compressive strength tests were performed on concrete specimens taken from the building. They have concluded about the effect of temperature on overall stability of structure (Ada, Yüzer, and Ayvaz, 2019).

Researchers (Jiang et al., 2015) has examined the fire resistance of key component, including the concrete core, mega columns, the composite floor, outrigger trusses and belt trusses. The results shows that the Shanghai Tower has a minimum of 3 h fire resistance against fire-induced progressive collapse. The concrete components have smaller residual displacements compared to the steel components. They have recommended to consider the effective fire protection of outrigger trusses to guarantee the connection between the core and mega columns. This paper presents preliminary results of a numerical study to investigate the impact of fire damage on the lateral load resistance of flexure-control RC structural walls. It indicates that the fire damage decreases the load-bearing capacity and the stiffness of RC walls under reversed-cyclic loads (Birely and Ni, 2016).

2.3 Materials Properties Assessment

The codes provide guidelines on fires and deterrents, e.g., the predictable degree of the temperature based on the duration dimension limitations, types of material for structural elements, combustible material, fire protection, and duration of active and passive safety systems. The researchers can differentiate between the structure's actual and predicted temperature by taking advantage of different codes. The variation may cause due to (a) the uncertainty of combustion fire loads; (b) the boundary conditions, non-uniformity, opening size, and discontinuity of concrete; (c) the size and shape of the structural elements, etc.(Han et al., 2012).

In general, steel structure is more vulnerable to fire than concrete structure. The cross-sectional integrity of reinforcement with aggregate and binding material will likely cause improved fire resistance (Topçu and Karakurt, 2008). The chemical and physical properties of concrete change when it is exposed to elevated temperatures. Interestingly, the reinforced lightweight concrete shows improved performance compared to normal- weight concrete in terms of ultimate load, yield load, cracked load, stiffness, ductility, and inter-storey drift after high-temperature fire resistance. A significant issue of concern in fire events is the degradation of material strength due to the excessive temperature rise. Experimental studies evidenced that the mechanical properties of concrete and steel, i.e., compressive strength, tensile strength, elongation, and modulus of elasticity, change with temperature (Tao, Wang and Uy, 2013). The effects of high temperatures on exposed reinforcing steel have been simplified and statistically analyzed earlier (Arioz, 2007). The physical characteristics of

concrete, i.e., surface texture and color, change by elevated temperature (Hager, 2013; Osman et al., 2017; and Fletcher et al., 2007). The capacity of structural elements changes due to material deterioration during the elevated temperature fire (Khoury, 2000; Kodur, 2014; and Hertz, 2005).

The temperature is a critical parameter to stabilize the strength of concrete. The rate of temperature rise significantly influences the degree of destruction and structural loss. The variation of concrete compressive strength with temperature may be classified (Malhotra, 1956; Torić, Boko and Peroš, 2013; and Ma et al., 2015) into three categories: a) up to 300°C, wherein the concrete compressive strength decreases slightly or remains constant. b) At 300°C-550°C, the compressive strength of concrete decreases sharply and may be reduced up to 50%. c) Above 690°C, the concrete compressive strength will remain at 20% of the specified concrete compressive strength.

The intensity of vapor increases as the burning of the combustible materials progresses, particularly in the case of ventilation-controlled fire. The vapor causes the hydration operation of dehydrated cement grain (Hertz, 2005). As a result, the compressive strength of concrete increases slightly. Exposure below 300°C temperature, concrete can recover to its initial circumstances by absorbing moisture from the environment (Luo, Sun and Chan, 2000). After rising 300°C, concrete should be removed due to micro-cracks piercing into the concrete. Residual compressive strength is not prominently influenced by elevated temperature exposure up to 400°C, whereas mean compressive strength decreased by 32% after exposure to 400°C. It may occur due to less sensibility to micro-cracks (Hsu et al., 1963). Heating up to 400°C may create a small number of micro-cracks that do not reduce immediate compression capacity; instead, a small amount of cracked concrete could work as a highly redundant member (Reifenstein et al., 1999; and Shang and Lu, 2014). However, the compressive strength of concrete reduces drastically by 50% and 80% up to 550°C and above 690°C, respectively (Arioz, 2007).

Above 1150°C, feldspar melts, and the remaining mineral components of cement change into the glass phase (Shoukry et al., 2011). For concrete, the compressive strength, flexural strength, splitting tensile strength, and modulus of elasticity have an inverse relationship with the temperature rising (Lin, Lin and Powers-Couche, 1996). Moreover, these parameters also have an inverse relation with moisture content (Hager and Tracz, 2010).

The effect of temperature on the reduction of compressive strength of concrete is associated with the chemical and physical modification and configuration of concrete. It is possible to assess the temperature-induced loss of strength in steel (rebars) and concrete layers by knowing the temperatures in those layers. Typically, after cooling, reinforcing steel regains the majority of its strength and stiffness. Nevertheless, the residual strength of steel decreases as the maximum temperature in rebars increases, especially when that temperature approaches 500°C. According to temperature-residual strength test results published by some researcher (Neves, Rodrigues and Loureiro 1996) that, the loss of strength in reinforcing steel is anticipated to follow in the suggested design method. Fig 2.1 depicts the change in steel and concrete residual strength as a function of maximum temperature.

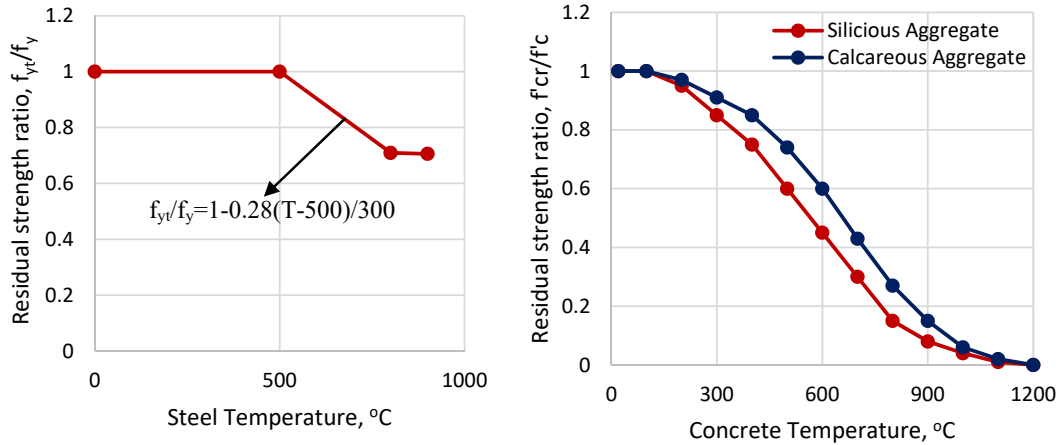


Fig 2.1: Variation of residual strength of rebar and concrete as a function of maximum temperature (EN, 2004).

At temperatures up to 800°C, volumetric shrinkage and expansion occurred due to the successful result of dehydration and rehydration of Ca(OH)_2 and CaO , respectively (Hertz, 1998). A notable expansion of the aggregate creates enlargements in the concrete crack (Hsu et al., 1963). Due to the temperature increase, vapor pressure intensifies the pore of concrete, which exerts excessive internal stress inside the concrete and results in concrete spalling and bonding failure. As a result, the effective cross-sectional area of structural elements reduces, and buried reinforcements become exposed to flame directly. Concrete spalling depends on concrete's physical and mechanical properties, such as strength, moisture content, and density. Besides the thermo-physical properties, temperature gradient, distribution of the temperature, external loads, geometry, and aggregate type, the

inclusion of fiber also influences the behavior of concrete during fire (Bratina, Saje and Planinc, 2007; Kizilkanat, Yüzer and Kabay, 2013; Kodur and Agrawal, 2017; Ozawa et al., 2012; and Tanyildizi and Coskun, 2008). The bond properties of the rebar/concrete interface can significantly affect RC members' strength degradation and deflection. Thus, structural components subjected to a fire provide poor fire resistance (Dwaikat, 2009; Gao, Dai and Tang, 2016; and Kodur and Dwaikat, 2008).

The concrete cover is a safeguard for the reinforcement against several effects of the external environment, including corrosion and physical, chemical, and thermal effects. An increase in concrete cover plays extra protection for reinforcement against fire (Shi et al., 2004; Subramanian and Geetha, 1997; and Topcu, Boğa and Demir, 2011). Concrete cover may be removed at the early stage of fire based on the amount of volumetric change in aggregates and spalling. An increase in cover may increase the fire-resisting capacity but provides slight improvement (Helmy, 2003; Ünlüoğlu, Topçu, and Yalaman, 2007), whereas retrofitting using advanced composite material may be an alternative (Okba, Helmy and Morsy, 2003). A 25 mm cover can protect high temperatures up to 400°C, almost the same as exposure to plain steel (Zhu et al., 2014). If the peak temperature increases beyond 500°C, the 25mm concrete cover thickness would be impractical. The frame structure decreases its load limit up to 36.9% and 48% under 600°C and 800°C, respectively. Under 1000°C, the frame losses its bearing capacity up to 57.3% (Lee, Choi and Hong, 2010; and Yüzer, Akbaş, and Kızılkana, 2007).

The tensile strength of cold-formed and hot-rolled steel is different at elevated temperatures. The hot-rolled bar regains its strength before the strength reduction happens at elevated temperatures. However, the strength of cold-formed steel was reduced compared to the actual tensile strength before cold-formed (Gunalan and Mahendran, 2014; Kankanamge and Mahendran, 2011; and Singh and Singh, 2019). The reduction of the rebar's tensile strength reduces the elements' ultimate capacity (Chiang and Tsai, 2003; Desnerck, Lees and Morley, 2017; Ichinose et al., 2004; and Yin, Han and Liu, 2011). The alteration of the aggregates and cement paste dehydration results in color variations, which can be determined by measuring carbonation depth. The level of temperature and damage to the mechanical properties of concrete can be related to the carbonation depth. Few researchers have also performed similar (Beck et al., 2016; and Wróblewski and Stawiski, 2020).

The load-carrying capacity can also be reduced by decreasing the bonding and anchorage capacity of concrete and reinforcement (Rodriguez, Orteza and Casal, 1997; Zandi, Kettil and Lundgren, 2011). The anchorage capacity refers to the minimum bond and splitting capacity. The sectional geometry, reinforcement, and concrete strength affect the splitting capacity, whereas rebar diameter, rib geometry, clear cover, rebar confinement, and concrete properties control the bonding capacity (Khaksefidi, Ghalehnovi and Britto, 2021). Generally, a splitting capacity test is performed to determine the anchorage capacity, whereas bond capacity represents the anchorage capacity for fire-damaged structures (Hertz, 1982). Yin, Han and Liu (2011) studied the anchorage of strength with temperature and applied the cooling method. Anchorage strength decreases slightly up to 300°C, whereas the strength reduces quickly, and ultimate slippage decreases gradually at high temperatures (Sharma, Bošnjak and Bessert, 2019).

Non-destructive testing (NDT) techniques have recently drawn significant importance for structural health assessment of reinforced concrete structures. The concrete structures undergo deformation, cracks, honeycombing and voids due to service, fatigue loads, environmental conditions and other extreme events. These defects can further deteriorate the integrity of concrete structures due to corrosion/damage of steel reinforcement and concrete itself. Various NDT techniques have been established to monitor these defects and update the health of structure accordingly during the service life of structure. Hobbs and Tchoketch (2007) have used ultrasonic pulse velocity (UPV) and impact rebound hammer (IRH) for predicting compressive strength of concrete structure. Similarly, health assessment of concrete has been carried out by combination of non-destructive techniques (Aseem et al., 2019)

2.4 Thermal Stress Analysis

The effect of real fires on the structural performance of RC member needs to be quantified to achieve a more rational approach for fire resistance design. Fig 2.2 illustrates the development of a possible real fire, which involves four stages – growth, flashover, fully developed and decay (Purkiss and Li, 2013). In the growth stage, structural integrity is not significantly influenced as the fire does not reach a high temperature (i.e. the temperature is normally lower than 300°C). However, once the fire temperature reaches about 600°C,

flashover occurs and the fire enters the fully developed stage, when the temperature may exceed 1000°C.

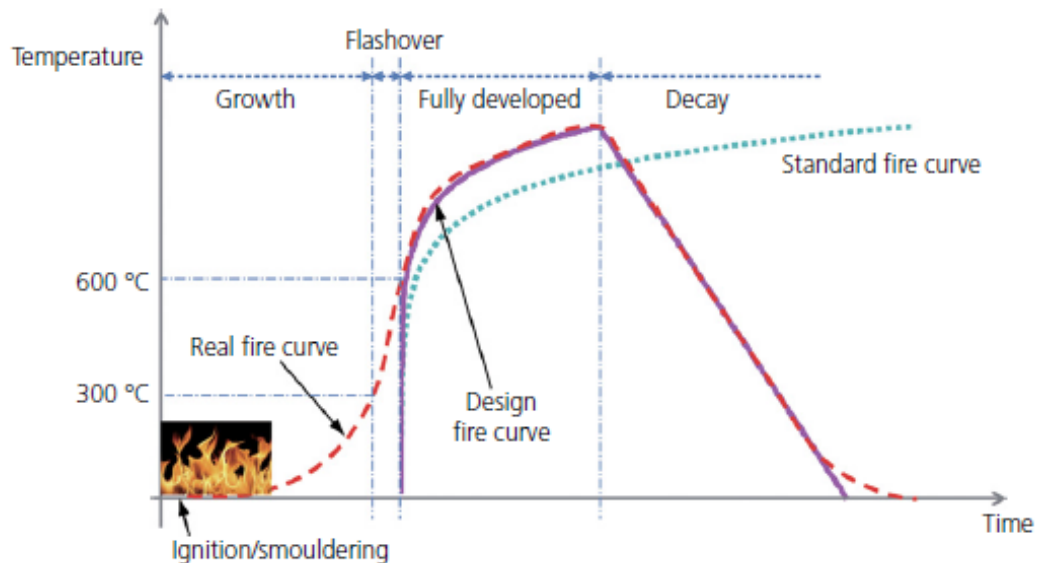


Fig 2.2: Temperature development of a real fire and a standard fire (Bisby and Stratford, 2013).

A number of mathematical models have been developed over the past 40 years in an attempt to describe the time–temperature curve of a post-flashover fire for use in structural design. These models are commonly referred to as design fires, and the notable ones include the model development (Magnusson and Thelandersson, 1970; Lie, 1974; Babrauskas, 1981; Wickstrom, 1985; Tanaka et al., 1997; Ma and Makelainen, 2000; Barnett, 2002, 2007; Zehfuss and Hossler, 2007; and Du and Li, 2012) and the Eurocode. It is worth noting that analysis of postflashover fire behaviour is complex and the above-mentioned models are based on some simplified assumptions, notably that the temperature distribution after post-flashover is uniform throughout a fire compartment and that the fuel burns in a uniform way (Buchanan, 2001; and Law, 1983).

The reliability of these models is not discussed here, but can be found elsewhere (Hurley, 2005). Among these models, the Eurocode parametric fire curve (CEN, 2002) has been widely used in estimating the temperature evolution of a post-flashover fire (Wang, 1997). This fire curve is a function of compartmental characteristics including the fuel load (i.e. calorific values of the available combustible materials), the ventilation conditions (i.e.

dimensions of openings) and the thermal inertia of the boundary of enclosure. The heating phase of the fire curve is given by

$$T_d = 20 + 1325(1 - 0.324e^{-0.2t^*} - 0.204e^{-1.7t^*} - 0.472e^{-19t^*}) \quad \text{Equation 2-1}$$

where, T_d is the fire temperature (in °C) and t^* is the fictitious time (in hr)

There are different ways of obtaining the post-flashover design fire temperature T_f . ISO 834 (1999a) and ASTM E-119 are the easiest way to describe the development of fire temperature. ISO 834 (1999a) is based on an equation, whereas the ASTM E-119 is on a time-temperature curve with values similar to ISO 834. The ASTM E-119 and ISO 834 time-temperature relation curves have been shown in Fig 2.3.

This way of describing a curve is used when no other information is available. But in reality, it is often possible to find more information concerning geometry and fire information. There are two variations of the ISO 834 fire curve based on the scenario. The hydrocarbon and external fire curves used were considered applicable.

Gas temperatures can be estimated using a design fire. A nominal fire or a natural fire can be selected. A nominal fire is represented by a standard curve (Fig 2.3) of uniform gas temperature with time (ISO 834, 1999a). It is independent of fuel and ventilation conditions and continues with time without decaying. A natural fire depends on fuel, geometry, and ventilation conditions, and it decays following the stages of a typical fire, as described above. Simplified models can be used to predict gas temperature, such as one-zone models, two-zone models, and computational fluid dynamics. Nominal fires are often used for designing purposes.

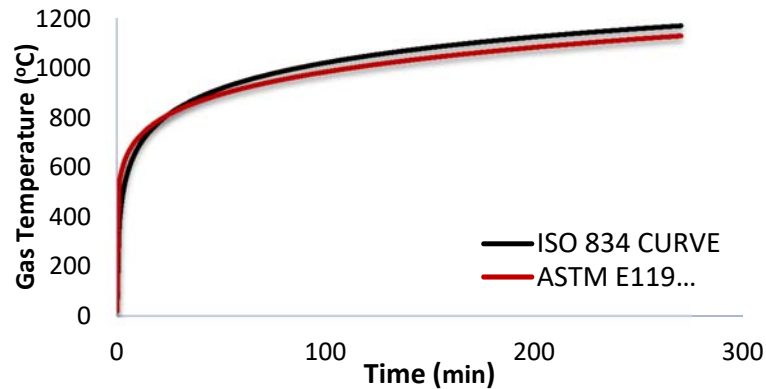


Fig 2.3: Temperature time curves.

The opening factor method uses information on fire load and ventilation openings, as shown in Fig 2.4. The Euro code parametric fire curves approximate the opening factor method using an equation with parameters regarding geometry, fire load, ventilation, and thermal properties of surrounding fire compartment surfaces.

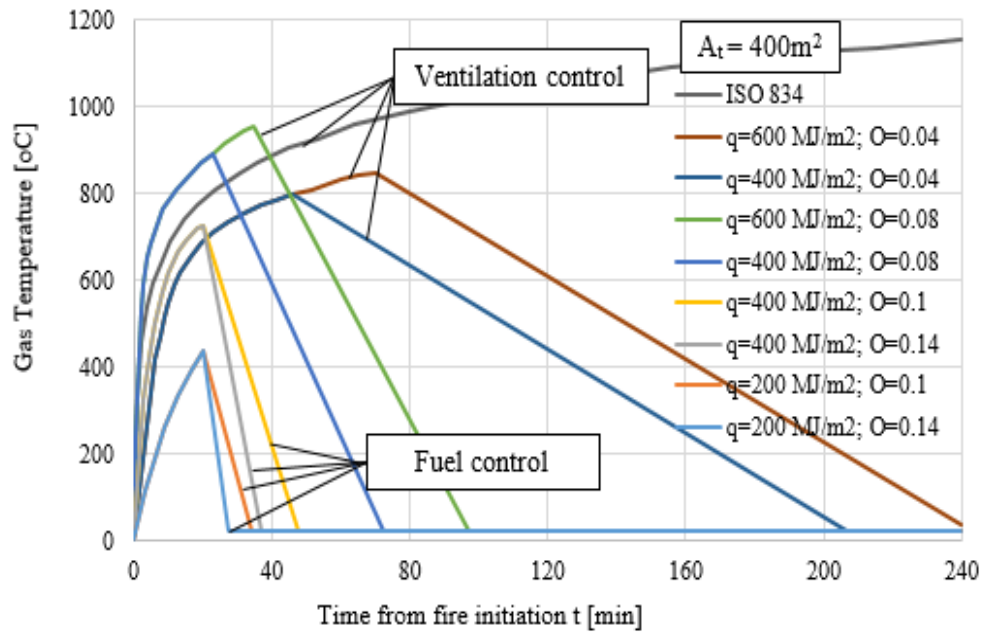


Fig 2.4: Temperature time curves for various opening factors and fire load (Van Coile, 2015).

The behavior of structures exposed to fire depends on several factors, including construction materials, the developer temperatures, the duration and the opening factor of the fire. The temperatures developed inside structural members must be estimated either for design purposes or for a damage assessment of a structure exposed to fire. These temperatures can be estimated if the gas temperature throughout the burning time is known. The gas temperature developed from a wildfire is more difficult to predict and depends on weather conditions (Butler, 2010).

2.5 Seismic Analysis

The structures, in a seismically active region, need to be designed and evaluated in accordance with modern earthquake engineering tools as the increasing earthquake losses is a burning issue of the present day world. Most often, a sudden rupture or unusual movement of a geological fault causes an earthquake (Kramer, 1996). This causes an

enormous amount of energy to be released, which travels to the surface of the earth as waves and causes vibrations. Buildings and other infrastructure systems may suffer serious damage or even collapse as a result of this ground shaking. Performance-based earthquake engineering (PBEE) is a modern method for dealing with building design and/or evaluation (Themelis, 2008). A building is designed using the PBEE method, which is logical and scientific, such that damage and performance are predicted in the event of an earthquake (Guo, Dong and Gu, 2020). Because there are no experimental or observable data available, determining the susceptibility of the entire building is a difficult undertaking. This is why it is preferred to evaluate RC frame constructions in terms of their constituent parts. The most important parts of an RC frame construction in terms of seismic performance are beams and columns.

The seismic design philosophy is predicated on permitting damage at certain areas in the structural elements, such as at beam ends and the bottom of the lowest storey columns in lateral force resisting systems. This is done for economic reasons. The response modification factor/force reduction factor, denoted by R , is used to implement this design concept in similar linear static force and code-based response spectrum analyses (FEMA-450, 2003; and IBC, 2012b). In the event of a seismic event, this factor regulates the seismic reaction of the structure. The force-deformation connection when the seismic design philosophy is used on a structure is shown Fig 2.5.

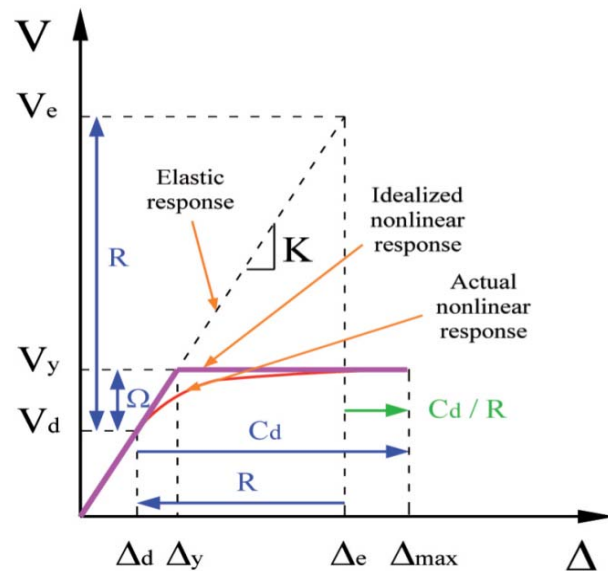


Fig 2.5: Assumed force-deformation relationship (Varela, Tanner and Klingner, 2004).

Equivalent static analysis (ESA) is the most commonly used, simple, easy, and quick method for analysis of structures. It is based on the simple concept that a static lateral force equivalent to dynamic force resulted from ground shaking is applied to the structure and then structure is analyzed accordingly. UBC-97 puts a limit for the use of ESA and permits this procedure only when a regular structure is of height upto 240 feet or when an irregular structure is of height upto 65 feet. When the height exceeds more than 240 feet or 65 feet in case of regular or irregular structures, respectively, or when the structure is lying on soil profile type SF with time period of more than 0.7 sec, dynamic response spectrum analysis is recommended. ESA is mostly used for the design of regular structures. For irregular structures dynamic analysis is best suited (ACI 318, 2008).

According to some scientist, ESA is a streamlined technique that distributes lateral loads along the height of a structure for evaluation in the context of the impact of dynamic loading from a foreseeable seismic event. In both the X and Y axes, the induced seismic force or base shear (V) is assessed. If the structure reacts in its fundamental lateral mode and is same in both the X- and Y-directions, precise design may be achieved.

Seismic events around the globe in the last quarter of the 20th century became a reason for collapse or extensive damage of many buildings that were designed in accordance with prevailing codes. The buildings were incapable to withstand the effects of seismic event despite of the fact that safety factors against earthquake had been taken into consideration while designing the structure. The probable reason for this was that there are many restrictions and limitations in code based design techniques. The stockholders of the building had concerns about safety and damage of the building. The scenario also became a challenge for structural engineers that how to evaluate the vulnerability and damage assessment of existing buildings as well as design of new structures. There was a need for new analysis and design approach. Performance based seismic design (PBSD) emerged as an effective solution.

Observing the damage following the San Fernando (1971), Northridge (1994), and Kobe (1995) earthquakes building owners, managers, and design professionals realized that buildings designed by following minimum code standards could suffer extensive and costly damage in response to the moderate earthquake-induced ground shaking.

A building may be designed to protect life safety and enable continued post-earthquake occupancy and functionality. In response to these concerns, structural engineers have developed a seismic design concept called Performance-Based Seismic Design (PBSD). PBSD approach permits a building owner/operator to select an acceptable level of building damage for a given intensity of earthquake ground shaking, which can serve as an objective for the seismic design. The fundamental objective of PBSD is to design a building with known approximation of damage in a seismic event. The PBSD approach has been in practice since the performance level of the building in case of earthquake is pre-defined. In PBSD, extent of damage in case of earthquake can be analyzed. In PBSD methodology, two parameters are required to be calculated for analysis and design purposes i.e. seismic capacity and seismic demand (ATC-40, 1996). The seismic capacity is the capability of the building to resist seismic effects whereas; the seismic demand is the earthquake effects imposed to the structure. The structure must be designed in a way that the seismic capacity always exceeds the seismic demand. International Code Council (IBC, 2012c) defines performance based design as, "An engineering approach to design elements of a building based on agreed upon performance goals and objectives, engineering analysis and quantitative assessment of alternatives against the design goals and objectives using accepted engineering tools and methodologies".

Table 2-1: Structural hazard level definition (Pekelnicky et al., 2012)

Hazard Level	Description
Frequent, minor EQ (SLE)	Return period: 43 years (50% probability of occurrence in 30 years)
Infrequent, moderate EQ (DBE)	Return period: 475 years (10% probability of occurrence in 50 years)
Worst EQ ever likely to occur (MCE)	Return period: 2475 years (2% probability of occurrence in 50 years)

A performance objective is a combination of two components called hazard level and performance level as detailed in Table 2-1 and Table 2-2, respectively. Association of performance level with a hazard level is called a performance objective. The leading advantage of PBSD is that any performance objective can be achieved when the structure is subjected to any specified hazard level. Fig 2.6 illustrates the performance levels of a

building as per ASCE 41-13 along with tentative expected approximate repair cost and time.

Table 2-2: Structural performance level definition (Pekelnicky et al., 2012)

Performance Level	Description
Operational (O)	Negligible impact on building. Building can be occupied. No repair work required.
Immediate Occupancy (IO)	Building is safe to occupy but will need little repair work.
Life Safety (LS)	Building is safe during the event but possibly not afterward. Building can be occupied after subsequent repair.
Collapse Prevention (CP)	Building is on the verge of collapse, probable total loss. Building is far beyond the economically feasible repair.

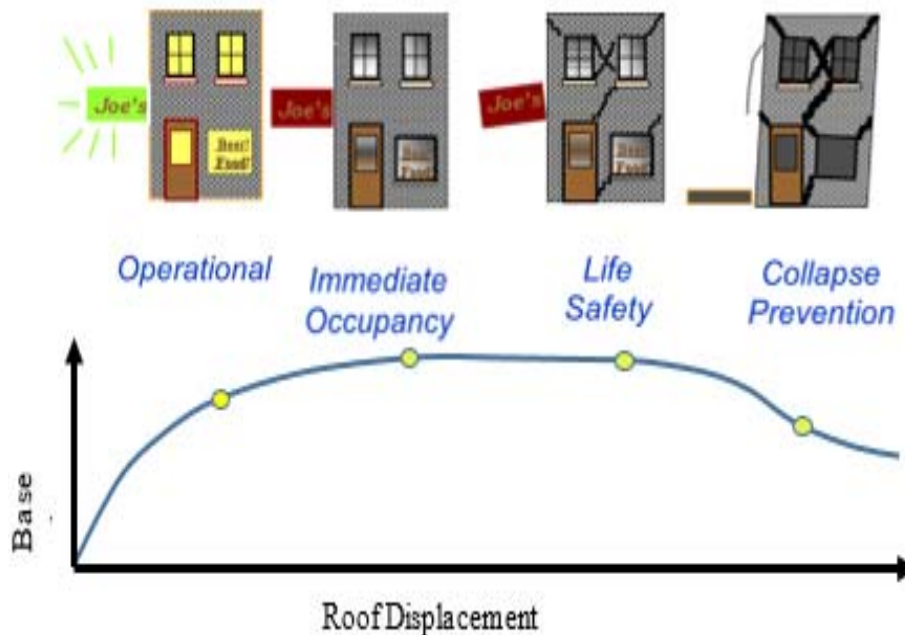


Fig 2.6: Illustration of performance level (Pekelnicky et al., 2012).

Some researcher has outlined four analytical methods for analysis and design purposes known as Linear Static Procedure (LSP), Linear Dynamic procedure (LDP), Nonlinear Static Procedure (NSP) and Nonlinear Dynamic Procedure (NDP). In the present study, only nonlinear time history analysis is done for the damage assessment of a case study building. Performance criteria of building for different seismic level has been shown in Fig 2.7.

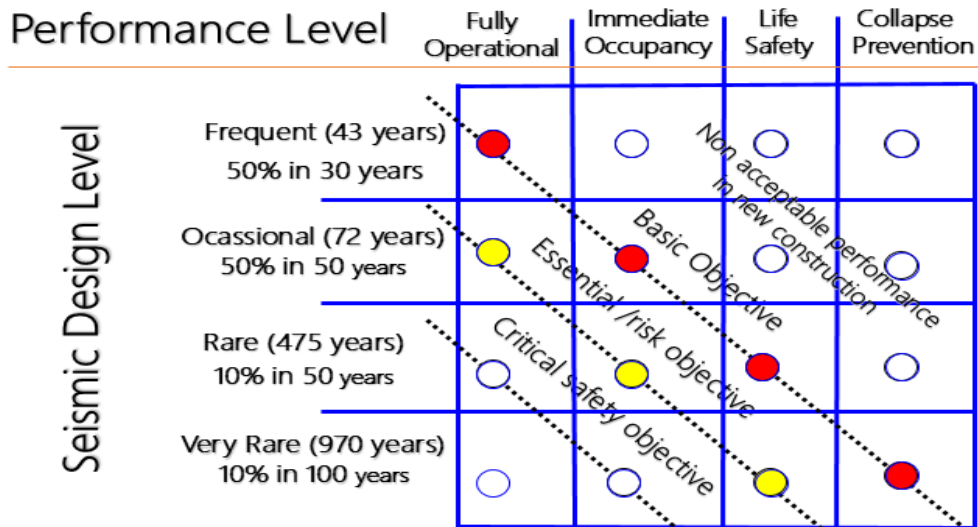


Fig 2.7: Structural performance criteria (Pekelnicky et al., 2012).

Target displacement and yield mechanism are the two design parameters that are required for calculation of seismic base shear up to specific hazard level and are directly linked with degree and distribution of structural damage, respectively (Goel et al., 2010). The whole structure is then pushed to a calculated target displacement to balance the work-energy principle (Zhang et al., 2017). Nonlinear analysis is then performed to design the frame elements and joints to attain the desired yield mechanism and behaviour. The described procedure is reasonably expedient for multistorey high-rise buildings (Wei and Qing-Ning, 2012). Recently PBSO has been a globally known methodology for advanced seismic design in the future.

2.6 Summary

Post-fire seismic assessment of any structure is becoming an essential nowadays. Competitive knowledge, skill and analysis requisitions are developing day by day. Several computer codes are currently available to perform this sort of analysis. The model used to describe the fire action must be carefully coupled with the mechanical model available, in order to obtain sound and realistic results. To simulate the actual behaviour of concrete structures exposed to fire the transient effects must be considered, by means of adequate calculation models and constitutive laws both for concrete and steel at elevated temperatures. Only the advanced calculation models that consider these features are able to output a rational, safe and cost-effective structural fire assessment. Moreover, structural

analysis also predict the performance of building. Numerous studies have focused on the seismic performance of RC structures. Performance based analysis over the force based design becomes notable development. Over the last few decades, various researchers and engineers have made significant contributions on the development of the PBD design process. This research provides a brief overview of PBD's progress. The key summury of this literature review are highlighted below.

- a. Damage assessment and thermal analysis for material properties following some features are able to output a rational, safe and cost-effective structural fire assessment.
- b. Within the performance-based design (PBD) paradigm, displacement-based design (DBD) is a viable design strategy. Researchers and engineers have made numerous efforts to broaden the applicability of PBD. A vast amount of regional data must be made available to accurately estimate the repair cost effective. There is a need for more research into improving repair processes and construction. Governmental agencies, practitioners, and researchers must all work together to address this issue.

CHAPTER 3

METHODOLOGY

3.1 Introduction

The study work was completed sequentially to reach the expected goals. The complete works were done in such a manner so that the experimental data could be used for finite element analysis. The damage states of different building components are determined using on-site visual inspection and some non-destructive and destructive testing for engineering judgment. Several on-site and laboratory-based techniques are available to aid in diagnosing the RCC building. Among them, the best way to know the compressive strength of concrete and the tensile strength of rebar is to collect concrete cores and rebar from buildings and test them in the laboratory. The UPV test estimates concrete strength based on the relationship between pulse velocity and compressive strength. Carbonation depth is found by spraying phenolphthalein indicator on a freshly broken/drilled surface.

3.2 Damage Evaluation Methods

Several documents describe existing techniques for the post-fire assessment of concrete structures. Many of these techniques are aimed at evaluating the residual strength of structures after a fire. Material testing and a site inspection are mandatory for evaluating the existing condition of any reinforced concrete structure. In this study, a series of destructive and non-destructive tests, such as the concrete core test, ultrasonic pulse velocity (UPV) test, carbonation depth test, and rebar tensile strength test, have been conducted to understand the properties of concrete and rebar. As a result, the following inspections and tests have been carried out:

- a) Visual Inspection
- b) Damage Classification
- c) UPV Test
- d) Carbonation Test
- e) Concrete Core test
- f) Rebar Tensile Strength Test

Visual inspection and non-destructive testing approaches are most suitable for a rapid inspection protocol since laboratory methods may take weeks to perform. On the other hand, laboratory methods may give a more accurate and thorough assessment of the residual capacity of the structure. The following flowchart (Fig 3.1) helps to delineate the whole study procedure.

3.3.1 Visual Inspection

A visual inspection has been performed on almost every part of the building. More emphasis and importance have been given to the seventh, eighth, and ninth floors affected by the fire. Initially, a site visit was conducted to assess the existing conditions, including all burnt furniture, mattresses, interior decoration, and debris from the ceiling that had fallen due to the fire-generated heat. The visiting team suggested cleaning the compartments for a more precise and in-depth picture of the fire so that an accurate inspection could be performed. Later, the fire-damaged areas of the building were inspected again.

3.3.2 Damage Classification

Based on the visual inspection, the fire-burned floor of the building has been subdivided into a 900x900 mm grid. This grid helps us to specify the damage location and intensity. The entire fire-damaged zone of the building structure, particularly the seventh to ninth floors, has been divided into six types based on the intensity of the damage. Damages to the zones and relevant structural components were classified based on the description mentioned in Table 3-1. Moreover, a damage intensity plan by color code has been prepared.

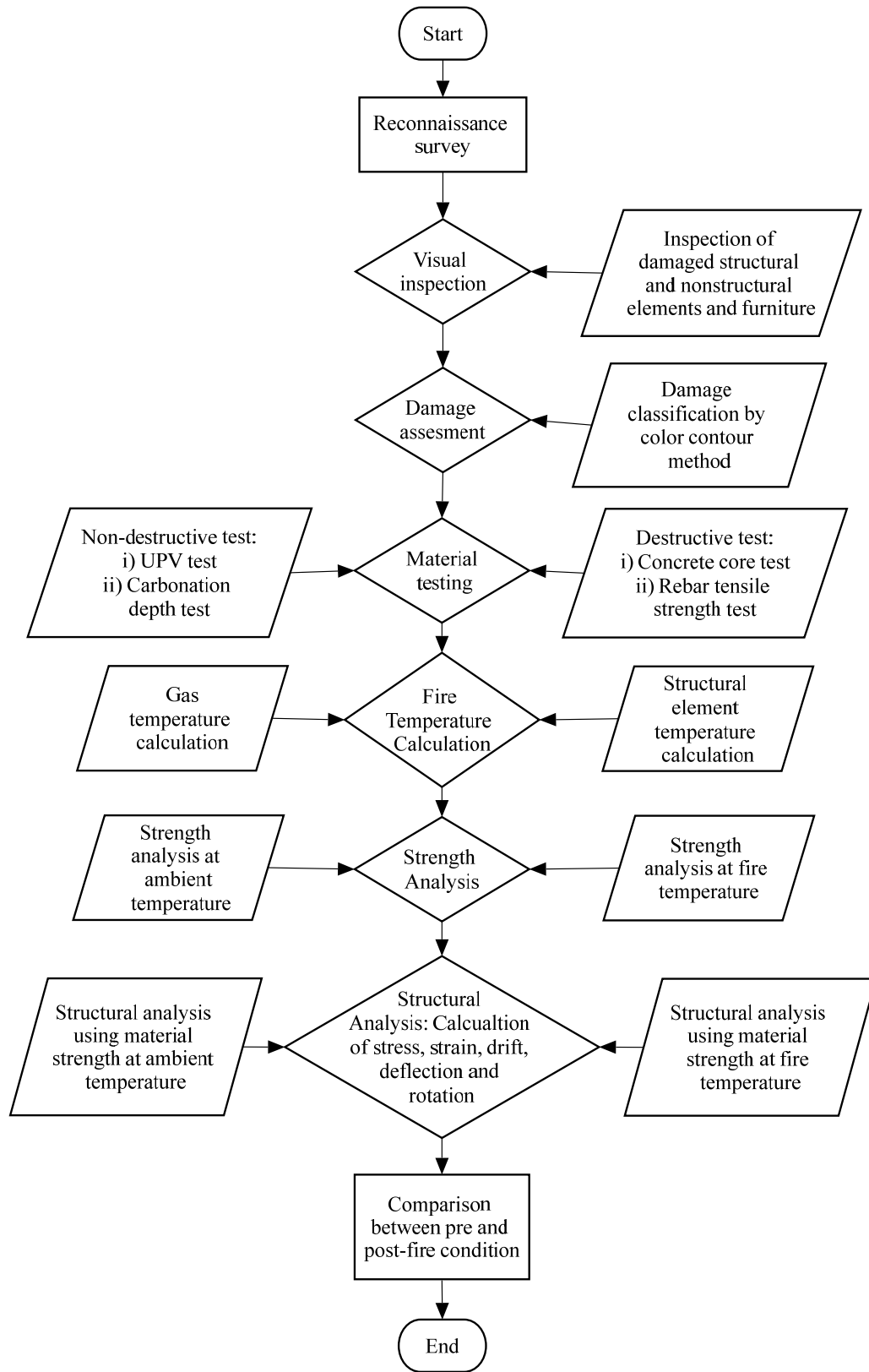


Fig 3.1: Flow chart for assessment of fire-damaged RC building.

Table 3-1: Post-fire Damage Ratings and descriptions (FIB 2008)

Sl No.	Damage Rating	Classification	Description
1	0	No visible damage	Floor not affected by fire. Equipment in that area remains in operational condition
2	1	Paint/cosmetic damage, spilling of surface coat	Characterized by powder deposits and discoloration. The patchy distribution of soot deposits. Permanent discoloration on surfaces
3	2	Technical damage, surface	Characterized by damage to surface treatments. The surfaces can be repaired using paints. Plastic-coated surfaces may need replacing or covering. Minor concrete spalling may remain or can be plastered
4	3	Structural and Non-structural damage at the surface	Characterized by some concrete cracking and spalling in the plaster of structural and non-structural member.
5	4	Structural damage, cross-section (interior)	Characterized by major concrete cracking and spalling and degraded plastics. Damage can be repaired on the existing structure in many cases. Within the class deformations of structures are also significant in that the load-bearing capacity is reduced
6	5	Structural and non-structural component damages	Classified as severely damaged structural members and components, structural cracking, and large deformations. Extensive concrete spalling, exposed/damaged reinforcement. Changes in material properties are expected after the fire.

3.3.3 Ultrasonic Pulse Velocity Test

The ultrasonic pulse velocity (UPV) method, as described in ASTM C597, is a non-destructive method used to determine the quality and integrity of concrete structures. It is performed by monitoring the transmission of elastic waves through concrete. An emitter transducer generates elastic waves in the concrete, which vibrate at their resonant frequency when short pulses of high-voltage electricity are sent. A receiver transducer detects these pulses placed nearby, and the time of transmission is determined by a device containing a timer connected to both transducers. From this, the pulse velocity, C , can be determined by the equation $C = L/t$, where L is the distance traveled and t is time. Three different

configurations of transducers can be used to perform a UPV test. This includes direct, semi-direct, and indirect (surface) transmission. The principle and method of wave transmission schematic of this system are shown in Fig 3.2.

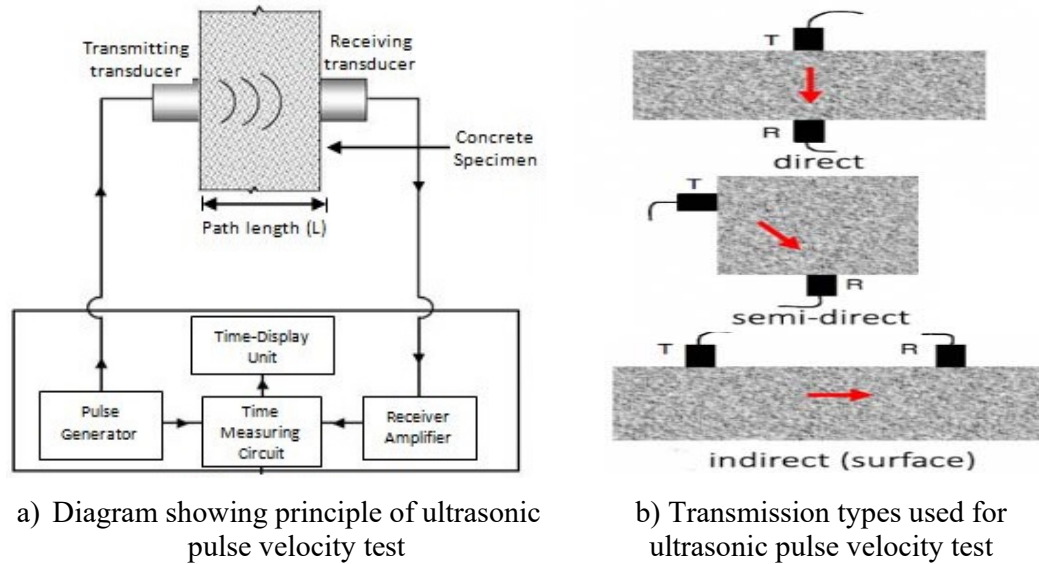


Fig 3.2: Principle and method of wave transmission used in UPV.

UPV test has been performed on the collected core sample of the column and slab. The direct wave transmission method has been used. A UPV test has been conducted on 18 concrete cores of columns and 13 cores of slabs. Two equations are proposed for the column and slab based on the concrete compressive strength data and UPV measured from the concrete core samples. Pictorial evidence of the concrete core UPV test has been shown in Fig 3.3.



Fig 3.3: UPV data collection from the concrete core sample.

3.3.4 Carbonation Depth Test

Carbonation testing is a method used to determine the level of carbon dioxide that has penetrated concrete. Carbon dioxide can react with the calcium hydroxide in concrete, causing a chemical reaction known as carbonation. This reaction can weaken the concrete and reduce its structural integrity.

There are several methods for testing carbonation in concrete, including the rebar corrosion method, the pH method, and the surface carbonation method. The carbonation test was performed by drilling a hole in the concrete surface to a different depth. The dust was removed by brush, and air was blown to clean the hole. The 0.2% phenolphthalein solution was injected with a physician's injection syringe or needle and sprayed on freshly drilled or broken concrete, and the color change was observed. The depth of the uncolored layer (carbonated layer) was measured from the external surface at 4 to 8 positions. A measured, uncolored distance indicates the depth of carbonation. The depth of concrete carbonation is estimated by the change in color profile and the degree of carbonation that can be measured in millimeters (Fig 3.4).

Carbonation depth tests were conducted on-site at various locations. A total of 29 carbonation tests were done on the seventh-floor roof, whereas 29 and 23 tests were done on the eighth and ninth floors, respectively.



a) Surface preparation for indicator spray b) Measurement of carbonation depth

Fig 3.4: Onsite carbonation test and depth measurement.

Carbonation depths of 20 nos. (3 nos. for the seventh-floor roof, 9 nos. for the eighth-floor roof, and 8 nos. for the ninth-floor roof) in periphery beam and 66 nos. (30 nos. for the seventh floor, 13 nos. for the eighth floor, and 23 nos. for the ninth floor) in the column were also measured in the fire affected floor.

3.3.5 Concrete Core Test

A concrete core test is the most reliable way to determine the compressive strength of concrete. In this study, the existing strength of the concrete was obtained through compression tests. The core sample is collected from the structural components of the building using a core cutter following the ASTM C42 standard. Fig 3.5 depicts pictorial evidence of core sample collection and sample preparation.

The collection point for core samples was selected after a visual inspection of the fire-damaged structures. The fire-affected and unaffected column sections were selected for core collection, considering the minimum disturbance of the existing structure. Since the column and shear wall are the key structural components of the building's stability, 23 core samples were collected from the seventh, eighth, and ninth-floor columns and shear walls.



a) Collection of concrete core samples

b) Extracted concrete core sample for column (designation: D3/E1, 7th floor)

Fig 3.5: Concrete Core Test, sample collection and preparation.

Many concrete core samples have also been collected from the seventh, eighth, and ninth roof slabs. Since visual inspection revealed that the seventh-floor roof slab had been damaged more severely than others, more samples were collected from there. The structures have only perimeter beams, i.e., no interior beams. A few core samples were also collected from the seventh and eighth-floor roof beams. The core samples have been collected carefully by avoiding reinforcement. The grid location is also mentioned in each sample so that the corresponding core can be identified straightforwardly. The concrete core test result of the beam and slab for fire unaffected and affected conditions has been presented in Table 4-5 to Table 4-8, respectively. Finally, the equivalent compressive strength of the concrete core has been calculated following the ACI 562 and is presented in Table 4-5 to Table 4-8.

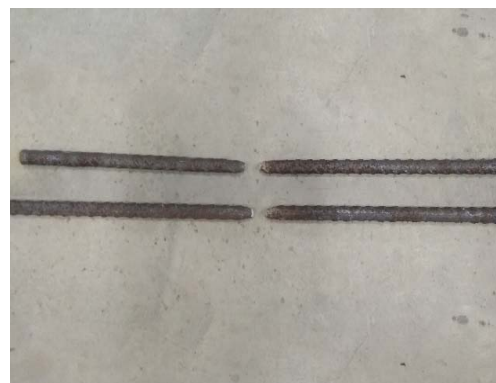
3.3.6 Rebar Tensile Strength Test

Rebar tensile strength testing is a method used to determine the tensile strength of reinforcing steel (rebar) used in concrete structures. Rebar is used to reinforce concrete, and its tensile strength is an essential factor in the overall strength and stability of the concrete structure.

There are several methods for testing the tensile strength of rebar, including the traditional tensile test, the bend test, and the torsion test. The tensile strength test is a procedure to determine rebar strength. Rebar samples were collected with great precaution from the existing structure. The sample is tested in the laboratory following the procedure and standard as described in ASTM A1034. Pictorial evidence of the rebar testing setup and sample has been shown in Fig 3.6.



a) Rebar tensile strength test setup



b) Rebar sample after breaking.

Fig 3.6: Rebar tensile strength test.

3.3 FEM Analysis Methods

The Finite Element Method (FEM) is a numerical method used to analyze and solve problems involving complex systems of interconnected components. In the context of a fire-damaged building, the FEM can be used to analyze the structural response of the building affected by the fire. Moreover, the determination of the extent of damage to the building's components can be done. This section presents the numerical models of the building for undamaged and damaged conditions. The RC buildings were modeled with the intent of evaluating the performance of the building for different seismic forces. FEM analysis has been performed in fire stress and seismic response analysis described below.

3.4.1 Fire Analysis by FEM

Information about the fire event is usually minimal. There is significant uncertainty about the fire as there is virtually no information about the considered apartment fire. Expert judgment and observation were not possible due to the apartment being inaccessible. Hence, the FEM model is needed in all generality to estimate fire development. The selection fire model for an analysis of the specific situation depends on some factors, i.e., the building layout, the type and distribution of fire load, and the observations reported by witnesses and the fire brigade. In this case, the fire was contained in a surface area of 400 m². Commercial building areas with fire load (80% fractile characteristic fire load of 948 MJ/m² following Eurocode) and firefighter observations indicate post-flashover compartment fire. A parametric compartment fire curve has been generated. Consequently, it was chosen to use the OZone software to model the fire (Cadorin and Franssen, 2003; and Cadorin et al., 2003) based on the resolution of mass and energy conservation equations. Considering parametric fire exposure and due to the level of complexity in the fire-response of common structures, advanced calculation methods such as numerical modeling has been used for analyzing the temperature distribution in the concrete sections (Column, beam, and slab). The concrete sections (Column, beam, and slab) were analyzed using the finite element analysis software FIN EC. Based on the fire-parametric curve, Wickstrom's method (Wickström, 1986), has been used to determine the temperature of rebars. Accordingly the temperature in rebars, T_{bar} , is given as:

$$T_{\text{bar}} = [\eta_w(\eta_x + \eta_y - \eta_x \eta_y) + \eta_x \eta_y] T_f \quad \text{Equation 3-1}$$

η_x , η_y and η_w are calculated as:

$$\eta_w = 1 - 0.616 t_h^{-0.88} \quad \text{Equation 3-2}$$

$$\eta_x = 0.18 \ln\left[\frac{t_h}{x^2}\right] - 0.81; \eta_y = 0.18 \ln\left[\frac{t_h}{y^2}\right] - 0.81 \quad \text{Equation 3-3}$$

where, T_f is the fire temperature, t_h is the time (h), and x and y are the depth of rebar from the surface in x and y direction, respectively.

This calculated temperature helps us to determine the strength loss of fire-heated concrete and rebar. Strength loss correlation has been used to estimate concrete and rebar residual strength.

3.4.2 Structural Analysis by FEM

To determine the parameters of the fire state, several finite element analyses of the sections were conducted using various layers of damaged and undamaged concrete material properties. Properties of typical damage classes, strengths, stiffness, and ductility were provided for a quick elastic analysis of the entire structure. To see the structure's original state and its undamaged structural performance under specified loading circumstances, structural design software created a 3D finite element model of the structure. Another 3D structural model was made using the loading data, damaged material, section parameters, and actual damaged state material properties to examine the structure's response to post-fire conditions. In the model, the mechanical and geometrical damage that occurred due to fire event has been considered and modeled for more accurate analysis.

The as-built drawing is prepared by the information collected from the building owner and site visits. The core strength collected from damaged and non-damaged portions is used to calculate equivalent concrete strength by ACI 562. Based on as-built drawings using equivalent core results, 3D analysis models have been prepared in ETABS for various earthquakes (MCE, DBE, and SLE) in pre- and post-fire conditions. In this case, the elastic properties of materials are used. The development of finite element models follows the static linear analysis for different earthquake conditions. Besides, BNBC (2020) has been used to select load cases and combinations during design. From the analysis and design, the

results obtained for different earthquakes (MCE, DBE, and SLE) in pre- and post-fire conditions, such as deflection, drift, stiffness, and the demand capacity ratio of columns, are compared. The causes of the change in pre- and post-fire conditions are described.

An as-built design has been used to develop 3D finite element models for various seismic scenarios in pre- and post-fire conditions. Concrete and rebar's nonlinear characteristics are applied in this study. The kinematic hysteretic type has been selected for rebar nonlinearity with a park parametric stress-strain curve. In contrast, the concrete hysteretic type with a mander stress-strain curve has been selected for concrete. There is a hierarchy of four levels of structural analysis appropriate for the evaluation of existing buildings (Charleston, 1997). Each higher level procedure provides a more accurate model of the actual performance of a building subjected to earthquake loads, but requires greater effort in terms of data preparation time and computational effort. The two most basic procedures, the Linear Static Procedure (LSP) and the Linear Dynamic Procedure (LDP), are mainly suitable for buildings which respond primarily in the elastic range. The Nonlinear Static Procedure (NSP) can evaluate buildings loaded beyond the elastic range but does not fully capture the response of dynamics, especially higher mode effects. The Nonlinear Dynamic Procedure (NDP) is the most complete form of analysis, modeling both dynamic effects and inelastic response. Ten well-known GMs have been chosen for analysis. The ground motions are correlated with the reaction spectrum of several earthquake circumstances, including MCE, DBE, and SLE. Deformation-controlled (ductile) type nonlinear hinges are assigned in beams and columns on both ends. Auto fiber nonlinear hinges are assigned in shear walls. Priority is given to performance-based nonlinear time history (NLTH) analysis. With the outcomes of the analysis, a comparative graph has been drawn. Under pre- and post-fire conditions, the building's performance is evaluated for various GMs with varying seismic intensities. The building's base shear, drift, and drift ratio are investigated. The rebar and concrete in the fire-damaged floors were measured for maximum and comparative stress-strain values for different hinges. It has been determined whether the strain caused by the stress is within the building code's permissible range. When the permitted maximum is exceeded, the cause is described. Additionally, moment rotation and fiber stress-strain states of beams, columns, and wall hinges have been examined at various ground movements. In NLTHA, the causes of the differences between pre- and post-fire situations are discussed.

3.4.3 Summary

In this chapter, damage evaluation and finite element analysis methods of a fire damaged RC structure have been discussed elaborately. For damage evaluation visual inspection, damage classification, ultrasonic pulse velocity and carbonation test, concrete core and rebar test has been described. Thermal as well as structural analysis software has been used to determine the thermal stress and structural response. Finite Element helps to predict the force, displacement, stress, strain behavior of the RC structure under static linear analysis and dynamic time history considering both geometric nonlinearities. The development of finite element model, regular loading, static analysis procedures, time history ground motion data are presented. In case of finite element structural analysis prior to fire damage, material property of fire undamaged condition has been used. To determine the response of fire effect, fire damaged material property has been used. The proposed methodology starts from the observation of a fire event and the collection of data and goes through the different steps up to the estimation of the maximum seismic response of structural elements.

CHAPTER 4

DAMAGE ASSESSMENT AND FIRE ANALYSIS

4.1 Introduction

The assessment of the post-fire condition of the structure was the on-site inspection, including collecting data and information about the event. The preliminary purpose of the site inspections was to assess the fire severity. This assessment can be done based on expert judgment, on-site visual tests (e.g., color change of the concrete), non-destructive and destructive tests, models (e.g., numerical models), or a combination of these. In general, visual observations of the structural and non-structural damage resulting from the fire also inform about the fire severity.

4.2 Fire Information

The building is a reinforced concrete 23-storied commercial building with two (02) basements, as shown in Fig 4.1.



a) Source: The Daily Star (March 28, 2019)

b) Source: bdnews24.com (March 29, 2019)

Fig 4.1: General view of the building under fire.

The fire broke out at FR Tower around 12:52 pm on Thursday, March 28, 2019. It was reported in the newspaper that the fire at the FR tower originated from an electric short circuit from the eighth floor of the building and exploded on the adjacent floors. Twenty-one firefighting units of the Dhaka Fire Service and Civil Defence brought the fire under control around 4:45 pm (Dhaka Time). This accident was nearly a five-hour fire incident that caused a massive loss of properties and expensive lives. It caused about 25 deaths, and more than 70 others were injured. It was observed that the seventh, eighth, and ninth floors had been severely damaged with concrete cracking and spalling and excessive bending of steel reinforcement. All utility facilities, such as machinery and set-ups for heating, ventilation, air conditioning (HVAC), and lifts, become non-functional and devastated due to severe fire-induced burning and temperature. Two local broadcasting channels named, Duronto TV and Radio Today, were bound to shut down their transmission when the fire broke out because both offices were situated adjacent to the affected building.

The fire was initiated on the eighth floor of this commercial building, as reported in the newspaper. It is suspected that the fire originated from an electric short circuit. It started to spread ninth and seventh floors of the building. After the fire roll out, the whole building has become a deep sea of smoke, as shown in Fig 4.2.



a) Source: The daily star (31st March 2019)



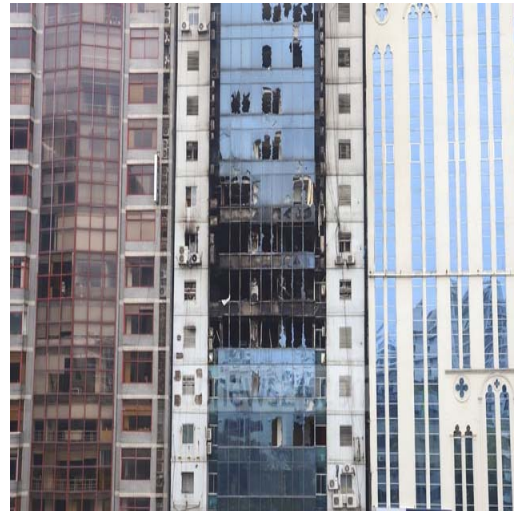
b) Source: ALJAZEERA (31st March 2019)

Fig 4.2: Rescuing operation during the fire incident.

The lift core and stairs have become a well of smoke during the fire. The external and internal fire-damaged views have been shown in Fig 4.3 & Fig 4.4, respectively. The glass of the periphery wall was heated, cracked, and gone to pieces for fire intensity. Fig 4.4 highlighted the condition of the building even before cleaning burned debris inside the compartments, the development of cracks, and burning of the structural and non-structural components.

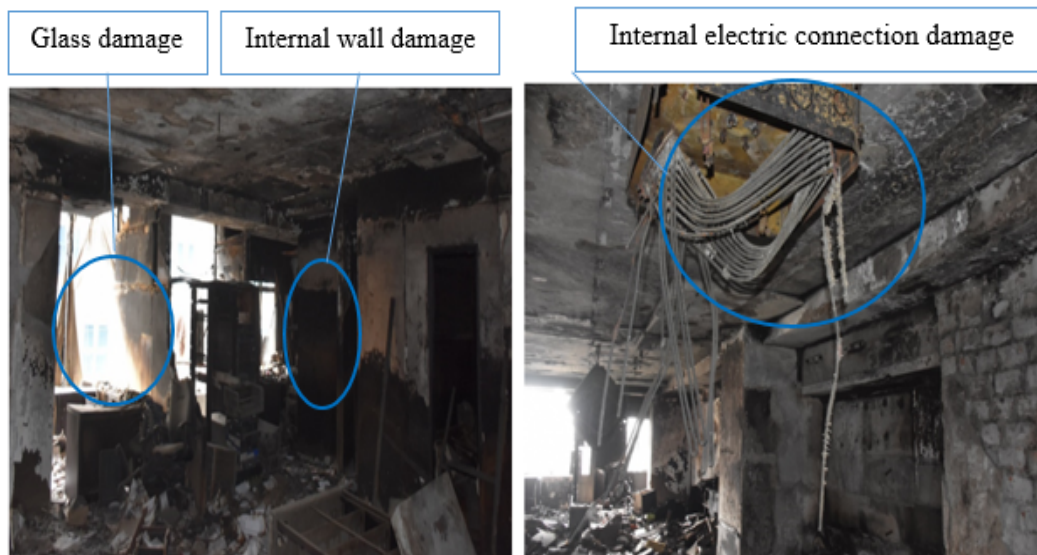


a) Source: The Daily Star (March 31, 2019)



a) Source: bdnews24.com (30st March, 2019)

Fig 4.3: The external appearance of the building after the fire.



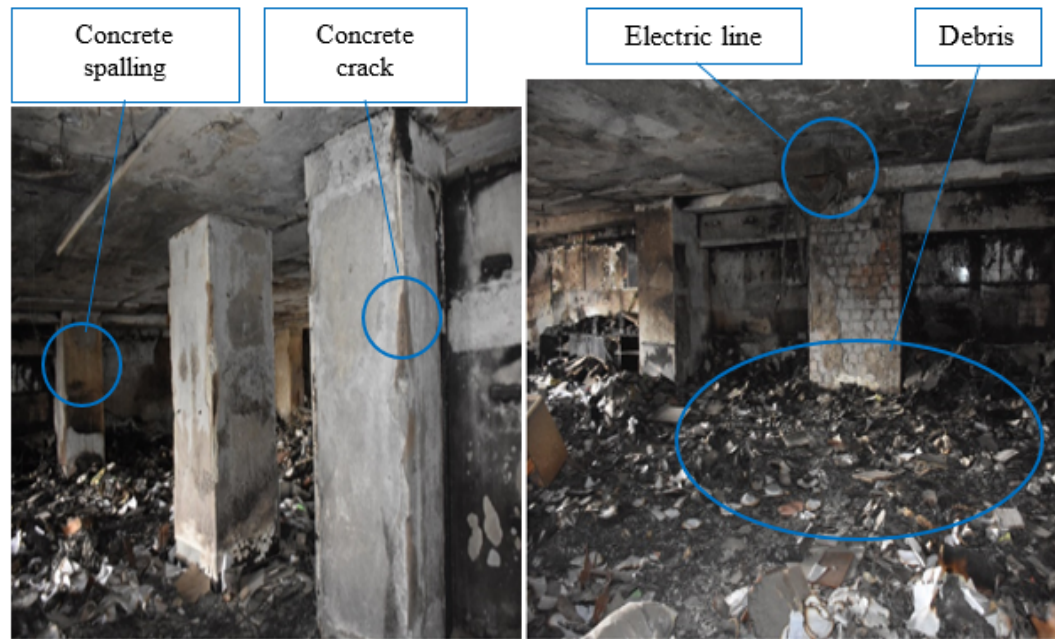
a) Damage to the internal wall and peripheral glass partition on the 7th Floor (Grid-D/3,4)

b) Damage to the internal electric connection on the 7th Floor (Grid-A, B, C/1)



c) Plaster removal in front of the stair on the 8th Floor (Grid-B,C/3,4)

d) Damage to internal furniture in front of the toilet zone on the 8th Floor (Grid-C, D/4)



e) Some concrete cracking and spalling on the 9th Floor (Grid-B, C, D/2)

f) Damage to the electric line, debris of partition, concrete cracking, and spalling on the 9th Floor (Grid-C, D/4)

Fig 4.4: Floor damages inside the building.

4.3 Fire Damages to the Structural and Non-structural Components

There are a few critical concerns in determining the damages caused by the fire on RC structures. Those points may be categorized as a) the deformation of structural components as well as the global structure with significant distress, movement, and settlement, b) the effect of heat inside the concrete; depth of damage or loss of strength and integrity of the concrete, c) Strength reduction of the reinforcing bars or embedded structural steel elements. Based on the above points, damage to several nonstructural elements at different temperature ranges has been shown in Table 4-1.

Table 4-1: Effect of temperature on common materials (Concrete Society, 2008)

Substance	Typical example	Conditions	Approximate temperature °C
Paint		Deteriorates Destroyed	100 150
Polystyrene	Thin-wall food container foam, light shades, handles, curtain hooks, radio casings	Collapse Softens Melts and flows	120 120-140 150-180
Polyethylene	Bags, films, bottles, buckets, pipes	Shrivels Softens and melts	120 120-140
Polymethylmethacrylate	Handles, covers, skylights, glazing	Softens Bubbles	130-200 250
PVC	Cables, pipes, ducts, linings, profiles, handles, knobs, house ware, toys, and bottles (Values depend on the length of exposure to temperature)	Degrades Fumes Browns Charring	100 150 200 400-500
Cellulose	Wood, paper, cotton	Darkens	200-300
Wood		Ignites	240
Solder lead	Plumber joints, plumbing, sanitary installations, toys	Melts	250 300-350

Substance	Typical example	Conditions	Approximate temperature °C
		Melts, sharp edges rounded Drop formation	350-400
Zinc	Sanitary installations, gutters, down pipes	Drop formation Melts	400 420
Aluminum and alloys	Fixtures, brackets, small mechanical parts	Softens Melts Drop formation	400 600 650
Glass	Glazing, bottles	Softens, sharp edges rounded Flowing easily, viscous	500-600 800
Silver	Jewelry, spoons, cutlery	Melts Drop formation	900 950
Brass	Locks, traps, door handles, clasps	Melts (particularly edges) Drop formation	900-1000 950-1050
Bronze	Windows, fittings, doorbells, ornamentation	Edges rounded Drop formation	900 900-1000
Copper	Wiring, cables, ornaments	Melts	1000-1100
Cast Iron	Radiators, pipes	Melts Drop formation	1100-1200 1150-1250

The location, melting condition, and charred materials for both structural and non-structural elements provide evidence of damages caused by the fire. Table 4-1 shows the effect of temperature on different building materials and their corresponding temperature. After the fire, photographic evidence was taken from the building site, as shown in Fig 4.4.

There is some technic to estimate the fire temperature. Table 4-1 is a guideline to evaluate the fire temperature level by assessing both structural and non-structural damage. This study investigates a multi-used high-rise commercial building. The offices' interior decoration was burnt due to the fire exposure. The columns, beams, and slabs have been burned and deformed due to the fire. The observed damage (as shown in Fig 4.5) to the interior elements indicates high temperature. It is a matter of concern for all stakeholders about the strength of the concrete and steel.

Damages caused by the fire on different structural and non-structural components were similar. The amount and patterns of damage depend on the heating time, fire load, lining materials of the surface, ventilation type, loading conditions, evacuation plan, and active and passive fire resistance systems. Damage assessments of structural components such as columns, shear walls, beams, and floors are critically important for a structure's stability. However, the degradation of the strength and integrity of concrete and the reduction of the cross-sectional area due to spalling at the elevated temperature result in diminishing both vertical and lateral load-bearing capacity.



a) The column on the 7th floor (Grid: D/3)

b) Slab at 7th floor roof (Grid: B1/9-9, B2/1-9)

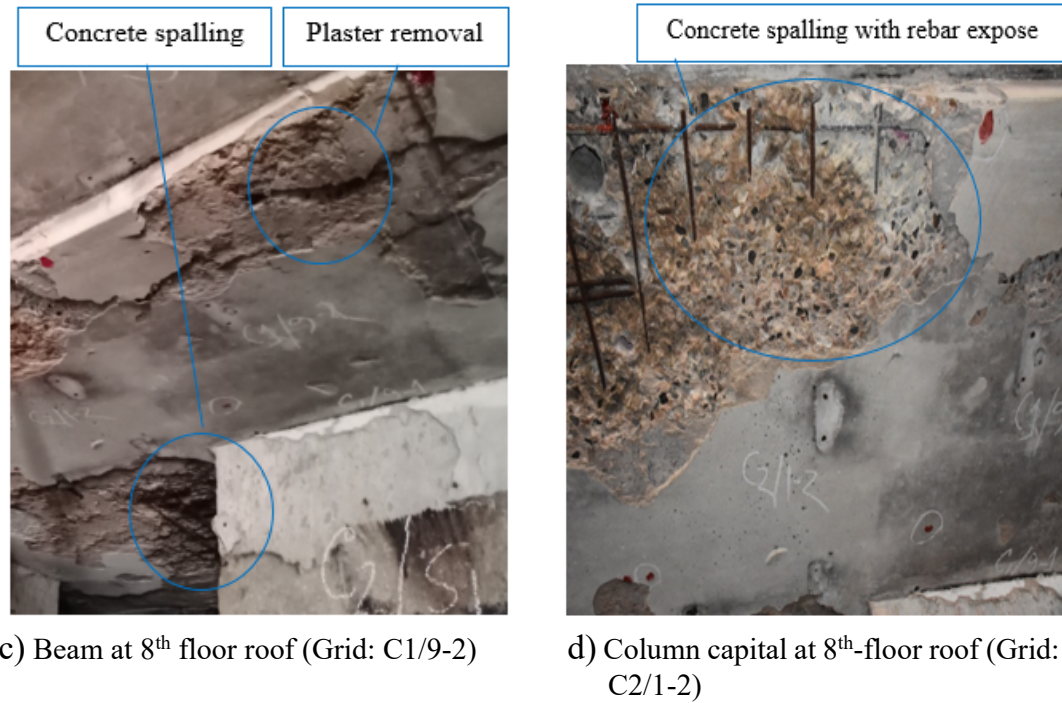


Fig 4.5: Some pictorial evidence of structural concrete damage.

Due to the fire, the bonding between the concrete and the reinforcement has been weakened significantly. The concrete cover has fallen from the surface of the roof slab and column capital, as shown in Fig 4.5. Therefore, the reinforcement of column capitals is visible.

4.4 Damage Classification

To determine the intensity of fire at different zones of the floor, the entire fire-burnt area of the building structure, particularly the seventh to the ninth-floor roof, has been classified into six types based on the intensity of the damage. The column, beam & roof slab of the seventh, eighth and ninth floor has been subdivided into finite sizes of 900mm X 900mm (Fig 4.6) grid. The subdivided grid system helps the stakeholders understand the damages' location (Fig 4.7) and their corresponding intensity. As a result, post-fire potential retrofitting or strengthening plans can be developed accordingly.

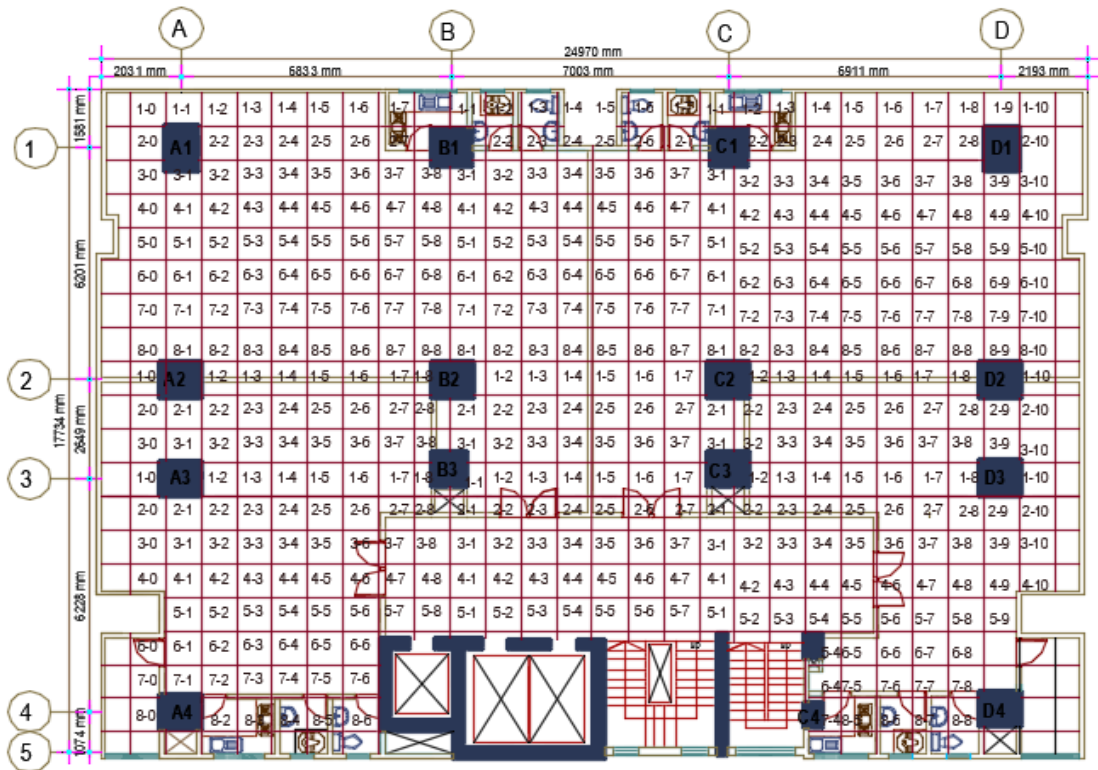


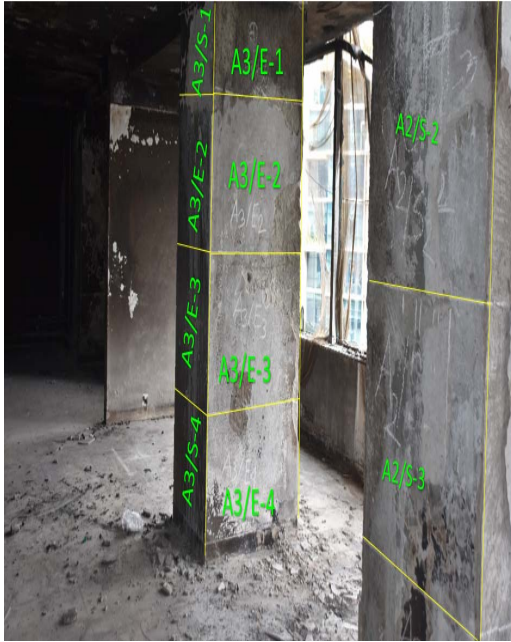
Fig 4.6: Typical floor subdivided into 900 mm X 900 mm grid.



a) 900 mm X 900 mm subdivision at the 7th floor roof slab (Grid-A, B/1,2)



b) 900 mm X 900 mm subdivision at 8th floor roof slab (Grid-1,2/A, B,C)



c) 900 mm X 900 mm subdivision at 7th floor column (Grid-A/2; A/3)

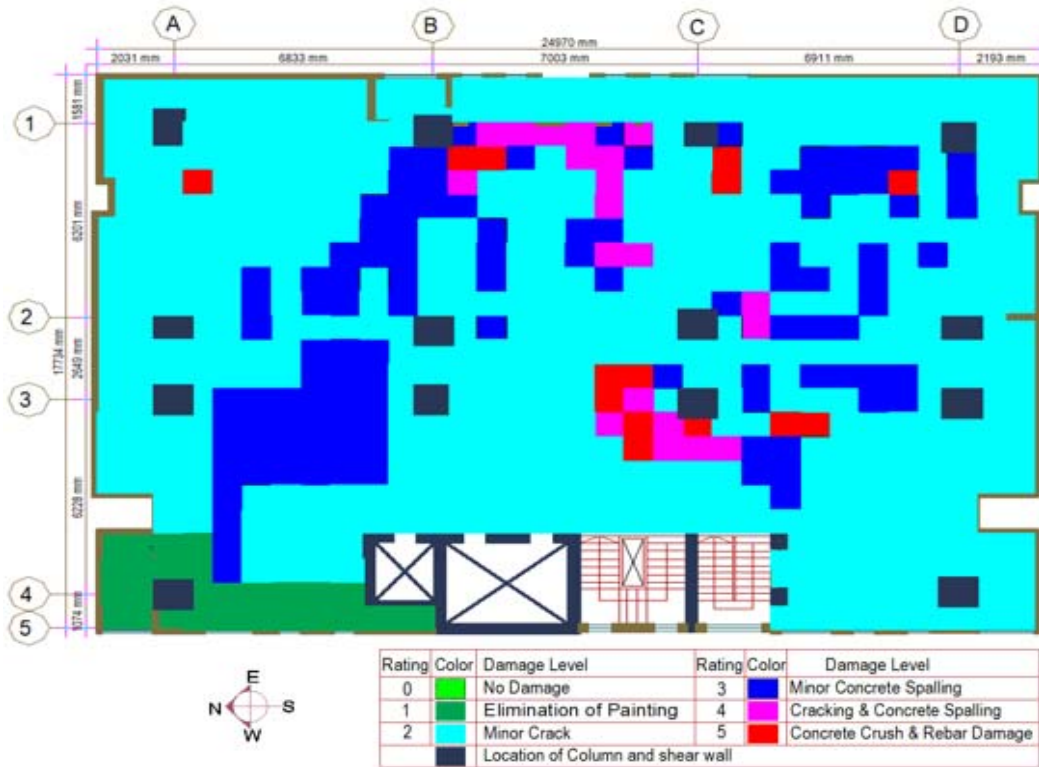


d) 900 mm X 900 mm subdivision at the 7th floor column (Grid-C/2)

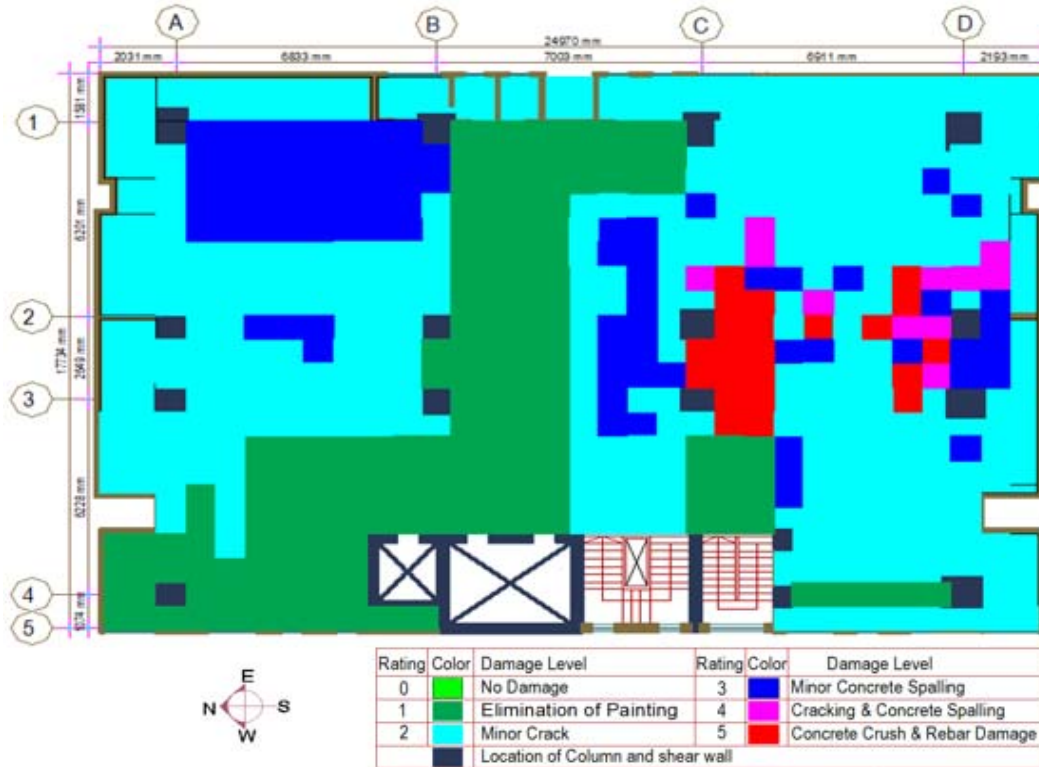
Fig 4.7: Column and slab subdivided into 900mm X 900mm.

Based on the existing condition of the fire-damaged floors, the damage intensity of different zone is presented on the floor layout plan using different colors, as shown in Fig 4.8. Color code indicates the severity or intensity of damage that started from no damage to severe damage based on cracking to concrete spalling and rebar damage.

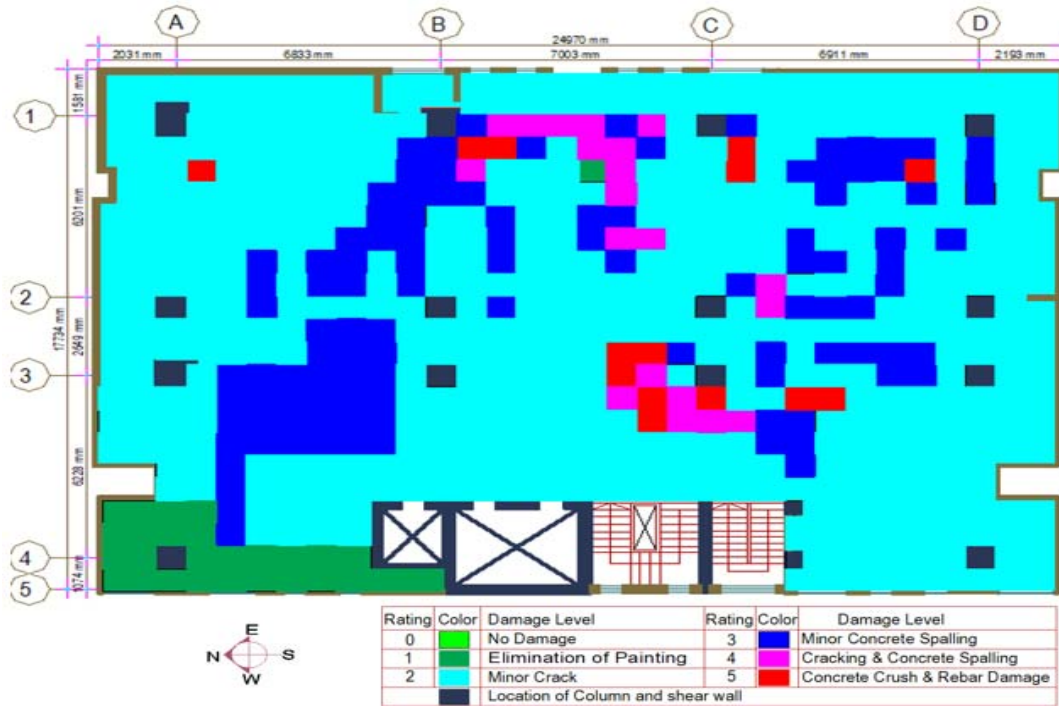
Classification has been made on the damage of the zones and relevant structural components based on the description mentioned in Table 3-1. The damage intensity shows that the entire area of the floors is affected by the fire as there is no zero damage zone. The damage intensity contour shows that nearly 72% of the seventh-floor roof, 80% of the eighth-floor roof, and 75% of the ninth-floor roof have burnt moderately (damage rating 0 to 2)(Table 4-2). It shows at least minor cracks on different structural and non-structural components. The damage intensity contour also shows that nearly 28% of the seventh-floor roof, 20% of the eighth-floor roof, and 25% of the ninth-floor roof are damaged at different intensities (damage rating 3 to 5) (Table 4-2) for both structural and non-structural components. Moreover, severe damages on the structural components have been observed at 5% on the seventh and ninth-floor roofs. The eighth-floor roof, which is the place of fire initiation, has been 8% severely damaged.



a) Damage intensity layout for the 7th floor roof



b) Damage intensity layout for the 8th floor roof



c) Damage intensity layout for the 9th floor roof

Fig 4.8: Damage Intensity layout with color code.

.Table 4-2: Summary of visual inspection

Parameters	7 th Floor	8 th Floor	9 th Floor	Remarks
Visual Inspection Burning	Moderate	Minor	Moderate	
Minor crack to moderate (Damage rating 0-2)	72	80	75	More green area
Concrete spalling to rebar expose (Damage Rating 3-5)	28	20	25	Blue to Red

4.5 Evaluation of the Material Properties

After a fire, the properties of the building materials, such as concrete and steel, can be affected, which may lead to reduced strength and stiffness. In concrete, fire can cause spalling, cracking, and loss of compressive strength. In steel, it can cause loss of yield strength, change in ductility, and buckling instability. Therefore, it is crucial to determine the damage's extent and evaluate the materials' remaining properties. This study has

conducted a series of destructive and non-destructive tests such as ultrasonic pulse velocity (UPV), carbonation depth, concrete core, and rebar tensile strength tests to understand the properties of concrete and rebar for pre and post-fire conditions.

4.5.1 Ultrasonic Pulse Velocity Test

The ultrasonic pulse velocity (UPV) is a non-destructive testing method that uses high-frequency sound waves to determine concrete materials' elastic properties and integrity, as described in ASTM C597. It measures the velocity of the waves passing through the concrete.

Based on the concrete compressive strength and UPV test data measured from the concrete core samples of the column and slab section, a regression equation has been proposed, as shown in Fig 4.9. The proposed equation may help predict the compressive strength of existing column and slab sections without conducting further harmful drilling into the column. The result shows a linear correlation between the core strength and UPV test data. The coefficient of determination is 0.5056 for the column and 0.0345 for the slab, which is reasonably good for the compressive strength of these fire-burnt concrete cores.

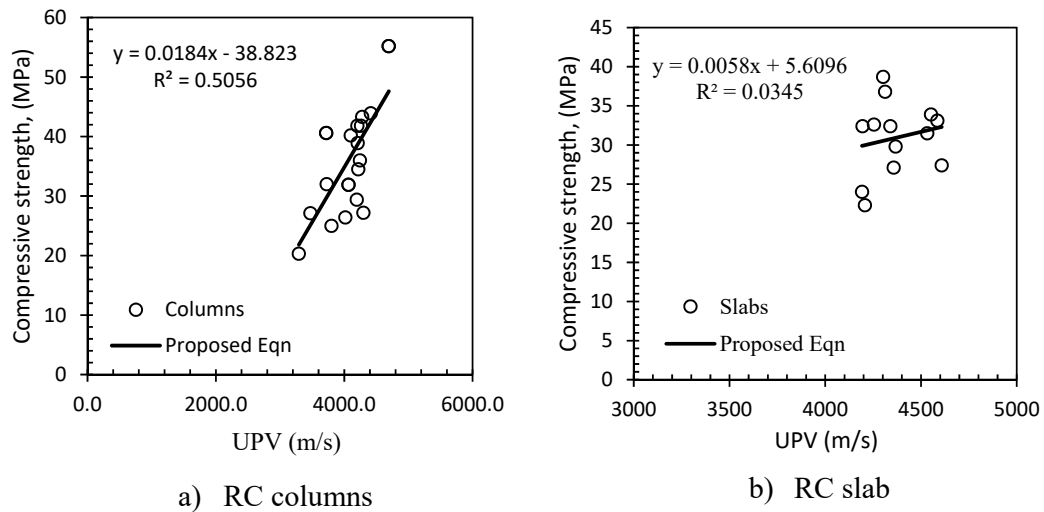


Fig 4.9: Compressive strength vs. ultrasonic pulse velocity plot for RC columns and slab.



4.5.2 Depth of Carbonation Test

The carbonation test is a quick, simple method that can approximate the depth of damage in a concrete member. As concrete is heated, several reversible and irreversible chemical reactions can produce a notable temperature. It is the procedure in which CO₂ from the air penetrates the concrete, which is responsible for corrosion in reinforcement. The presence of moisture content helps carbon dioxide to dilute into carbonic acid, reducing the alkalinity of concrete. Phenolphthalein solution is used as an indicator sprayed on the broken concrete surface. In the presence of alkaline concrete, the phenolphthalein indicator shows pink color. Colorless surfaces indicate the presence of acidity that is highly susceptible to rebar corrosion.

Carbonation depth tests have been conducted on-site at various locations. From the seventh-floor roof slab, 29 carbonation depths have been measured. The carbonation depths varied in a range of 13 mm to 35 mm. A total of 29 carbonation tests were done at the eighth-floor roof slab, and the depth found ranged between 5 mm and 30 mm. Finally, from the ninth-floor roof slab, 23 carbonation test has executed, and carbonation depths varied between 5 mm to 33 mm.

Carbonation depths for beams of 20 locations have also been measured. Carbonation depths are found as 20 – 31 mm, 5 – 27 mm, and 7 – 17 mm for the seventh, eighth, and ninth-floor roof beams, respectively. Moreover, 66 nos. carbonation tests have been performed from the seventh, eighth, and ninth-floor columns. Carbonation depths varied between 10 mm to 29 mm for the seventh floor, 7 mm to 19 mm for the eighth floor, and 10 mm to 38 mm for the ninth-floor columns, respectively. Based on the carbonation depths, it is evident that the seventh and ninth-floor columns have been affected by fire more than the eighth floor. The testing result with location and an overall summary of carbonation depths has shown in Table 4-3 & Table 4-4 respectively.

Table 4-3: Location & Picture of Carbonation for column shear wall and slab

Sl No.	Sample Id Mark	Carbonation Depth (mm)	Pictures
01	Column: B2/N1 -9 th Floor	21	
02	Column: A2/S2-7 th Floor	25	
03	Column: A3/E1 -7 th Floor	23	




Sl No.	Sample Id Mark	Carbonation Depth (mm)	Pictures
04	Core-A2/3-5 (Slab)- 7 th Floor	24	
05	Core-SW2 (Shear Wall)-8 th Floor	16	
06	Core-3A Front (SW)- 9 th Floor	18	

Table 4-4: Summary of inspection and test results

Parameters		7 th Floor	8 th Floor	9 th Floor	Remarks
Carbonation Test Depth (mm)	Floor Slab	13- 35	5-30	5-33	Maximum carbonation depth is 38mm
	Column	10-29	7-19	10-38	
Average(mm)		21.75	15.25	21.5	
Standard Deviation		12.14	11.61	16.42	

4.5.3 Concrete Core Test

It is known that the compressive strength of the concrete not only varies with temperature but also changes with other factors, including the rate of heating, duration of the fire, loading status of the element, type of aggregate, and water/cement ratio. However, it is necessary to obtain the resultant compressive strength of the concrete to determine the level of damage and take the required precautions for structural stability. A concrete core test is the most reliable way to determine the compressive strength of concrete. In this study, the strength values of the damaged concrete were obtained through compression tests. The core sample is collected from the structural components of the existing building using a core cutter. Pictorial evidence of core sample collection and sample preparation has been shown in Fig 3.5. Since water is applied at the time of core cutting, about five days waiting period is intended to reduce the effect of moisture gradients used during core drilling. The standard procedure for extracting and testing concrete core samples has been followed as described in ASTM C42.

Locations of core were selected after visual inspection of the fire-damaged structures. The fire-affected & unaffected column sections were selected for core collection considering the minimum disturbance of the existing structure. Since the column and shear wall is the key structural component of the building's stability, 23 core samples were collected from the seventh, eighth, and ninth-floor column and shear wall. The equivalent compressive strength of concrete has been calculated following the ACI 562 & the result of fire-unaffected column sections is presented in Table 4-5. The results show that the equivalent compressive strength of the concrete cores collected from fire-unaffected columns is 36.62 MPa for all three floors, which meets the design strength of 29 MPa.

Moreover, the core test result of fire-affected column sections is presented in Table 4-6. The results show that the equivalent compressive strength of the concrete cores collected from fire-affected columns is 24.46 MPa which doesn't meet the design strength of the column as 29 MPa. Core samples of . 9 and 10 nos. have been collected from the fire-undamaged and damaged beam slab, respectively. The variation of concrete may occur due to the uneven burning or heating of different column sections, and hence mechanical strength of the concrete core changes in different areas. The equivalent concrete

compressive strength for the beam slab of fire unaffected and affected condition is 30.33 MPa and 23.501 MPa respectively whereas the design strength for beam slab was 24 MPa.

Table 4-5: Fire Unaffected Column/Shear wall Concrete Equivalent Comp. Strength as per ACI 562

Sl. No	Location	Length (l) (mm)	Diameter (d) (mm)	Correction Factor for diameter, F_{dia}	Core Compressive Strength, f_{core} (MPa)	Corrected Core Strength, $f_{cc} = f_{core} \times \frac{F_{dia}}{F_{dia}}$
1	Core-1 (A3/S3-8F)	134.62	67.06	1.03	41.3	42.539
2	Core-2(B2/W1-8F)	134.62	67.06	1.03	39.5	40.685
3	Core-3 (A2/S2-9F)	134.62	67.06	1.03	41	42.23
4	Core-4 (A3/E1-9F)	134.62	67.06	1.03	43	44.29
5	Core-5 (B3/N1-9F)	134.62	67.06	1.03	42.5	43.775
6	Core-6 (D3/N1-9F)	134.62	67.06	1.03	39.8	40.994
7	Core-7 (D4/E2-9F)	134.62	67.06	1.03	54.1	55.723

Equivalent Strength Conversion According to ACI 562-12, Section 6.4.3, Page No-22

Average Core Strength, f_{cc}	44
Standard Deviation, S.D	5
Co-efficient of variation, V	0.1173
Number of observation, n	7
Co-efficient of variation modification factor, kc	1.15
Equivalent Compressive Strength, f_{ceq} , MPa	36.62

Table 4-6: Fire Affected Column/Shearwall Concrete Equivalent Compressive Strength as per ACI 562

Sl. No	Location	Length (l) (mm)	Diameter (d) (mm)	Correction Factor for diameter, F_{dia}	Core Compressive Strength, f_{core} (MPa)	Corrected Core Strength, $f_{cc} = f_{core} \times \frac{F_{dia}}{F_{dia}}$
1	Core-1 (A2/E3-8F)	134.62	67.056	1.03	29.4	30.28
2	Core-2 (A4/S3-8F)	134.62	67.056	1.03	33.8	34.81

Sl. No	Location	Length (l) (mm)	Diameter (d) (mm)	Correction Factor for diameter, F_{dia}	Core Compressive Strength, f_{core} (MPa)	Corrected Core Strength, $f_{cc} = f_{core} \times \frac{F_{dia}}{F_{dia}}$
3	Core-3 (D3/N1-8F)	134.62	67.056	1.03	32	32.96
4	Core-4(C3/W2-8F)	134.62	67.056	1.03	26.7	27.50
5	Core-5 (C3/W2-8F)	134.62	67.056	1.03	21.5	22.14
6	Core-6 (D2/W1-8F)	134.62	67.056	1.03	39.1	40.27
7	Core-7 (A1/S1-9F)	134.62	67.056	1.03	31.3	32.23
8	Core-8 (C2/N1-9F)	134.62	67.056	1.03	23.3	23.99
9	Core-9(C2/S2-9F)	134.62	67.056	1.03	18.8	19.36
10	Core-10 (A3/S1-10F)	134.62	67.056	1.03	25.9	26.67
11	Core-11 (B2/N1-10F)	134.62	67.056	1.03	26.7	27.50
12	Core-12(D1/W1-10F)	134.62	67.056	1.03	28.3	29.14
13	Core-13 (C2/S2-10F)	134.62	67.056	1.03	19.9	20.49
14	Core-14 (D2/N2-10F)	134.62	67.056	1.03	33.8	34.81
15	Core-15 (C1/W1-10F)	134.62	67.056	1.03	35.3	36.35
16	Core-16 (C3/N1-10F)	134.62	67.056	1.03	37	38.11

Equivalent Strength Conversion According to ACI 562-12, Section 6.4.3, Page No-22

Average Core Strength, f_{cc}	30
Standard Deviation, S.D	6
Co-efficient of variation, V	0.2117
Number of observation, n	16
Co-efficient of variation modification factor, kc	1.07
Equivalent Compressive Strength, f_{ceq} , MPa	24.46

Moreover, concrete core samples has been collected from beam and slabs also. The equivalent concrete compressive strength for beam slab of fire unaffected and affected condition is 30.33 MPa and 23.501 MPa respectively (as shown in Table 4-7 & Table 4-8), whereas the design strength for beam slab was 24 MPa.

Table 4-7: Fire Unaffected Beam/Slab Concrete Equivalent Compressive Strength as per ACI 562

Sl. No	Location	Length (l) (mm)	Diameter (d) (mm)	Correction Factor for diameter, F_{dia}	Core Compressive Strength, f_{core} (MPa)	Corrected Core Strength, $f_{cc} = f_{core} \times F_{dia}$
1	Core-1 (A3/44-8F)	134.62	67.06	1.03	32.7	34
2	Core-2 (A2/32-8F)	134.62	67.06	1.03	39.9	41
3	Core-3 (B2/33-8F)	134.62	67.06	1.03	30.5	31
4	Core-4 (C2/22-8F)	134.62	67.06	1.03	43.1	44
5	Core-5 (A1/74-9F)	134.62	67.06	1.03	32.4	33
6	Core-6 (C1/56-9F)	134.62	67.06	1.03	32.6	34
7	Core-7 (B2/15-10F)	134.62	67.06	1.03	55.3	57
8	Core-8 (C3/34-10F)	134.62	67.06	1.03	32.4	33
9	Core-9 (C3/29-10F)	134.62	67.06	1.03	33.1	34

Equivalent Strength Conversion According to ACI 562-12, Section 6.4.3, Page No-22

Average Core Strength, f_{cc}	38
Standard Deviation, S.D	8
Co-efficient of variation, V	0.2181
Number of observation, n	9
Co-efficient of variation modification factor, kc	1.09
Equivalent Compressive Strength, f_{ceq} , MPa	30.33

Table 4-8: Fire Affected Beam/Slab Concrete Equivalent Compressive Strength as per ACI 562

Sl. No	Location	Length (l) (mm)	Diameter (d) (mm)	Correction Factor for diameter, F_{dia}	Core Compressive Strength, f_{core} (MPa)	Corrected Core Strength, $f_{cc} = f_{core} \times F_{dia}$
1	Core-1 (B2/32-8F)	134.62	67.06	1.03	27.9	29
2	Core-2 (C2/23-8F)	134.62	67.06	1.03	27.5	28
3	Core-3 (C2/36-8F)	134.62	67.06	1.03	29.8	31
4	Core-4 (A2/35-8F)	134.62	67.06	1.03	24	25
5	Core-5 (C3/43-8F)	134.62	67.06	1.03	24	25
6	Core-6 (C1/35-8F)	134.62	67.06	1.03	27.1	28
7	Core-7(A3/63-9F)	134.62	67.06	1.03	31.3	32

Sl. No	Location	Length (l) (mm)	Diameter (d) (mm)	Correction Factor for diameter, F_{dia}	Core Compressive Strength, f_{core} (MPa)	Corrected Core Strength, $f_{cc} = f_{core} \times F_{dia}$
8	Core-8 (C2/27-9F)	134.62	67.06	1.03	22.3	23
9	Core-9 (B2/27-9F)	134.62	67.06	1.03	27.4	28
10	Core-10(B3/16-10F)	134.62	67.06	1.03	31.3	32

Equivalent Strength Conversion According to ACI 562-12, Section 6.4.3, Page No-22

Average Core Strength, f_{cc}	28
Standard Deviation, S.D	3
Co-efficient of variation, V	0.1130
Number of observations, n	10
Co-efficient of variation modification factor, kc	1.08
Equivalent Compressive Strength, f_{ceq}	23.501

4.5.4 Rebar Test

The rebar tensile strength test is a procedure to determine rebar strength. The mechanical properties of steel were significantly affected by elevated temperature. Rebar has been collected from the selected place on the eighth-floor roof. The yield strength of new and fire-affected rebar has been compared. It is found that the rebar strength has been reduced by 15%, as shown in Table 4-9.

Table 4-9: Tensile strength test for rebar of used and new samples

Sl No	Sample Id & Location	Nominal Dia (mm)	Actual Dia (mm)	Yield Strength (Ys) (MPa)	Yield Strength avg. (Ys) (MPa)	Ultimate Strength (Ts) (MPa)	Ultimate Strength avg. (Ts) (MPa)	$\frac{T_s}{Y_s}$	Elon. (Gauge Length = 200 mm) (%)
1	Grid- C-2, (Col Capital)	10	9.56	402		520			27
2	8 th Floor roof	10	9.44	382	392	474	497	1.26	23
3	of existing structure	10	9.76	364		452			21

Sl No	Sample Id & Location	Nominal Dia (mm)	Actual Dia (mm)	Yield Strength (Ys) (MPa)	Yield Strength avg. (Ys) (MPa)	Ultimate Strength (Ts) (MPa)	Ultimate Strength avg. (Ts) (MPa)	$\frac{T_s}{Y_s}$	Elon. (Gauge Length = 200 mm) (%)
1	New rebar of same company	10	10.1	456		645			20
2		10	10.1	468	464	635	638	1.37	19
3		10	10.1	468		635			20

4.6 Evolution of Material by Fire Temperature

Fire is an unanticipated phenomenon that causes severe loss of lives and property everywhere in the world. Generally, fires occur either by man-made accidents or natural hazards i.e., post-seismic fire events, volcanic incidents, etc. Based on the temp-time relationship, fire may be categorized into several types: International Standards Organization (ISO) fire, hydrocarbon fire, natural fire, British Standards (BS) fire, and parametric fire. The major issue of concern in fire events is the degradation of material strength for both concrete and rebar yield strength, tensile strength, elongation, and modulus of elasticity. Fire of the studied building has affected the building at 7th to 9th floor roof which has been shown the Fig 4.10.

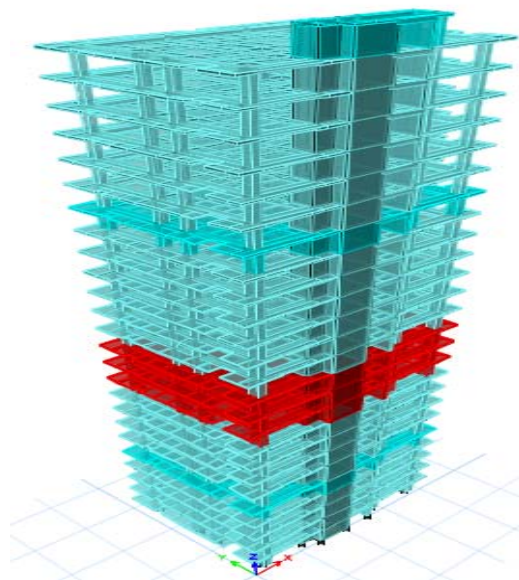


Fig 4.10: 3D View of FR Tower (Fire Affected 7th, 8th & 9th Floor).

4.6.1 Development of Parametric Fire Curve

It is required to choose a fire scenario and simulate structural components' fire resistance after specifying the structure's physical state following a fire incident. Regarding the seismic scenario, it should be considered that it will significantly impact the earthquake-damaged building.

Fire is assumed to happen at the center of the room space, and the temperature is uniform inside the compartment. It monotonically increases following the standard time-temperature fire curve. The standard fire curve is a purely conventional fire action model, which does not represent any particular fire that could develop in actual buildings. The standard fire curve is mainly used for design purposes. In this study, a parametric fire curve has been used to find the more realistic value of real fire.

The fire zone (Fig 4.11) has been used to calculate (Table 4-10 to Table 4-13) the parametric gas temperature and a fire curve has been developed (Fig 4.12) according to Eurocode (En, 2002) using FIN EC software.

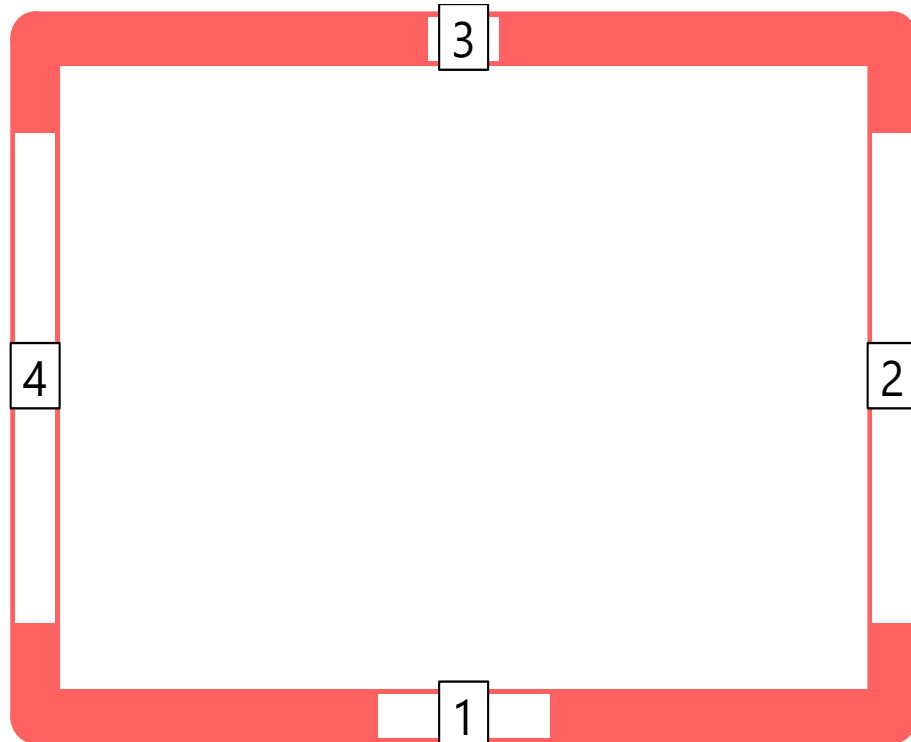


Fig 4.11: Fire zone walls.

Table 4-10: Fire Zone Properties

Wall No.	Start		End		Wall Material(Brick wall with Plaster)			Opening	
	X [m]	Y [m]	X [m]	Y [m]	density ρ [kg/m ³]	specific heat c [J/kg/K]	thermal conductivity λ [W/m/K]	width b [m]	height h [m]
1	0	0	24.97	0	1600	840	0.7	5.0	1.5
2	24.97	0	24.97	17.77	1600	840	0.7	13.0	1.5
3	24.97	17.77	0	17.77	1600	840	0.7	2.04	1.5
4	0	17.77	0	0	1600	840	0.7	13.0	1.5

Table 4-11: Material Combustion Properties

Parameter	Floor Material (Ceramic Tiles)	Ceiling Material (Combustible Interior Design Materials)
Density, ρ (kg/m ³)	2600	60
Specific Heat, c (J/kg/K)	1000	1030
Thermal Conductivity, λ (W/m/K)	2.8	0.03

Table 4-12: Considered Fire Parameters

Fire Parameters	Value
Time of fire development, t_{lim} (min.)	20
The characteristic fire load density per unit floor area, q_{fk} (MJ/m ²)	650
The factor of combustion, m	0.8
Factor related to the fire activation risk due to the size of the compartment, δ_{q1}	1.53
Factor related to the fire activation risk due to the type of occupancy, δ_{q2}	1.02
Factor related to the different active fire fighting measures, δ_n	1.2

Table 4-13: Results of Parametric Fire Curve

Fire Result	Value
Opening factor, O ($m^{1/2}$)	0.052
Thermal absorptivity, b ($J/(m^2s^{1/2}K)$)	1295.3
The design fire load density, $q_{t,d}$ (MJ/m^2)	378.4
Time for maximum gas temp. t_{max} (min.)	86.6
Maximum gas temperature, Θ_g ($^{\circ}C$)	1047.4

Ventilation Controlled fire

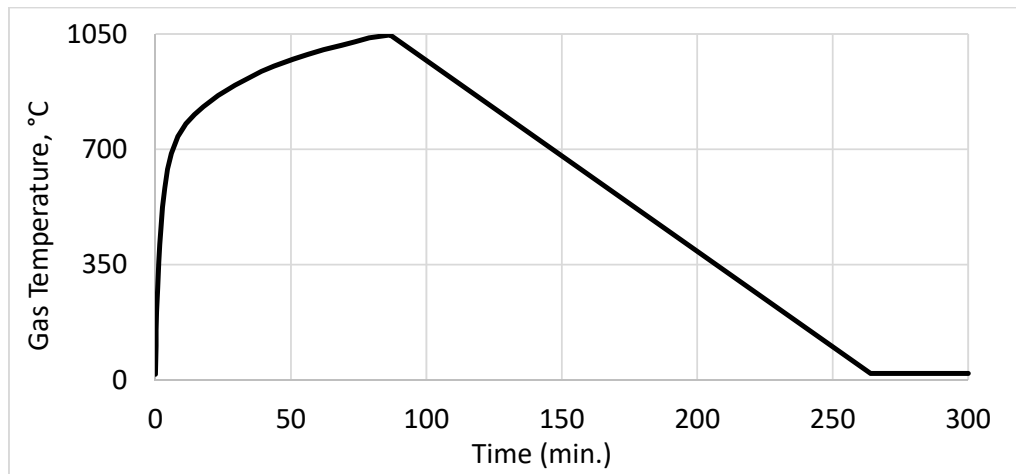


Fig 4.12: Time vs. gas temperature curve for parametric fire.

4.6.2 Calculation of Concrete and Rebar Temperature

Based on the fire curve constructed by the parametric method, concrete and rebar temperature has been calculated according to the Euro code. Fig 4.13 shows temperature development of concrete at depths 38 mm and 75 mm has been shown for different time duration. Moreover, in Fig 4.14, the rebar temperature has been shown also. The researchers (Kodur and Agrawal, 2016) proposed an equation for the temperature of the rebar:

$$T_{smax} = \lambda T_{fmax} \tag{Equation 4-1}$$

Here, $\lambda = 1.45(t_h + \frac{t_c}{w})^{0.2} (0.4 + 0.03 \frac{H}{B}) - 5a$

Where, T_{smax} = maximum rebar temperature; T_{fmax} = maximum fire temperature; λ = modification factor for the cross-section dimensions and fire exposure; t_h = duration of the heating phase (in hours), t_c = duration of the cooling phase (in hours); H = section depth (m); B = section width (m) and a = axis distance (m).

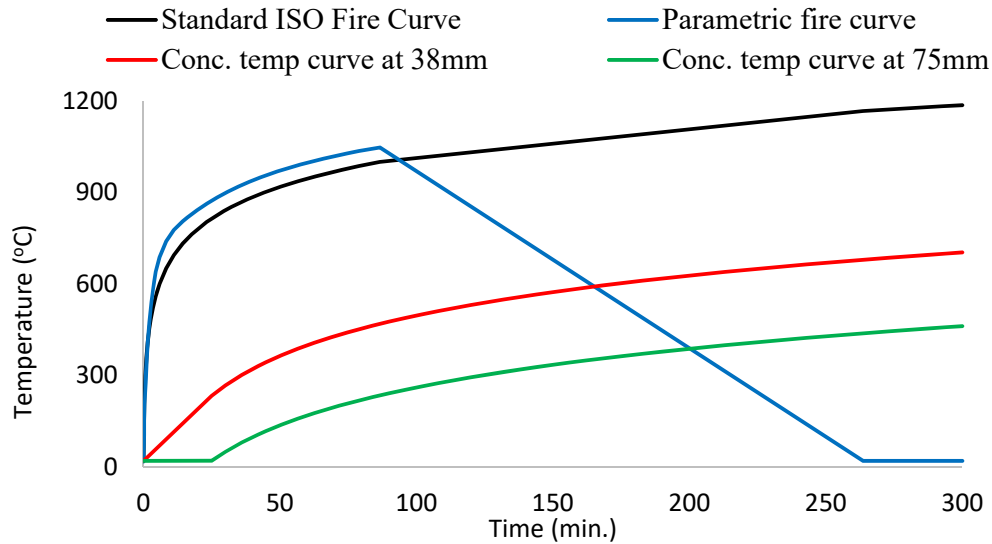


Fig 4.13: Time vs. concrete temperature at different concrete depths.

This empirical equation was developed based on the results of hundreds of finite element heat transfer analyses with 17 different design fires performed by the researchers. After estimating rebar temperature, the strength-temperature relationship can be used to calculate the residual strength.

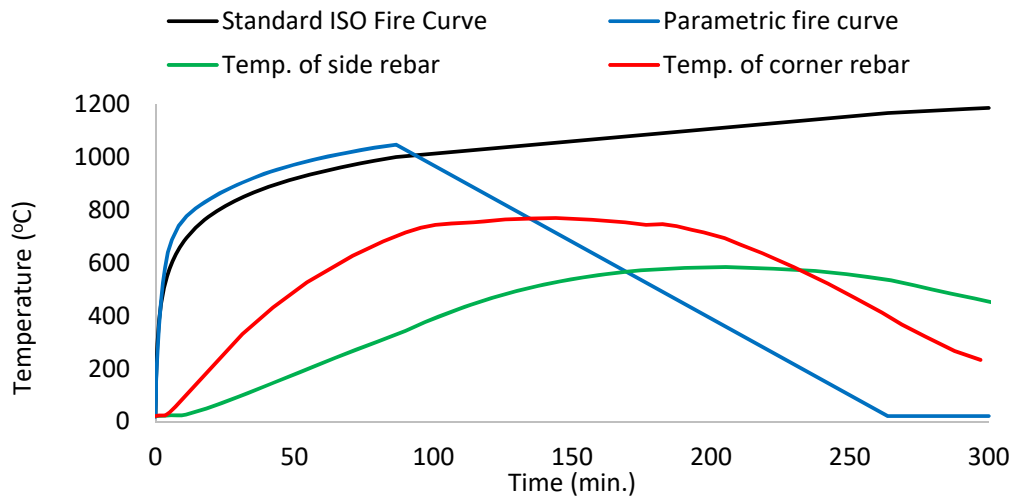


Fig 4.14: Time vs. Rebar Temp at a different location.

4.6.3 Heat Transfer Analysis of Column at FIN Software

The temperature distribution across the cross-section of the beam or column has been obtained from the 2D heat transfer analysis. During this analysis, heat transfer mechanisms were determined by assuming that heat was distributed through solid structures primarily by conduction at the section's boundary. The heat was exchanged with the environment by convection and radiation. Heat exchange was based on a Fourier equation for conduction in the solids. The section's temperature gradient is calculated using the FEM model using the FIN EC software package. The average and gradient temperatures of the section have been extracted for thermal stress analysis. Temperature distribution has been shown in Fig 4.15 and Fig 4.16 for the column and beam sections, respectively.

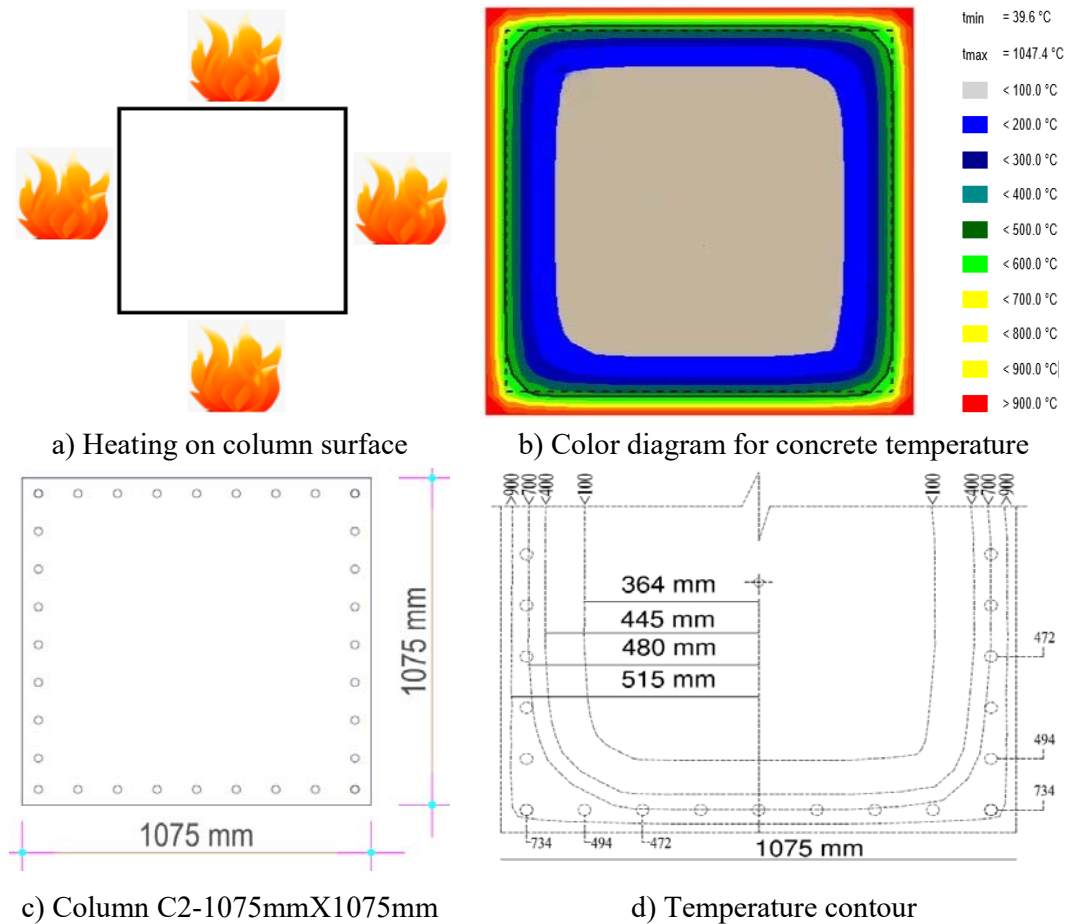


Fig 4.15: Heat Transfer analysis by FIN software for C2 on the 8th floor.

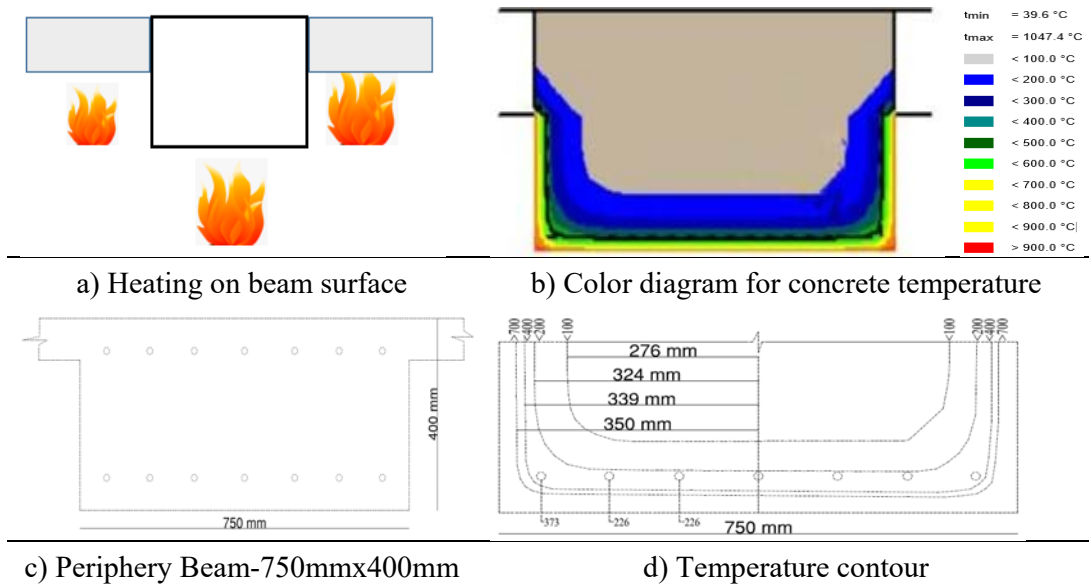


Fig 4.16: Heat transfer analysis by FIN software for periphery beam on the 8th floor.

4.6.4 Residual Concrete Compressive Strength Based on Heat Analysis

Based on the calculated fire temperature, concrete residual compressive strength has been estimated per the building code. As per Eurocode (EN 2004), damaged concrete strength has been calculated (Table 4-14) using the weighted average method of member cross-section. Finally, this residual strength has converted to a residual strength curve (Fig 4.17) for different temperatures.

Table 4-14: Constitutive relationships of high-temperature properties for concrete of column (EN, 2002)

Length mm	Width mm	Develop Temp.	Area mm ²	Affected area mm ²	Core equivalent compressive strength for undamaged condition f _c (Mpa)	Residual strength f _{c,r} (MPa)	Concrete strength, f _{c, eq} (MPa)
1000	875	1047.4	875000	143600	36.61	0	24.7 (very close to core strength of damaged condition)
920	795	800	731400	124564	36.61	6.432	
844	719	600	606836	90180	36.61	23.665	
784	659	500	516656	56120	36.61	32.281	
744	619	400	460536	68172	36.61	36.619	
692	567	300	392364	48760	36.61	36.619	
652	527	200	343604	159588	36.61	36.619	
496	371	100	184016	184016	36.61	36.619	

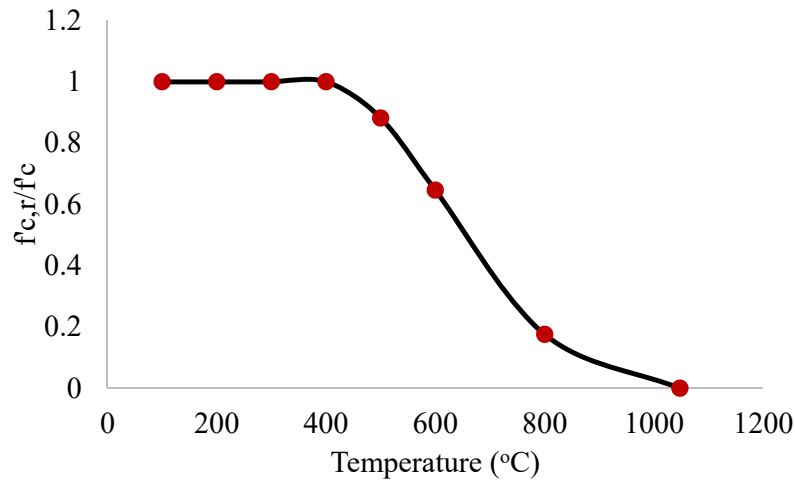


Fig 4.17: Concrete compressive strength reduction with temperature.

4.7 Summary

Three main inspection methods have been applied: visual Inspection, non-destructive, and laboratory testing. Visual Inspection methods are generally the quickest but least accurate. Laboratory testing methods are generally time-consuming and expensive but the most accurate. Non-destructive techniques are medium in quickness and accuracy.

Visual methods have been used to gain a general sense of the extent of damage and to identify the bounds of damage. Several methods have been developed primarily based on previous experiences with real fires in building structures. A damage classification chart (Table 4-1) is used to rate the condition of certain areas of a structure. The damage intensity shows that the entire area of the floors is affected by the fire as there is no zero damage zone, nearly 72% of the 7th-floor roof, 80% of the 8th-floor roof, and 75% of the 9th-floor roof are burnt moderately (damage rating 0 to 2)(Table 4-2) and 28% of the 7th-floor roof, 20% of the 8th-floor roof, and 25% of the 9th-floor roof are damaged at different intensities (damage rating 3 to 5) (Table 4-2) for both structural and non-structural components. Moreover, severe damages on the structural components have been observed at 5% on the 7th and the 9th-floor roofs, which are 8% for the 8th-floor roof. In addition, the visual condition of other non-structural materials, such as aluminum and PVC, are used to estimate the temperatures reached in various parts of the structure.

Various potentially available non-destructive testing methods are used to assess the post-fire condition of the concrete. Some methods even provided estimates of residual strength

loss. The two most popular methods at present, ultrasonic pulse velocity, and carbonation depth test, can both delineate areas of damaged concrete but are unsuitable for estimating residual strength.

The most common laboratory testing methods are the concrete core and rebar tensile strength tests. This method has determined the strength of concrete and rebar. Although it is very accurate, these kinds of tests are expensive and time-consuming. It provides the condition of the concrete at particular points in the structure. The column/shear wall concrete core equivalent compressive strength has been found as 36.62 MPa and 24.46 MPa for pre and post-fire conditions. The concrete core equivalent compressive strength of 30.33 MPa and 23.5 MPa has also been found for beam, and slab at pre and post-fire conditions, respectively. Moreover, the rebar tensile strength testing shows that it reduced by about 15 %. Furthermore, the maximum carbonation depth was 38 mm, indicating the concrete damage by fire.

Moreover, the magnitude of temperature and its distribution is a part that creates thermal stress effects (stresses caused by thermal expansion or contraction of the material). Temperature distribution has been estimated using FIN EC software. The following steps have been followed to estimate the temperature and stress:

- a) The parametric method has been used to calculate the maximum gas temperature. The calculated maximum gas temperature is 1047.4°C, and the fire is ventilation controlled.
- b) A heat transfer analysis is performed to determine the temperature distribution across the cross-section (i.e., the thermal gradient in the element).

Using the developed temperature across the cross-section, residual concrete compressive strength has been calculated using the Euro code. The residual concrete compressive strength of the fire-damaged column has been calculated as 24.7 MPa, which is close to concrete core equivalent compressive strength for damage condition.

CHAPTER 5

FINITE ELEMENT ANALYSIS OF DAMAGED BUILDING

5.1 Information

This chapter describes the step-by-step process from building geometry to finite element modeling for the integrated superstructure. Section properties, material properties, dead loads, superimposed dead loads, live load, earthquake loads for the peak ground accelerations for the 43, 475, and 2475 years return periods are discussed accordingly. The properties of fire damaged as well as undamaged concrete and rebar has been used to determine the actual performance of the structure. Loading properties for linear static analysis are discussed to examine the linear capacity of the structure. The nonlinear mathematical model of the structure has been incorporated several assumptions, from the selection of idealized inelastic component types for each structural member to estimate gravity and seismic loads to capture the expected dynamic behavior of structures. All of these effects on the behavior of tall buildings have been explained elaborately. NLTHA uses ten pairs of ground motions and checks the results in compliance with the determined target performance levels.

5.2 General Properties of the case Studies

The building is a reinforced concrete 23-storied commercial building with two (02) basements, as shown in Fig 5.1. The total height of the building is 67.85m above ground and 5.6m below the ground floor. Storey heights of the basement, ground floor to the third floor, and fourth to above floors are 2.8m, 3.3m & 3.05m, respectively. The building users use the basements for car parking. The building has two staircases, including one fire stair, though its width is only 1m.

The office space mainly occupies the floor area with a lobby area near the lift core and staircase. There are five and four grids in the global x and y directions. The grid spacing, office space arrangement, and location of the lift lobby and staircases are shown in . There are shear walls on the western part of the building. The thickness of all the shear walls is 300 mm. All shear walls are built to the full height of the building, i.e., from the basement

to the roof. The typical cross-sections of the beams and columns are shown in Fig 5.2. There are four types of columns, both square and rectangular, and the cross-sectional dimensions of columns C1, C2, C3, and C4 are 975 x 1225 mm, 1075 x 1075 mm, 1200 x 1200 mm, and 375 x 1050 mm, respectively, at the ground floor.

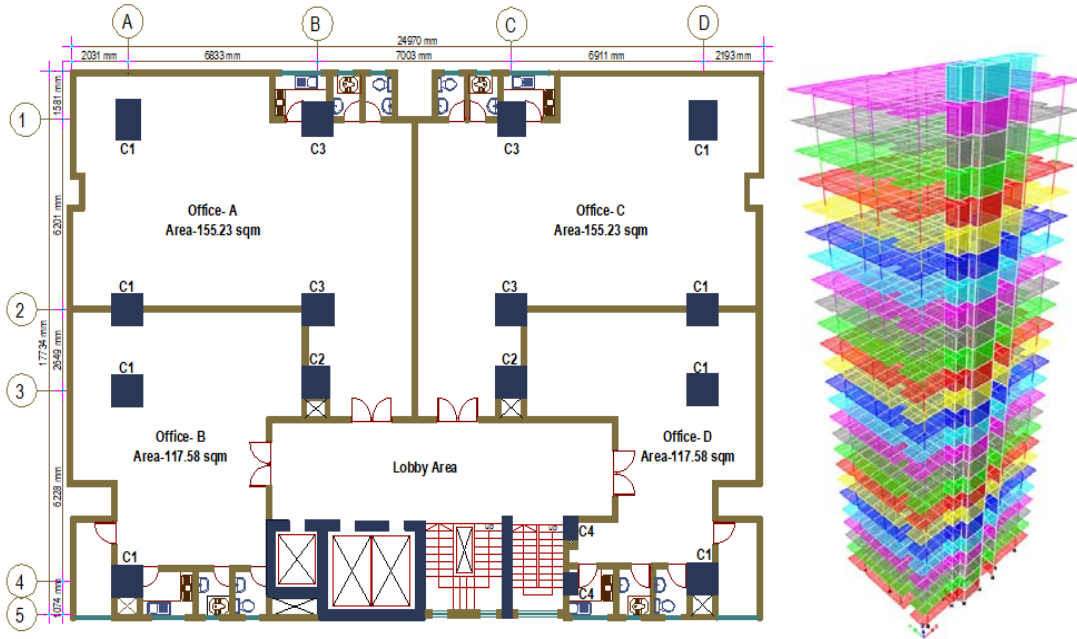


Fig 5.1: Typical floor plan & 3D view of the building.

Column size has changed at the ground, third, fifth, seventh, tenth, and seventeenth-floor levels. Columns C1, C2, C3, and C4 have cross-sectional dimensions of 750 x 1000 mm, 875 x 1000 mm, 1000 x 1000 mm, and 375 x 1050 mm, respectively, in the fire-affected zone (i.e., the seventh, eighth, and ninth floors). It is a flat slab building with perimeter beams. The cross-sectional dimension of the beam is 750 × 400 mm, as shown in fig. The center-to-center spacing of column ties and beam stirrups is 250 mm and 150 mm, respectively, for 10 mm diameter rebar. The overall slab thickness is 187.5 mm, with a column capital of 250 mm. The center-to-center spacing of the slab bottom rebar is 125 mm in both directions for a 12 mm diameter. Moreover, the spacing of slab top rebar at the mid-column strip is 125 mm and 100 mm, respectively, for 12 mm and 16 mm dia. rebar. The building is supported by a mat foundation that is 1450 mm thick. The clear covers for the mat foundation, column, shear wall, beam, and slab are 75 mm, 37.5 mm, 25 mm, 37.5 mm, and 19 mm, respectively.

As mentioned in the working drawing of the building, the specified concrete compressive strength of the columns was 29 MPa, whereas the specified strength of the beam and slab was 24 MPa. Moreover, the specified yield strength of the reinforcement was 420 MPa.

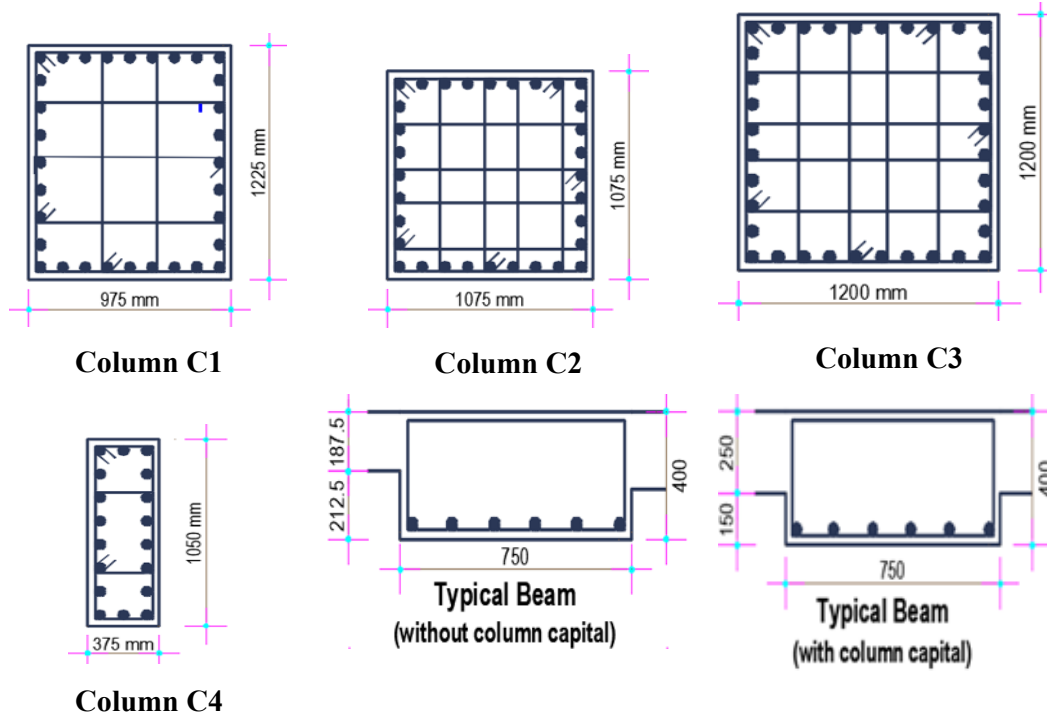


Fig 5.2: Cross-section of columns and beam with rebar arrangements.

5.3 Material Properties (Linear)

Table 5-1: Property of fire-affected and unaffected concrete (*Pekelnicky et al., 2012*)

Material Property			Value	
			Fire unaffected	Fire affected
Concrete compressive strength, f'_c (Mpa)	Column	36.6	24.5	
	Beam& Slab	30.3	23.5	
Modulus of Elasticity, E(Mpa)		$4700 \cdot \sqrt{f'_c}$		
Rebar Yield Strength, f_y (MPa)		420	392	
Expected Tensile Strength, f_u (MPa)		491*	458.6*	
Modulus of Elasticity, E (MPa)		21000		

*Expected tensile strength factor for nonlinearity-1.3(concrete) & .17(reinforcement);

5.4 Material Properties (Nonlinear)

The non-linear properties of concrete and rebar are shown in Fig 5.3. The meander model is considered for concrete, whereas the kinematic hardening model is considered for hysteretic responses of the rebar.

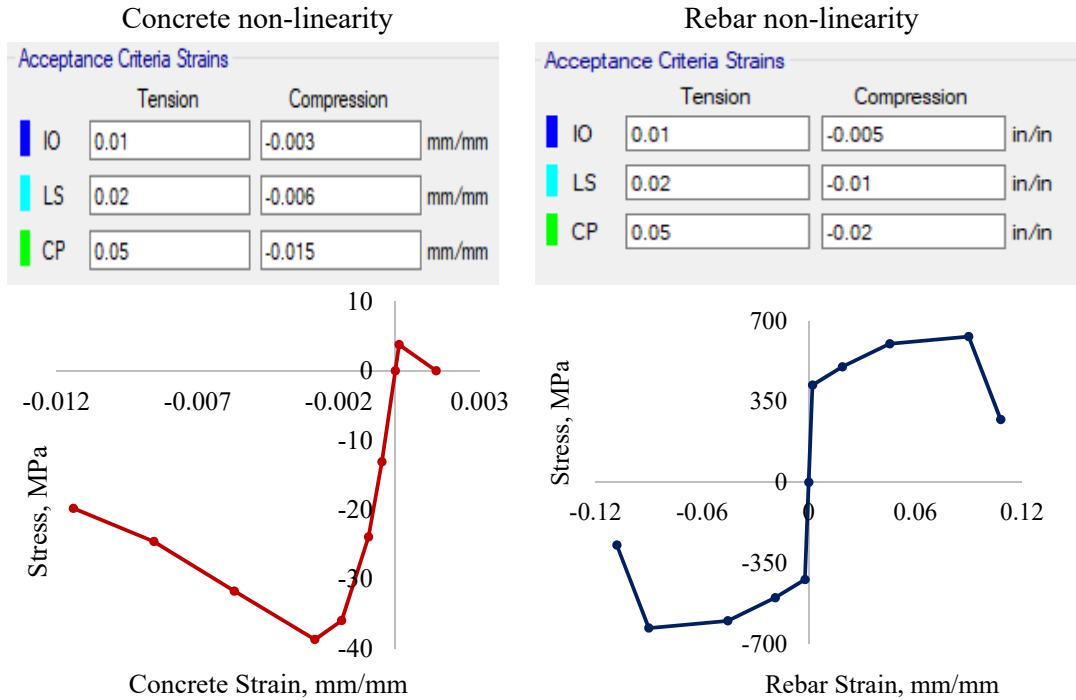


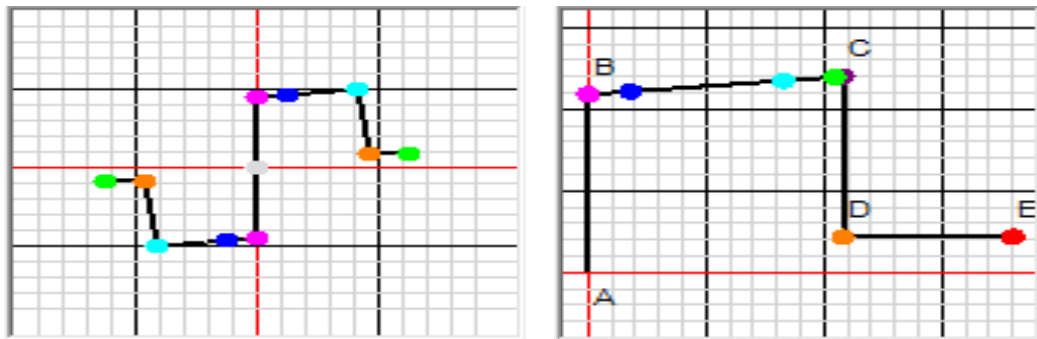
Fig 5.3: Material nonlinearity.

5.5 Nonlinear Hinge Properties

Beam and column elements were modeled as nonlinear frame elements with lumped plasticity by defining plastic hinges at both ends of beams and columns. In this study, user-defined deformation-controlled (ductile) hinge properties were implemented. The plastic hinge locations were assumed and defined on the two ends of the column and beam elements. The seismic performance evaluation was carried out following seismic codes (Fema356, 2000). Fig 5.4 presents the hinge properties and strain limit at different performance objectives and the nonlinear hinge behavior backbone curve.

Beam			Column		
Point	Moment/SF	Rotation/SF			
E-	-0.2	-0.0261	A	0	0
D-	-0.2	-0.0191	B	1	0
C-	-1.1	-0.0174	C	1.1	0.015
B-	-1	0	D	0.2	0.015
A	0	0	E	0.2	0.025
B	1	0			
C	1.1	0.0174			
D	0.2	0.0191			
E	0.2	0.0261			

a) Strain limit at a different point



b) Backbone Curve

Acceptance Criteria (Plastic Rotation/SF)		Acceptance Criteria (Plastic Deformation / SF)	
	Positive		
Immediate Occupancy	0.005	Immediate Occupancy	0.003
Life Safety	0.0174	Life Safety	0.012
Collapse Prevention	0.0261	Collapse Prevention	0.015

c) IO, LS, and CP strain levels

Fig 5.4: Beam & Column Hinge Properties.

5.6 Load Consideration

The load patterns and combinations considered for preliminary force-based analysis are presented in Table 5-2 and Table 5-3, respectively. The building has been analyzed by Etabs software. Since the torsional irregularity exist in the studied building, necessary steps has been taken as per building code during analysis (torsional amplification factor considered) and design (30% orthogonal seismic forces considered). The PMM (demand-capacity) ratio has been checked for the concrete columns and shearwall using load combinations before going into the non-linear analysis of the structure.

Table 5-2: Load Consideration

Load Pattern	Loads	Seismic Design Parameter
Self Wt. (DL)	As per frame weight	$S_1= 0.3, S_s= 0.75$ (MCE);
Floor Finish(DL)	1.2 kN/m ²	$S_1= 0.2, S_s= 0.50$ (DBE);
Floor Live Load(LL)	3.0 kN/m ²	$S_1= 0.13, S_s= 0.33$ (SLE);
Roof Live Load(LL)	1.4 kN/m ²	Site Class: C; SDC: C;
Partition Wall Load(DL)	2.4 kN/m ²	I=1; R=5.5; $C_d=4.5, w_d=2.5$
		*SDC- structural design category

Table 5-3: Load Combination

Load Combination
1. 1.4DL ^a
2. 1.2 DL + 1.6Lf + 0.5 Lr ^b
3. 1.2DL + 1.6 Lr + Lf ^c
4. 1.2D + 1.6W + Lf + 0.5 Lr
5. 1.2DL + 1.0 Lf + 0.5 Lr + 1.0E _{x/y} ^d ± 0.3E _{y/x}
6. 0.9D + 1.6W ^e
7. 0.9DL + 1.0E _{x/y} ^d ± 0.3E _{y/x}
^a Dead Load; ^b Roof Live Load; ^c Floor Live Load; ^d Earthquake Load; ^e Wind Load

5.7 Seismic Parameters for Different Earthquake Level

Seismic design parameters are also given in Table 5-4 considering intermediate moment resisting frames and soil type SC based on the soil investigation report following Bangladesh National Building Code, (2020). Moreover, the spectral acceleration curve for different earthquake level has been shown in Fig 5.5.

Table 5-4: Seismic parameters

Earthquake Level	Return Period (Years)	Probability of Exceedance	Seismic Parameters					
			S ₁	S _s	F _a	F _v	SDS	SD1
MCE	2475	2 % in 50 years	0.3	0.75	0.15	1.725	0.23	0.32
DBE	475	10 % in 50 years	0.2	0.5	0.15	1.725	0.38	0.23
SLE	43	50 % in 30 years	0.13	0.33	0.15	1.725	0.536	0.14

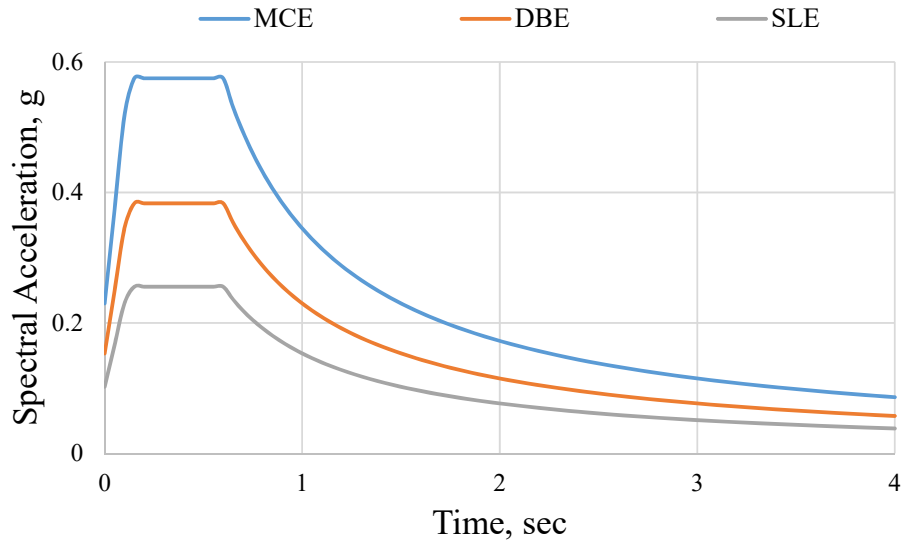


Fig 5.5: Spectral acceleration curve at different earthquake levels.

5.8 Linear Static Analysis

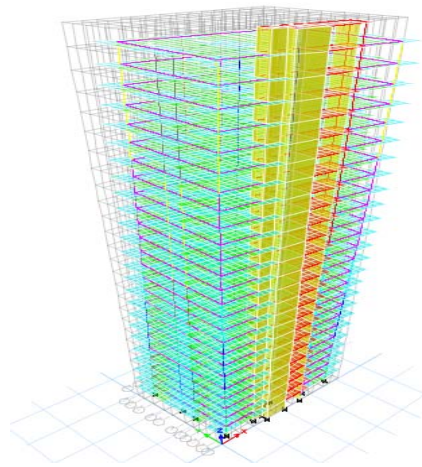
Based on the above mentioned considerations, a 3D finite element analysis model has been developed using commercially available finite element analysis software. The geometry, material properties, and loadings are strictly followed as per BNBC (2020), as mentioned earlier. In analysis, the crack section has been considered for beam, column, shear wall, and slab as per the National Building Code of Bangladesh.

5.8.1 Modal Analysis

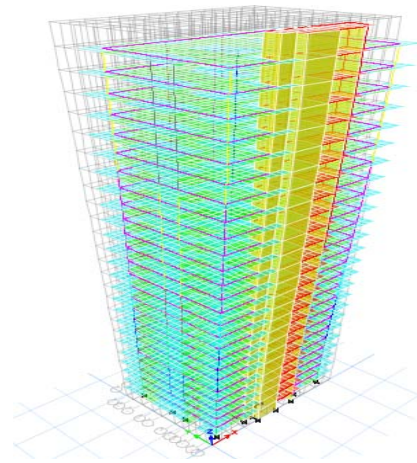
The properties of building under vibration was determined by modal analysis. The 1st vibration mode was translation in X direction with 4.02 and 4.19 sec time period, 2nd vibrational mode was translation in Y direction with 3.70 and 3.86 sec time period, 3rd mode was in torsion with 2.33 and 2.37 sec time period and 4th mode was also in torsion with 1.24 and 1.31 sec time period. Twenty six vibrational modes were considered for modal analysis and approximately more than 90% of the total mass from the ground level was participating in modal analysis. The time period for first three vibrational mode is considered as fundamental period. The time period, frequency and their shapes are shown Table 5-5 and Fig 5.6.

Table 5-5: Fundamental period and frequency

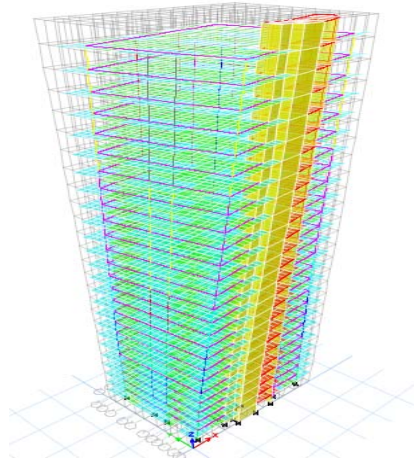
Mode	Before Fire Effect			After Fire Effect		
	Period	Frequency	Circular Frequency	Period	Frequency	Circular Frequency
	sec	cyc/sec	rad/sec	sec	cyc/sec	rad/sec
1	4.02	0.25	1.56	4.19	0.24	1.50
2	3.70	0.27	1.70	3.86	0.26	1.63
3	2.33	0.43	2.70	2.37	0.42	2.66
4	1.24	0.81	5.07	1.31	0.77	4.81



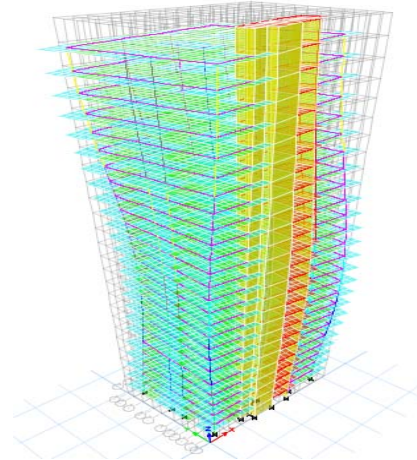
a) 1st Mode



b) 2nd Mode



c) 3rd Mode



d) 4th Mode

Fig 5.6: First four-mode shape.

5.8.2 Column Moment Curvature

A comparison of column moment-curvature between pre and post-fire conditions for columns C1 & C2 is shown in Fig 5.7. The curve shows that for same amount of moment, the rotation for post-fire condition is more than the pre-fire condition. Compressive strength of concrete, axial load on the RC sections, longitudinal and transverse reinforcing ratios are the parameter that affects moment curvature relationship. Column moment capacity decreases by 11-12% for the decrease of concrete compressive strength and rebar tensile strength due to the fire effect.

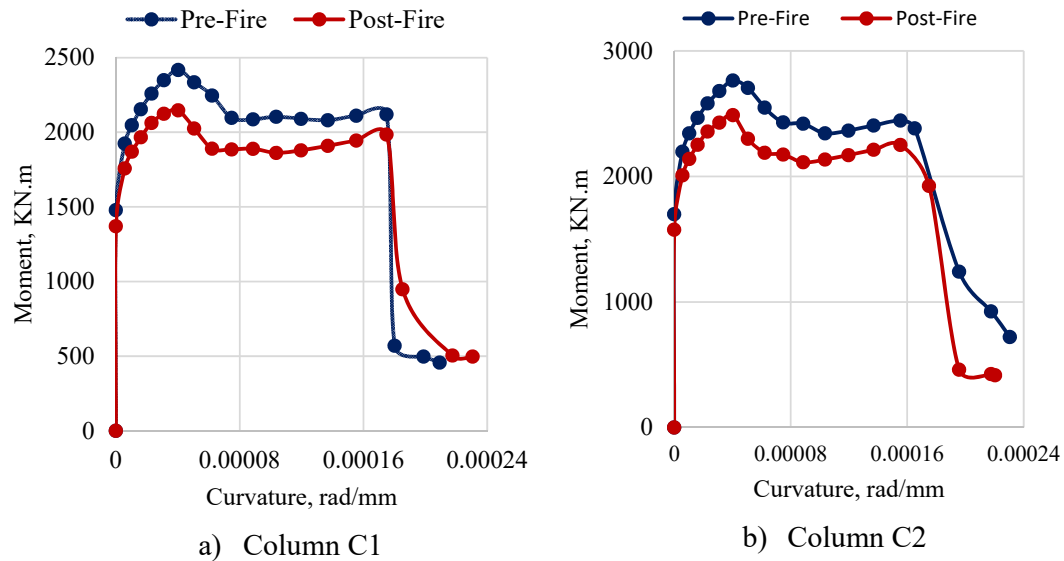


Fig 5.7: Column Moment Curvature.

5.8.3 Column Interaction Diagram

Column interaction diagram has been made for pre and post-fire conditions for C1 & C2 columns as shown in Fig 5.8. Compressive strength of concrete, tensile strength and arrangement of reinforcements are the parameter that affects column interaction diagram. Column axial capacity decreases 26 -27% at post-fire condition than the pre-fire condition. The column capacity may be result of the decrease of concrete compressive strength and rebar tensile strength due to the fire effect. The weak storey irregularity has been checked at post-fire condition following BNBC (2020) and found non susceptible due to fire effect.

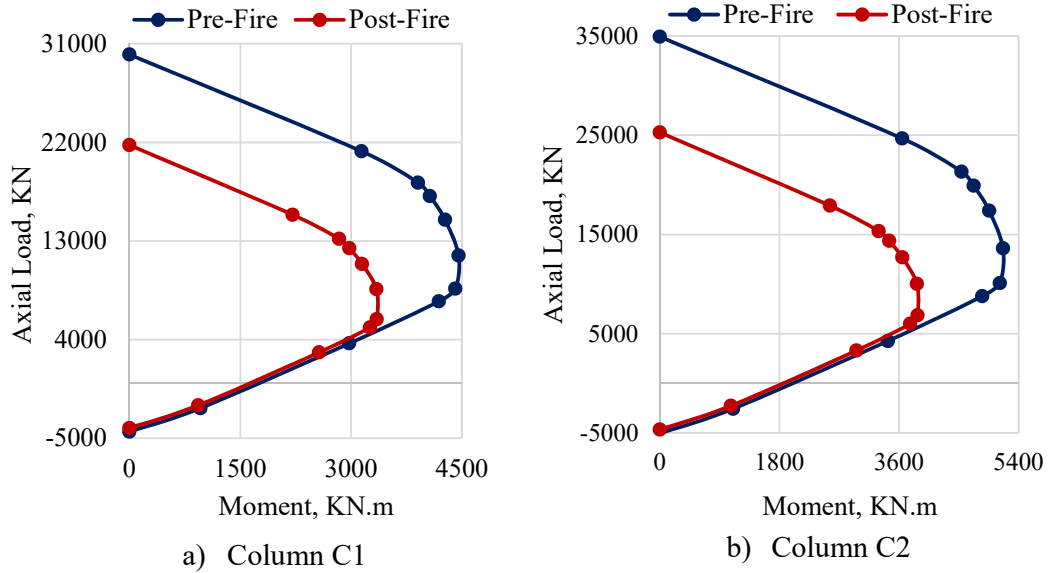


Fig 5.8: Column Interaction Diagram.

5.8.4 Deflection

The displacement demand of the building has been determined for both axes. The displacement demand for pre and post-fire conditions have been shown in Fig 5.9. Due to the fire effect, material strength & member sizes have been reduced. As a result, the lateral stability of the structure is also reduced. The maximum displacement at the 2475 yrs earthquake return period is 1.91m & 2.19m, which is 1.28m & 1.46m for 475 years return period and 0.85m & 0.97m for 43 years return period at pre and post-fire conditions, respectively. Maximum deflection increases by about 10-20% (Table 5-6).

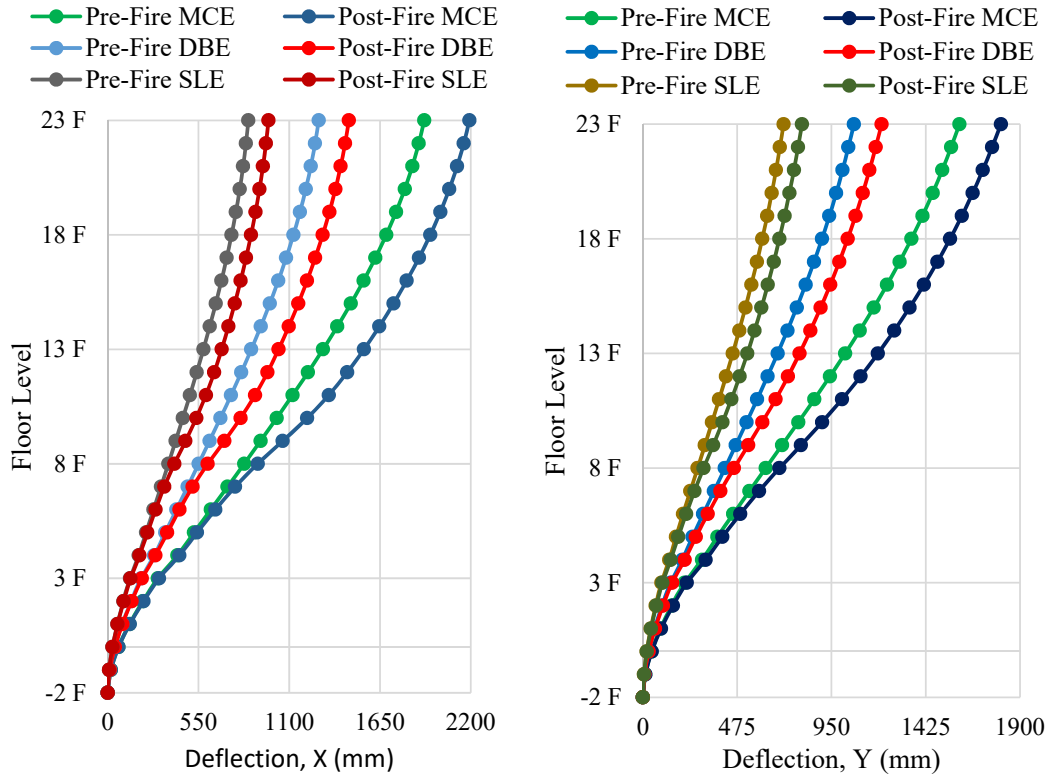


Fig 5.9: Maximum Deflection.

Table 5-6: Drift and deflection increase for fire effect

Floor	Deflection Increase		Drift Increase	
	X (%)	Y (%)	X (%)	Y (%)
14F	18	18	4	8
13F	18	18	5	10
12F	19	19	8	12
11F	20	20	14	15
10F	20	20	25	20
9F	18	18	37	26
8F	14	14	36	26
7F	10	10	25	20
6F	6	6	12	13
5F	5	5	7	10
4F	3	3	4	8
3F	3	3	3	6
2F	2	2	2	5
1F	2	2	2	4
GF	2	2	1	4

5.8.5 Drift

The fire effect has reduced material capacity and member sizes. Due to the structural lateral capacity reduction, the drift ratio also increases by 26-37 % (Table 5-6) for the fire affected floors. The storey drift in X direction has been found beyond the allowable limit as prescribed in BNBC (2020) whereas in Y direction found within allowable limit.

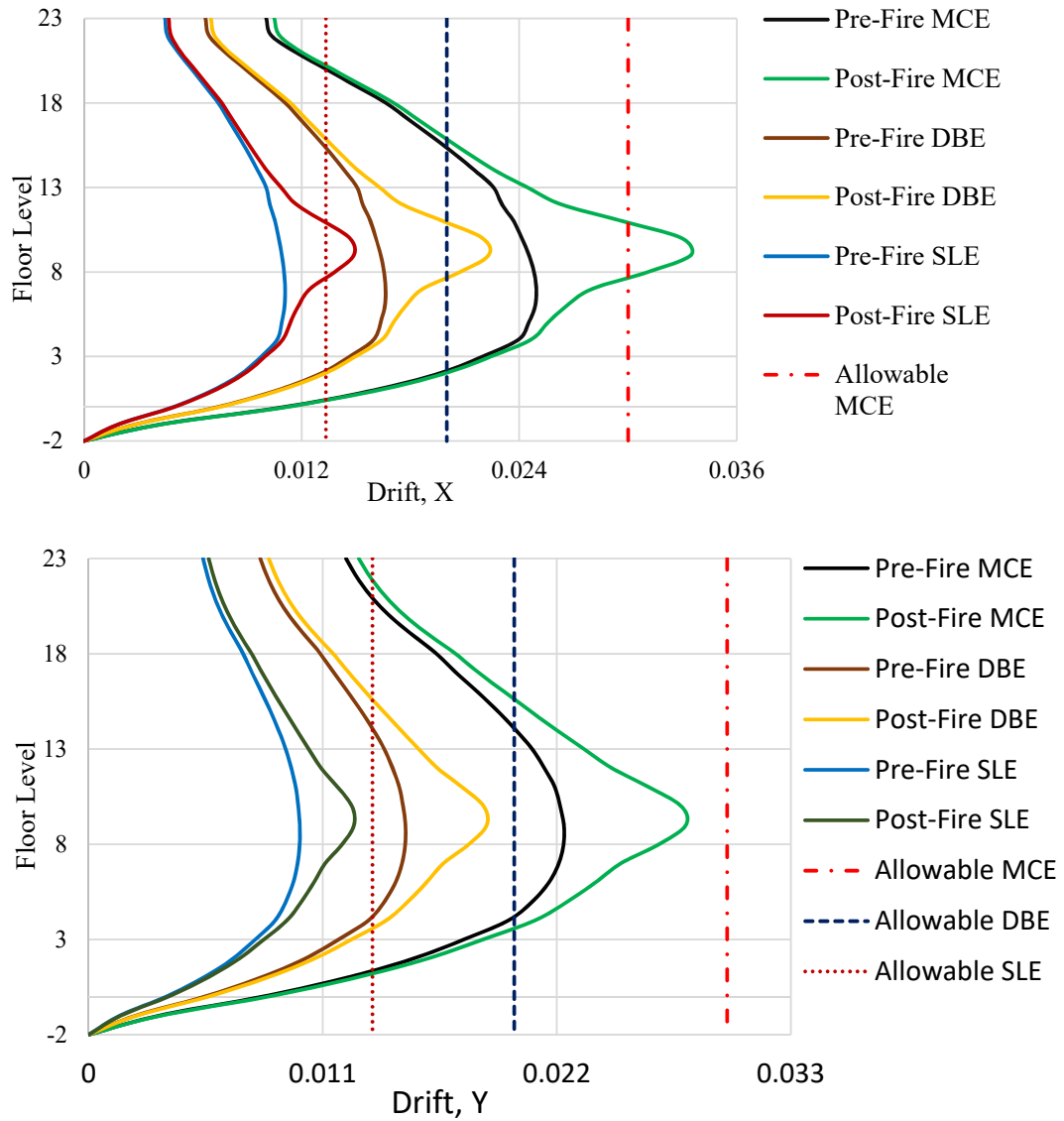


Fig 5.10: Storey drift.

5.8.6 Stiffness

The overall stiffness of the structure at different floor level is shown in Fig 5.11 for both pre and post-fire conditions. Generally, the stiffness depends on the modulus of elasticity & cross-sectional area of concrete. The stiffness of the fire-affected floor has been reduced by up to 28% as shown in Table 5-7. Since the strength and cross-sectional area have been reduced, the stiffness is also affected. Due to stiffness reduction the displacement of the structure increases, as a result soft storey irregularity may be developed. Stiffness and deflection based soft storey irregularity has been checked at post- fire condition and found non existence.

Table 5-7: Stiffness loss due to fire effect

Floor Level	Stiffness loss due to fire effect	
	Stiffness X (%)	Stiffness Y (%)
18 F	4	7
17 F	4	7
16 F	4	8
15 F	4	9
14 F	5	10
13 F	6	12
12 F	9	14
11 F	13	17
10 F	22	22
9 F	28	27
8 F	28	27
7 F	22	22
6 F	12	15
5 F	8	12
4 F	5	10

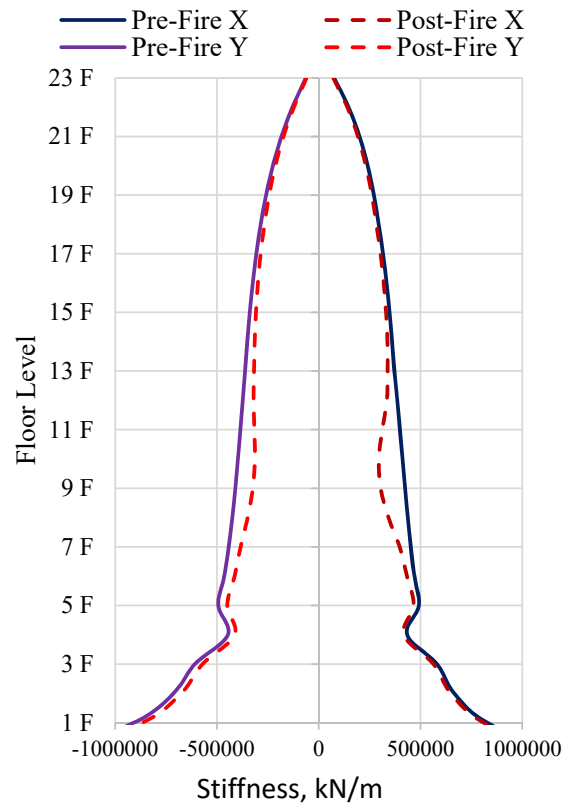
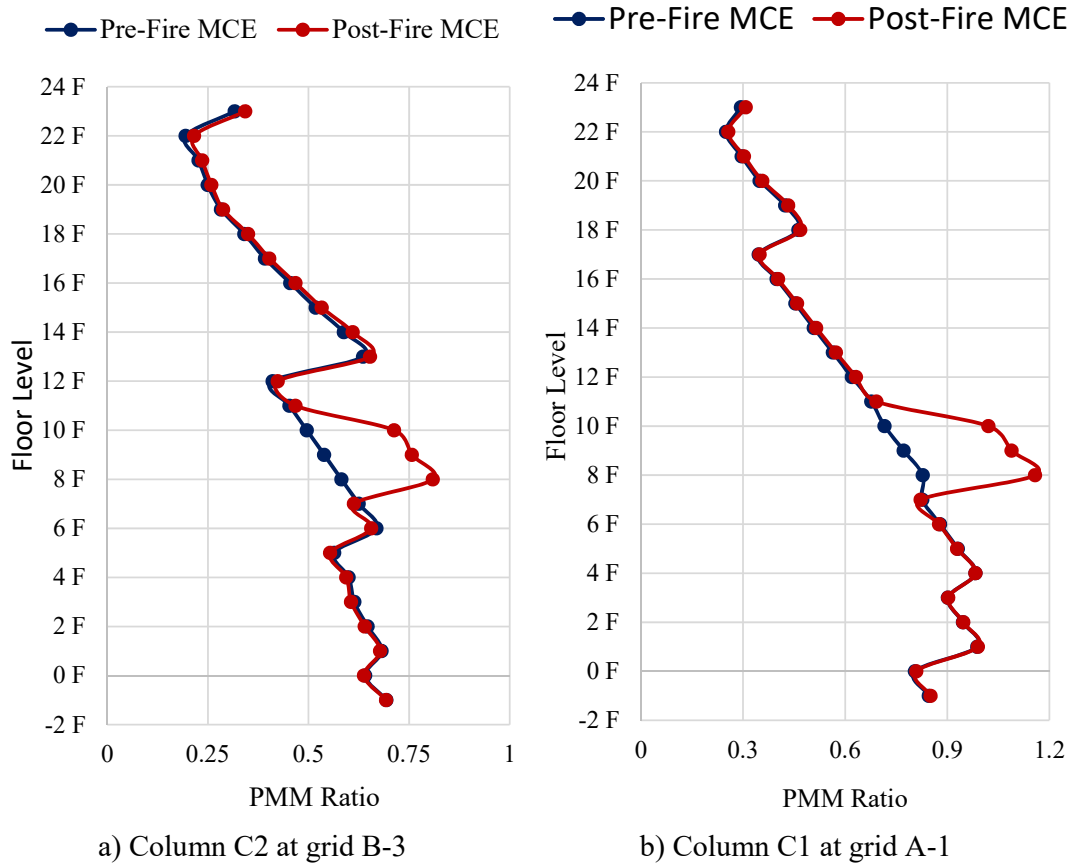
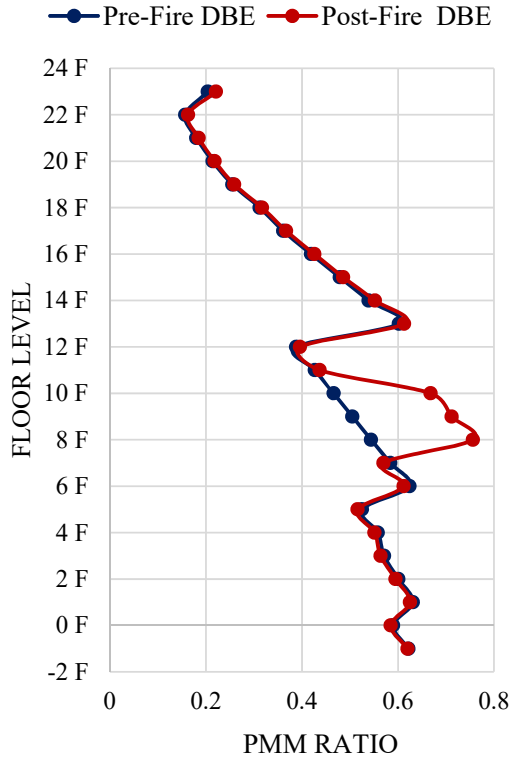


Fig 5.11: Storey Stiffness.

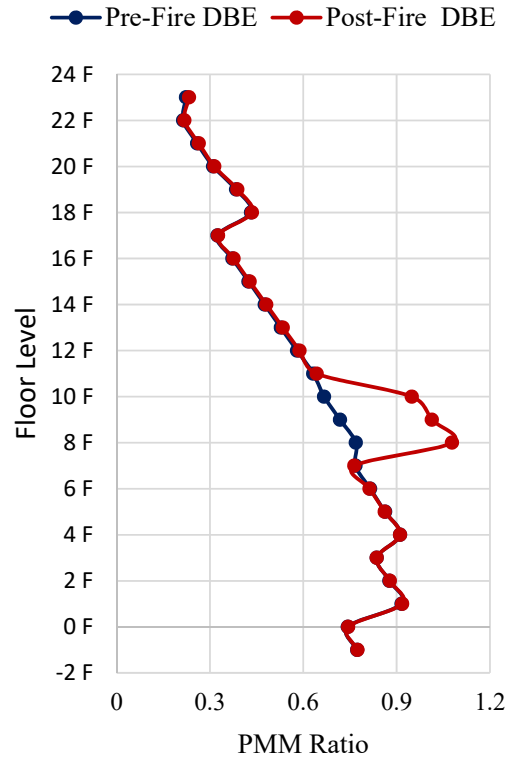
5.8.7 Column PMM Ratio

The column demand capacity ratio has been shown in Fig 5.12 & Table 5-8. The figure and table show that the column bearing capacity reduces. The column demand capacity ratio of column C2 at grid B/3 is found within the allowable limit (<1) for MCE, DBE, and SLE earthquake levels at pre and post-fire conditions. But the demand capacity ratio of the C1 column at grid A/1 is found within the allowable limit before the fire condition. In contrast, the demand capacity ratio is greater than 1 for the MCE, DBE, and SLE earthquake levels for post-fire conditions. The demand capacity ratio increases by 40-46% & and 39-44 % for columns C1 & C2, respectively. This may occur due to the structure's loss of strength and stiffness.

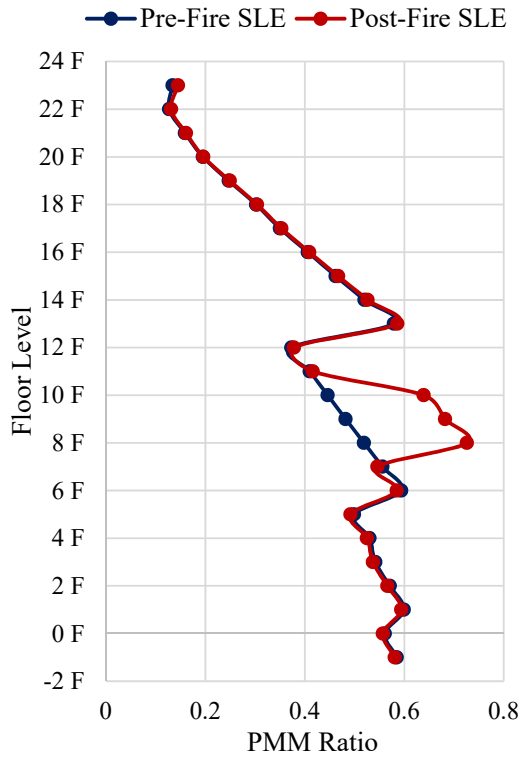




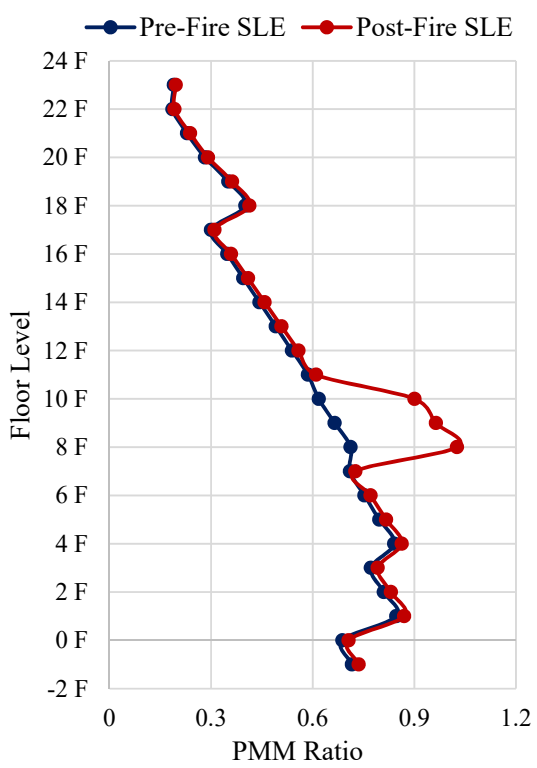
c) Column C2 at grid B-3



d) Column C1 at grid A-1



e) Column C2 at grid B-3



f) Column C1 at grid A-1

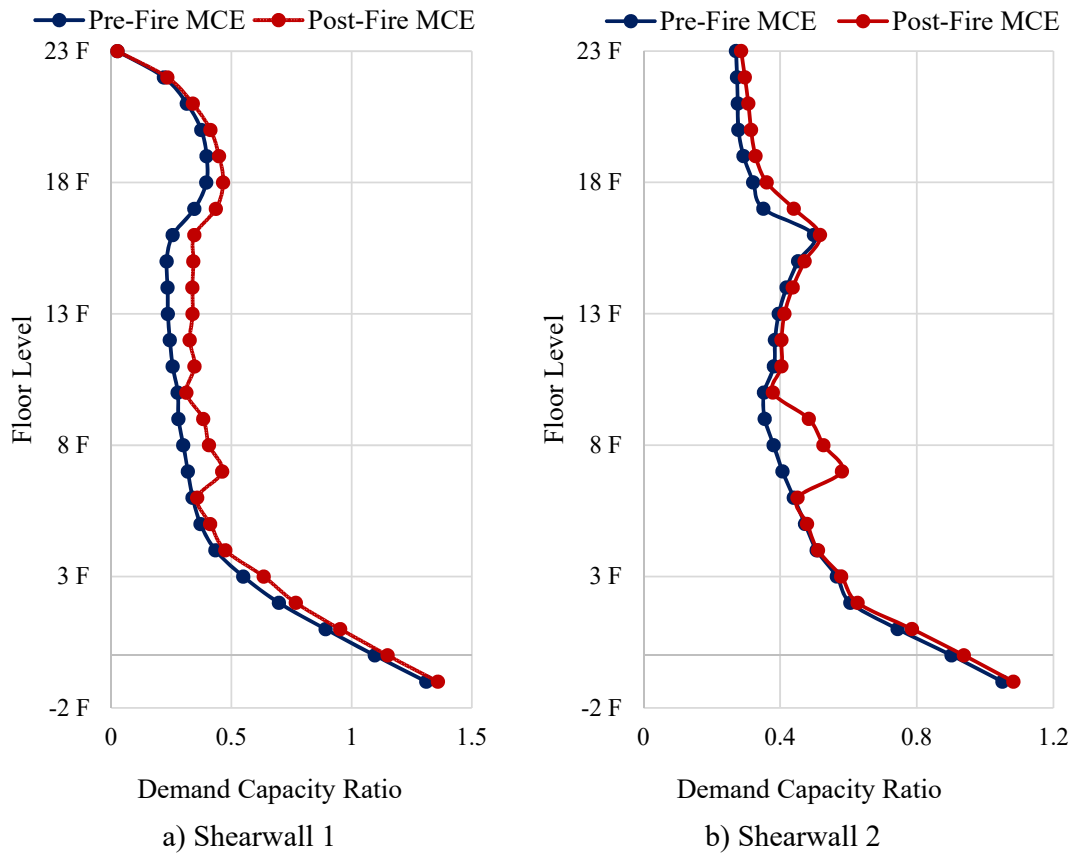
Fig 5.12: Column PMM ratio.

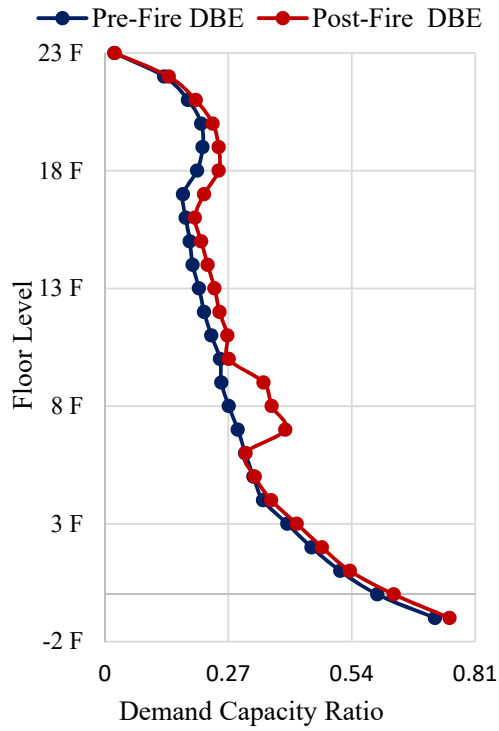
Table 5-8: Variation of column PMM ratio due to fire effect

FLOOR	PMM ratio variation due to fire effect for column C2 (Grid-E/7)			PMM ratio variation due to fire effect for column C2 (Grid-E/7)		
	MCE (%)	DBE(%)	SLE(%)	MCE (%)	DBE(%)	SLE(%)
21 F	4	3	1	2	2	4
20 F	4	3	1	2	2	4
19 F	4	2	1	2	1	3
18 F	2	2	1	2	1	3
17 F	3	2	1	1	1	3
16 F	3	2	1	1	1	3
15 F	3	2	1	1	1	3
14 F	3	1	1	1	1	4
13 F	4	2	1	1	1	3
12 F	3	2	1	2	1	3
11 F	3	2	1	2	1	4
10 F	3	2	1	2	2	4
9 F	44	43	43	43	42	46
8 F	40	41	41	41	41	45
7 F	39	39	40	40	40	44
6 F	2	2	2	1	1	2
5 F	2	2	2	0	0	2
4 F	2	2	1	0	0	3
3 F	1	1	1	0	0	3

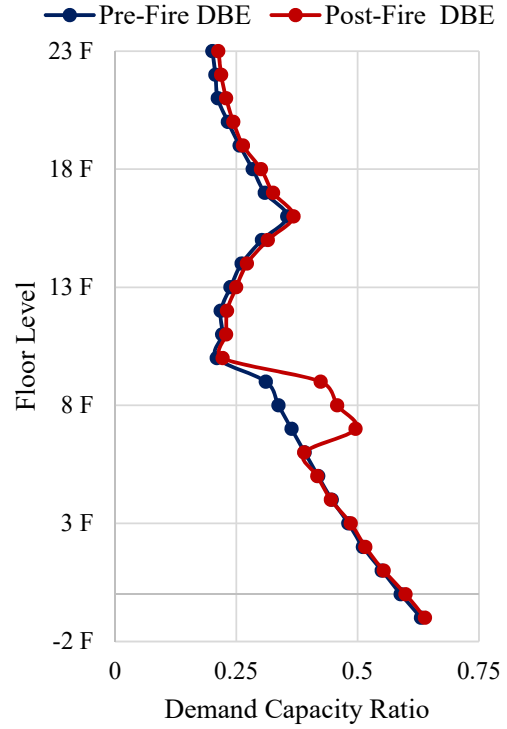
5.8.8 Capacity of Shearwall

Shear wall contributes maximum 47% and 55% of total base shear in X and Y directions respectively. The demand capacity ratio of shearwall has been shown in Fig 5.13. The figure show that the demand capacity ratios of shearwall for post-fire condition at 7th, 8th and 9th floor increases remarkably than pre-fire condition. The demand capacity ratio of shearwall W1 and W2 is found beyond the allowable limit (>1) for MCE earthquake levels at pre and post-fire conditions. In contrast, the demand capacity ratio is within the allowable limit (<1) for the DBE, and SLE earthquake levels. This may occur due to the structure's loss of stiffness and strength for concrete and rebar.

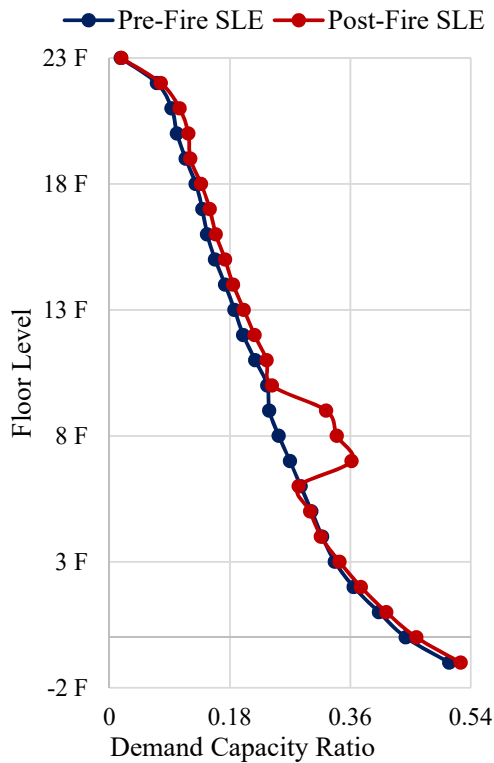




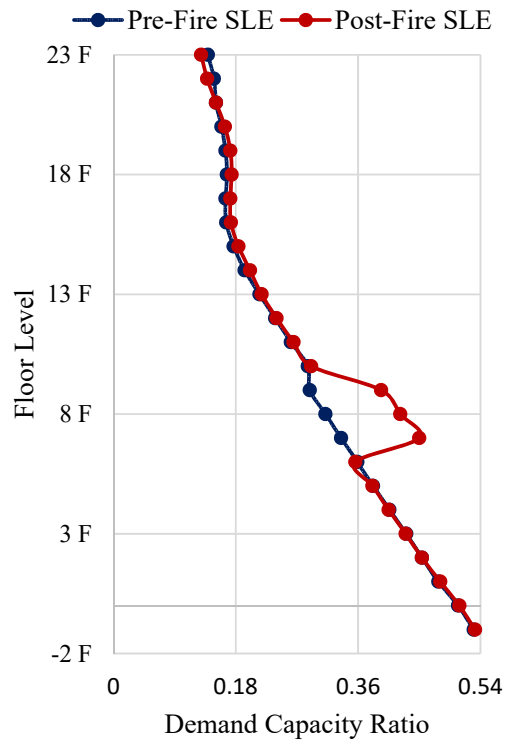
c) Shearwall W1



d) Shearwall W2



e) Shearwall W1



f) Shearwall W2

Fig 5.13: Shearwall demand capacity ratio.

5.9 Nonlinear Time History Analysis (NLTHA)

The investigation has been extended to Non-Linear Time History (NLTH) analysis to understand the actual response of the building under seismic excitation. In this study, ten nos. well-established ground motions have been selected for NLTHA. The ground motions are Chi-Chi, Hollister, Imperia, Kobe, Denali, Landers, Loma Prieta, Northridge, Trinidad, and Bhuj. The properties of the ground motions, magnitudes of the earthquake, PGA, and other seismic data have been shown in Table 5-9. These are recorded earthquakes and will be scaled to approximately 0.3g, 0.2g, & 0.13g to represent an MCE, DBE, and SLE condition, respectively. The earthquake ground motions are presented in terms of ground acceleration vs time in Fig 5.14. For nonlinear analysis, FNA usually uses a Ritz vector customized with P-Delta based on the gravity loads. It is important to use P-delta as it is critical in adequately determining stability behavior. Time history analysis uses the time history of input force or acceleration, which is then united to get the response. Finally, the motions are applied to the 3D finite element model developed by structural analysis software.

Table 5-9: Reference ground motions data used in the analysis

EQ Serial	EQ Name	Station	Year	Magnitude	PGA(g)
1	ChiChi	CHY002	1999	7.6	0.098
2	Hollister	Hollister City Hall	1961	5.6	0.036
3	Imperia	Aeropuerto Mexicali	1979	6.5	0.160
4	Kobe	Abeno	1995	6.9	0.138
5	Denali	Carlo (temp)	2002	7.9	0.074
6	Landers	Forest Falls Post Office	1992	7.3	0.080
7	Loma Prieta	Gilroy Array	1989	6.9	0.038
8	Nortidge	Alhambra - Fremont School	1994	6.69	0.046
9	Trinidad	Rio Del overpass	1983	5.7	0.028
10	Bhuj	Ahmedabad(ISC)	2001	7.7	1.038

Ground motions are matched with local seismic data i.e., the response spectrum that gives the actual seismic demand. The time functions have been scaled with seismo-match software for the target response spectra for the return periods of 43, 475, and 2475 years. The displacement demand is the expected outcome from the ten ground motion data. The original time functions have been scaled up to the target acceleration values for 2475 years, 475 years, and 43 years of earthquake events. The scaled period vs. acceleration for the time function and response spectrum have been plotted in Fig 5.15 to Fig 5.20.

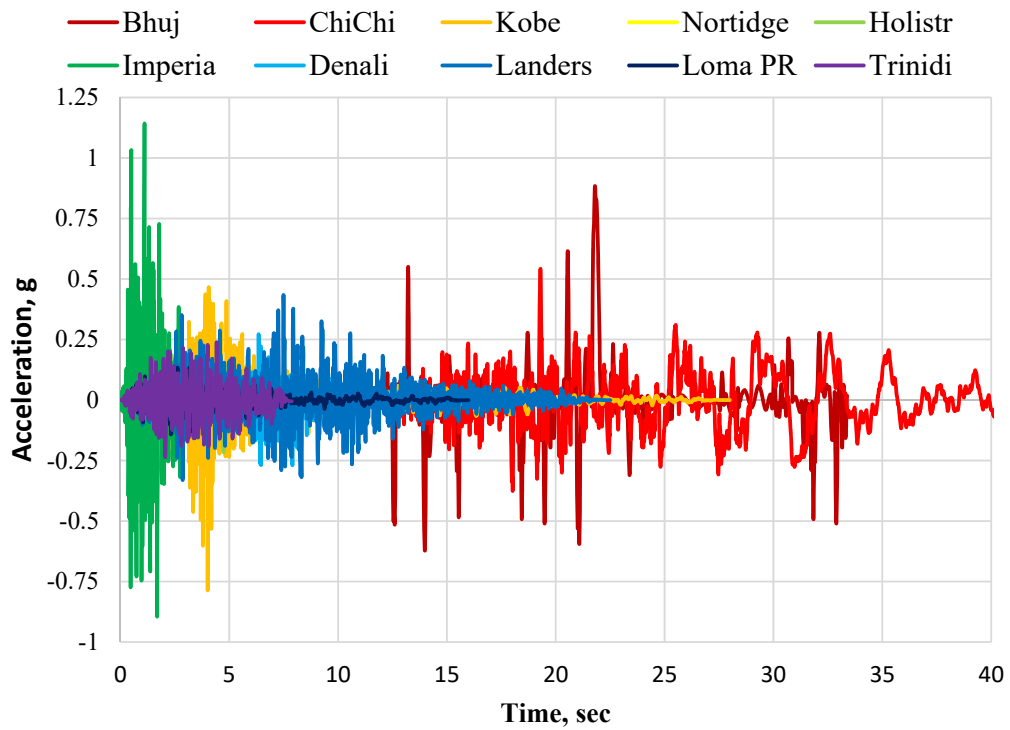


Fig 5.14: Time history functions of ten different ground motions.

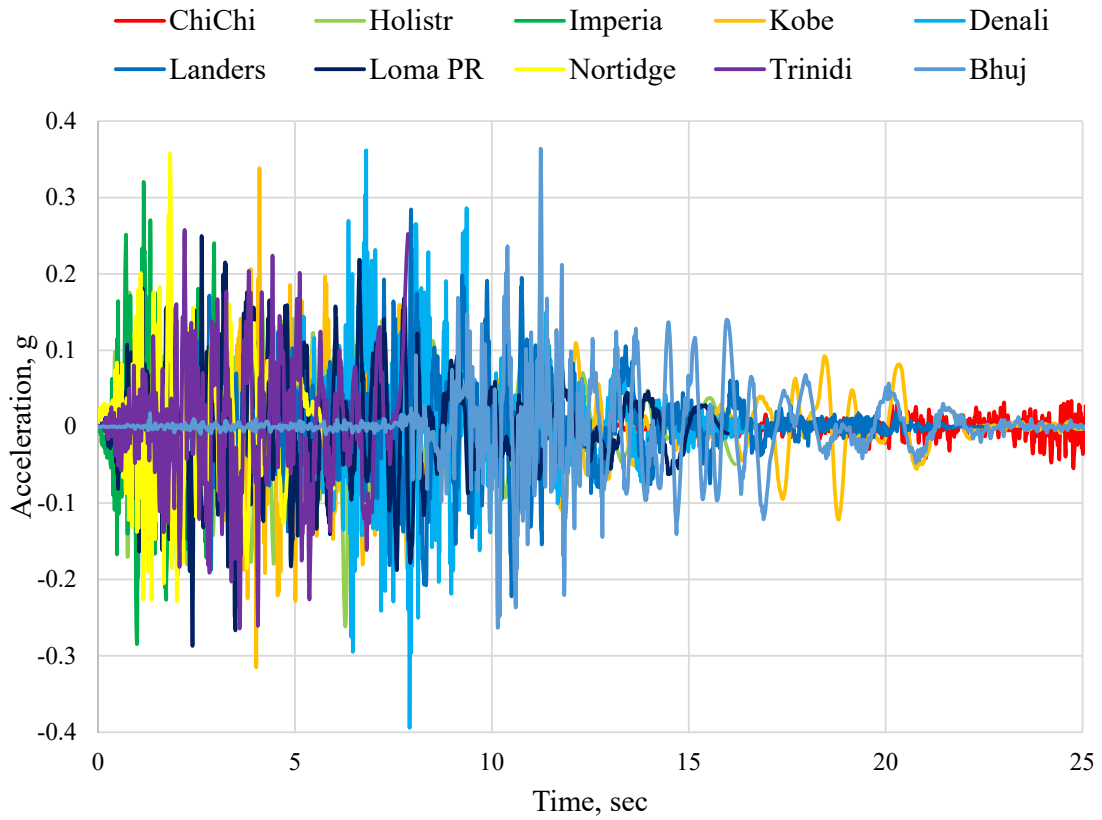


Fig 5.15: Scaled Time history function- 2475 Years.

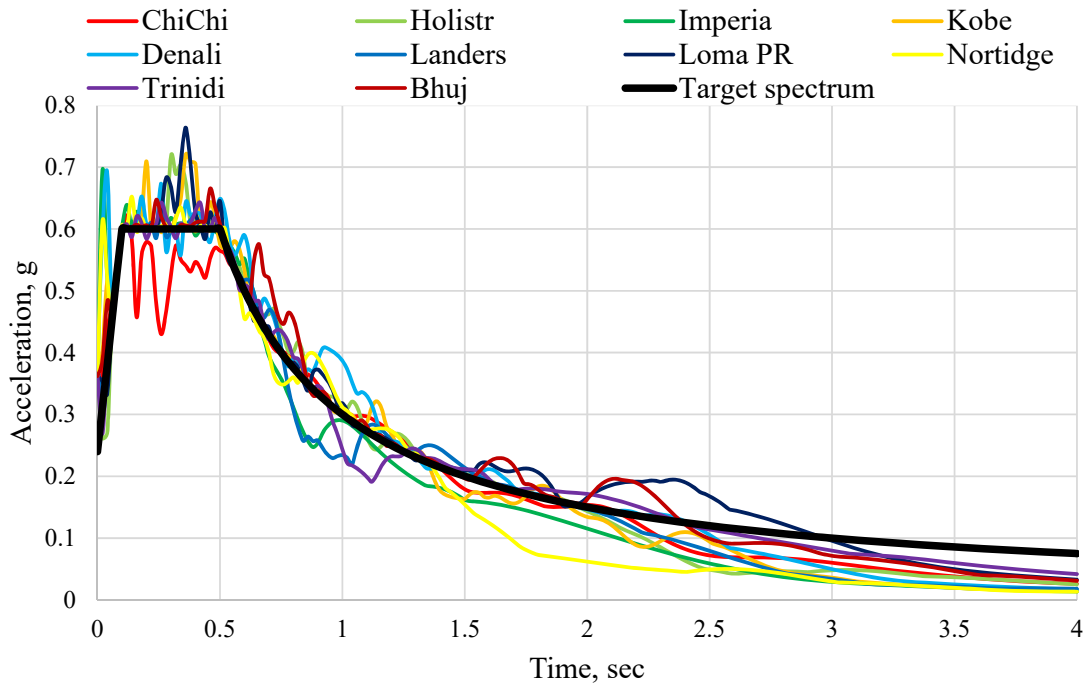


Fig 5.16: Scaled Response Spectrum- 2475 Years.

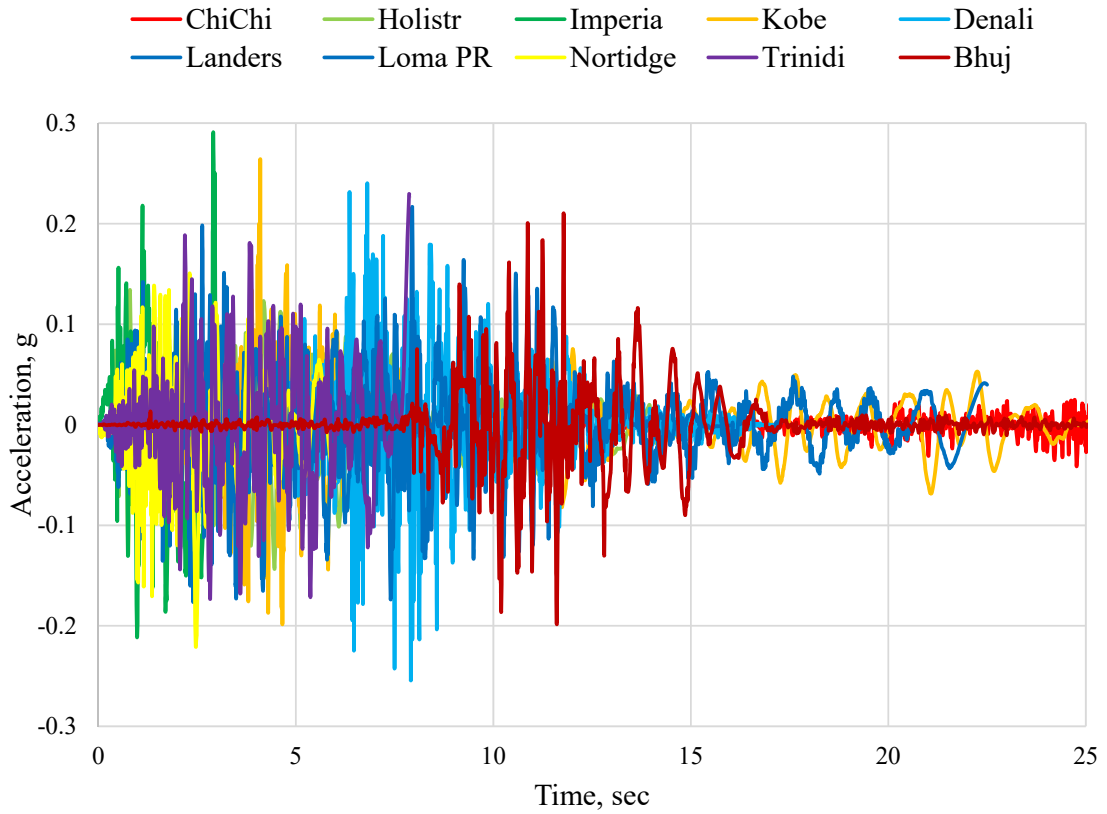


Fig 5.17: Scaled Time history function- 475 Years.

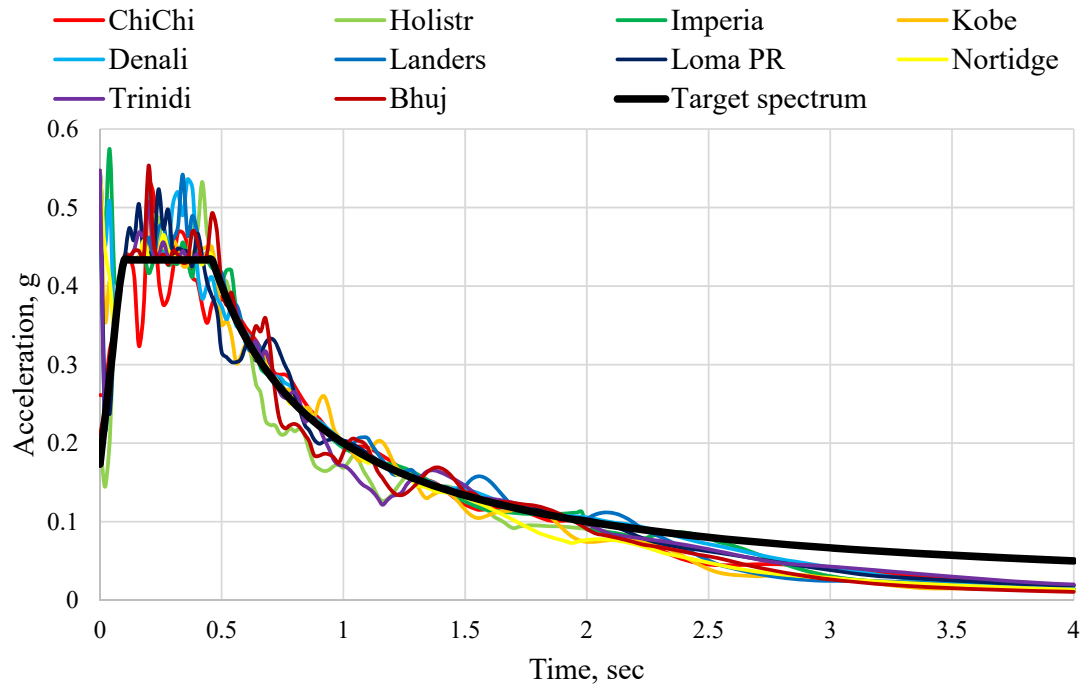


Fig 5.18: Scaled Response Spectrum- 475 Years.

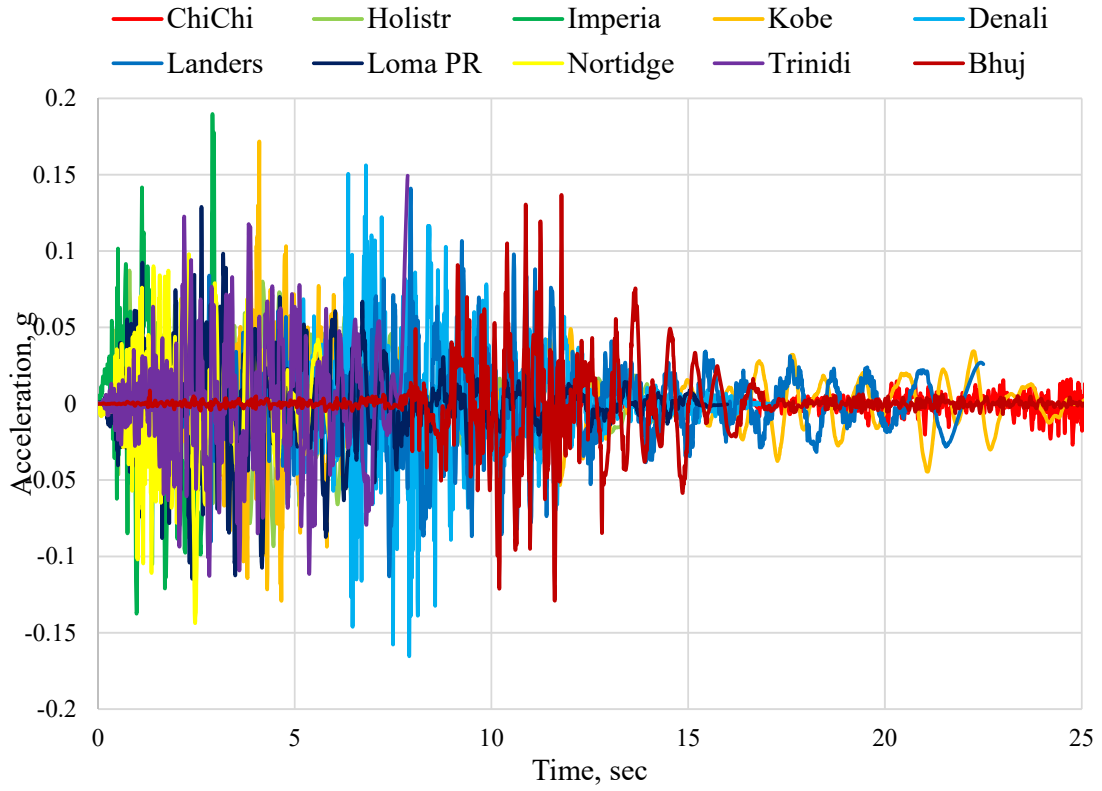


Fig 5.19: Scaled Time History Function- 43 Years.

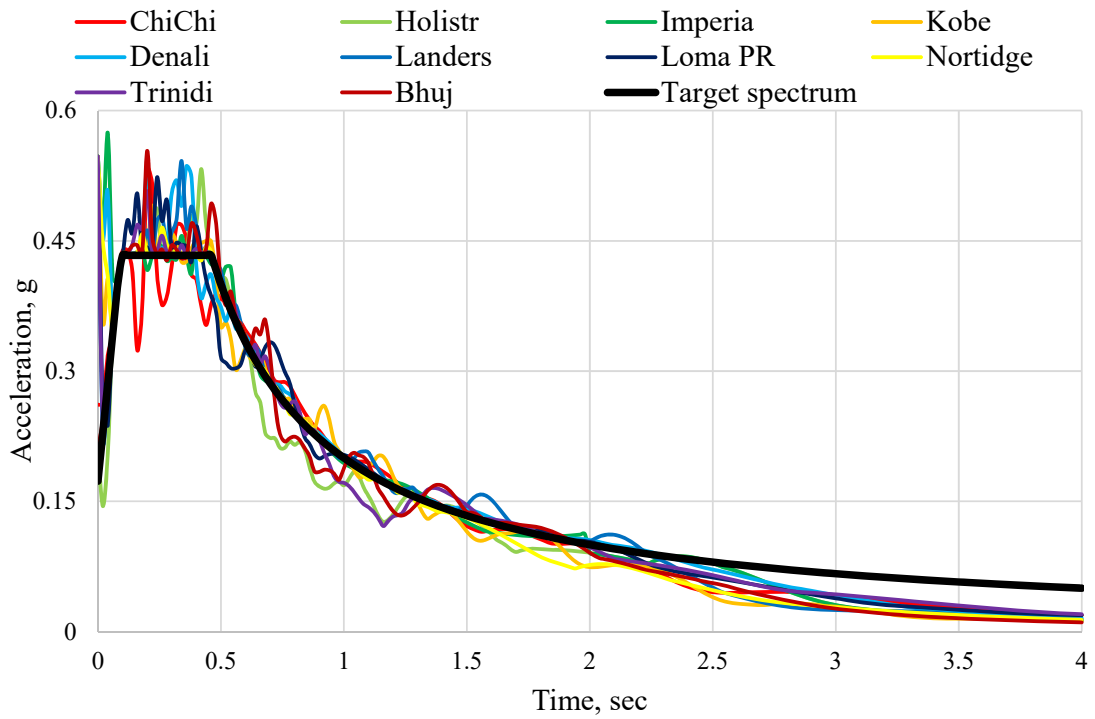


Fig 5.20: Scaled Response Spectrum- 43 Years.

5.10 Interpretation of Result for Performance-Based Analysis

Non-Linear Time History (NLTH) analysis includes ground motion with Period. Putting the Ground motion into NLTHA enables us to get seismic demand. It reflects the displacements demand of the structure due to the ground motion. Time history analysis uses the time history of input force or acceleration directly, which is then united to get the response. Based on the NLTHA following observations are made:

5.10.1 Base Shear

The base shear comparison from different analyses were made between pre-fire and post-fire conditions for different time history functions, as shown in Fig 5.21~Fig 5.26. The base shear obtained from nonlinear time-history analysis based on ten pairs of ground motions under MCE earthquake level was highest whereas that obtained from SLE earthquake level had lowest base shear. Moreover, the figure clearly shows that the base shear obtained from Trinidad & Hollister is considerably higher than resulting from other GMs. The maximum base shear of different GMs for pre and the post-fire condition is 60599 KN & 62532 (SLE); 144156 KN & 145426 KN (DBE), and 184393 KN & 187944 KN (MCE), respectively.

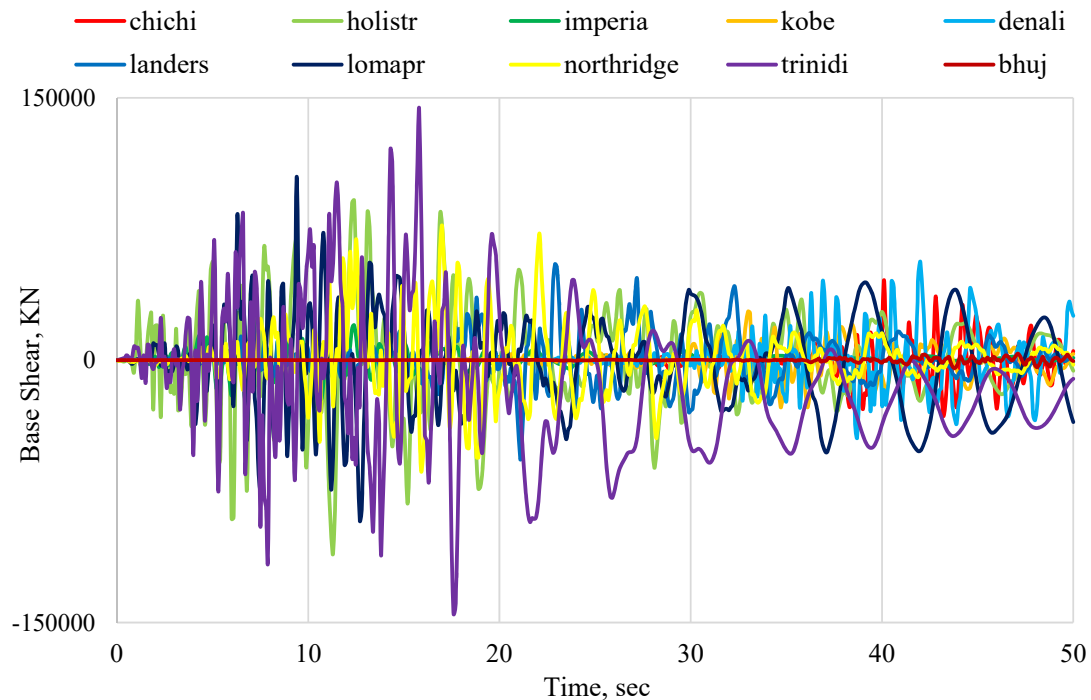


Fig 5.21: Base shear at different GMs for pre-fire MCE condition.

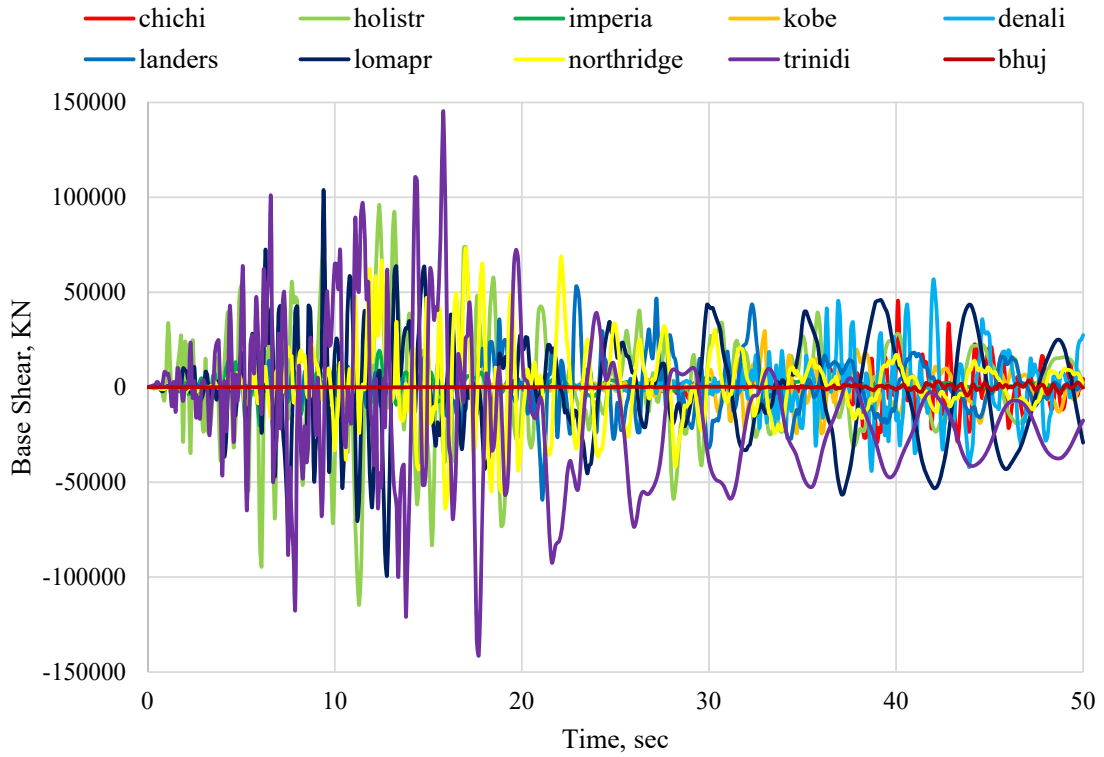


Fig 5.22: Base shear at different GMs for post-fire MCE condition.

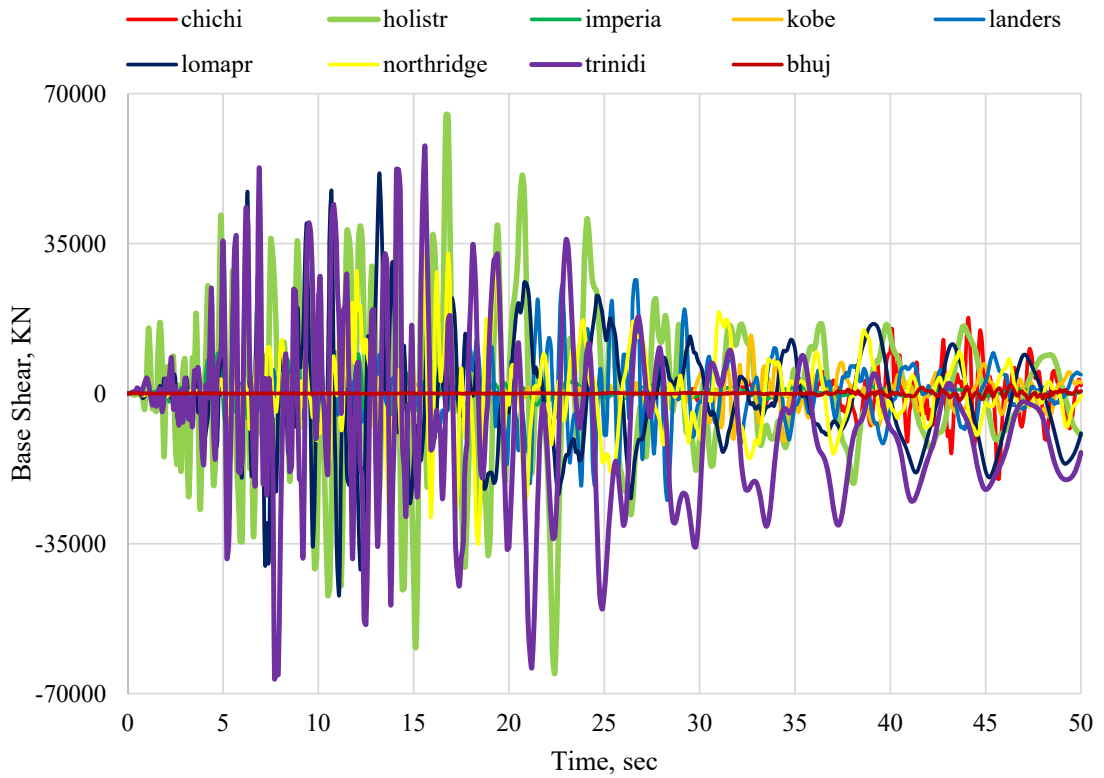


Fig 5.23: Base shear at different GMs for pre-fire DBE condition.

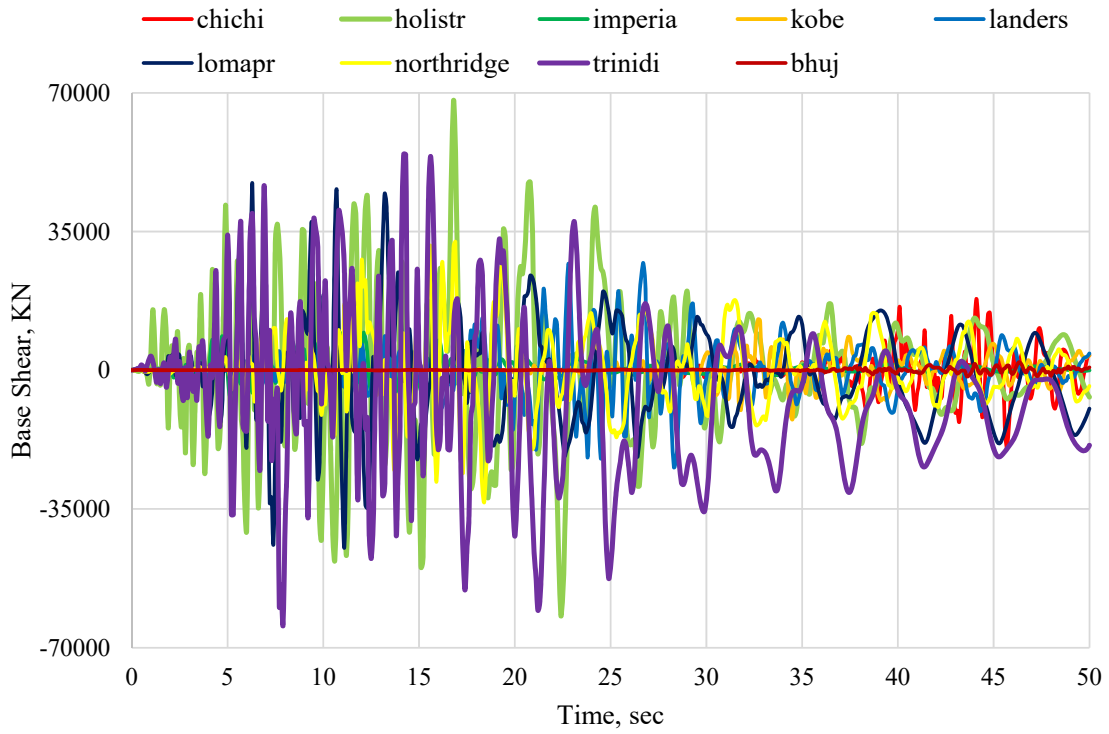


Fig 5.24: Base shear at different GMs for post-fire DBE condition.

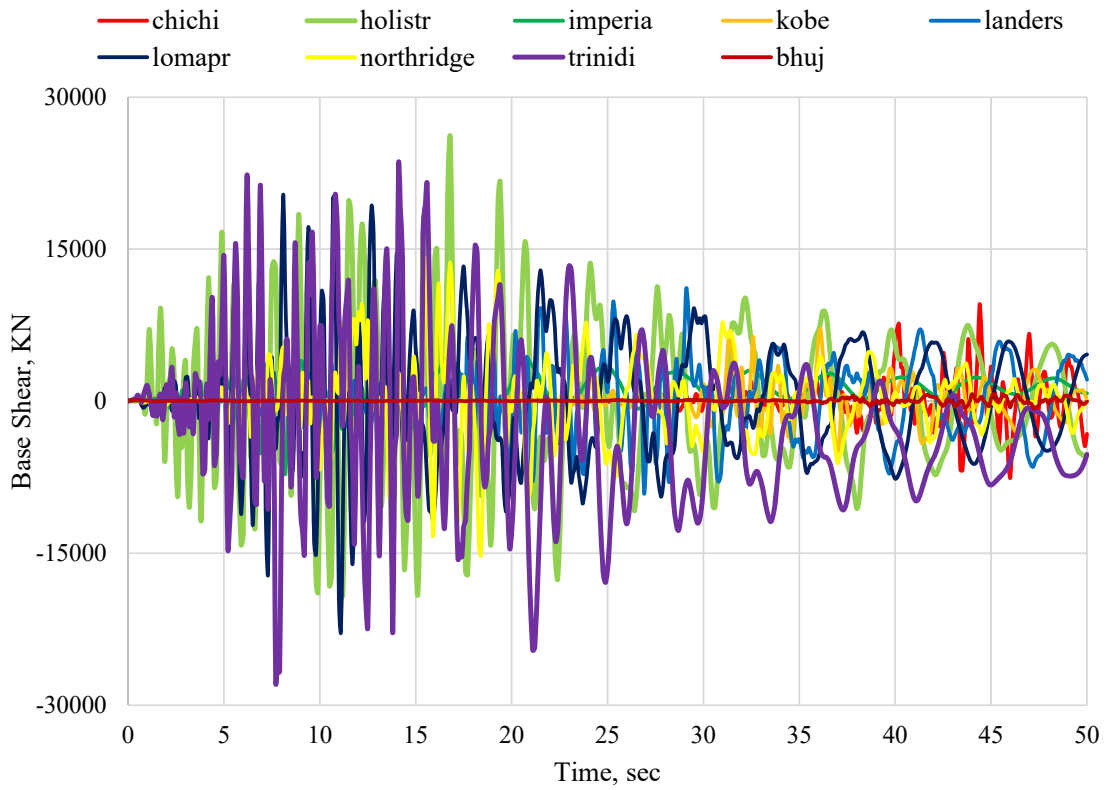


Fig 5.25: Base shear at different GMs for pre-fire SLE condition.

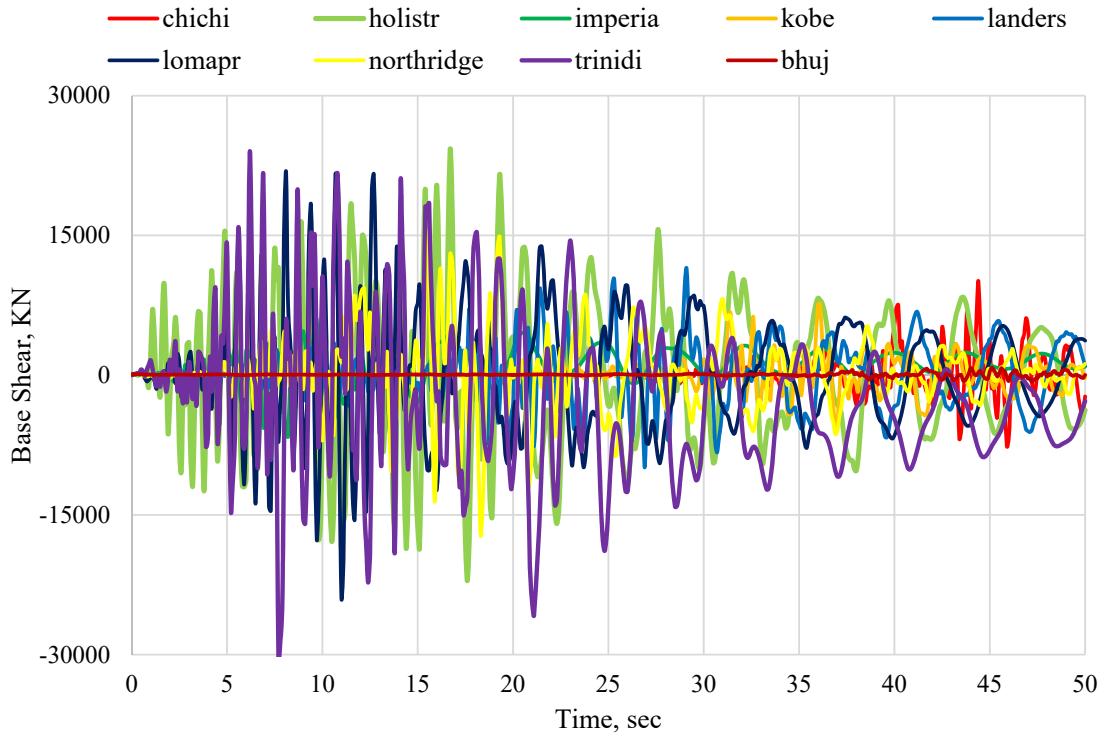


Fig 5.26: Base shear at different GMs for post-fire SLE condition.

5.10.2 Drift Ratio

The storey drifts of the structure for different ground motions are presented in Fig 5.27. The largest inter-storey drift is observed for Trinidad. Inter-storey drift ratio increased at 7th, 8th, and 9th due to the fire effect. The average inter-storey transient drift ratio values of each analysis for assessment of service level (SLE) and collapse prevention level (MCE) is 0.3% and 2.7% respectively. As per ASCE 41-13 the allowable limit states to check the performance criteria of the of structure service level (SLE) and collapse prevention level (MCE) is <0.5% and <4.5% respectively. The difference in behavior among different earthquakes is further appreciated by referring to Fig 5.28 to Fig 5.29

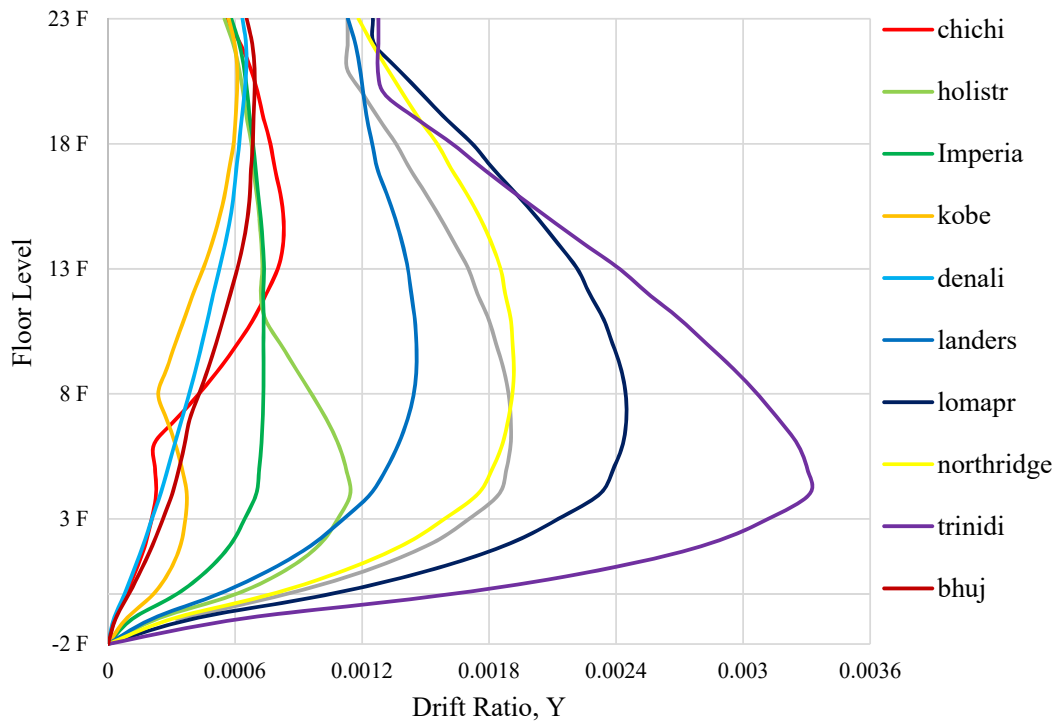
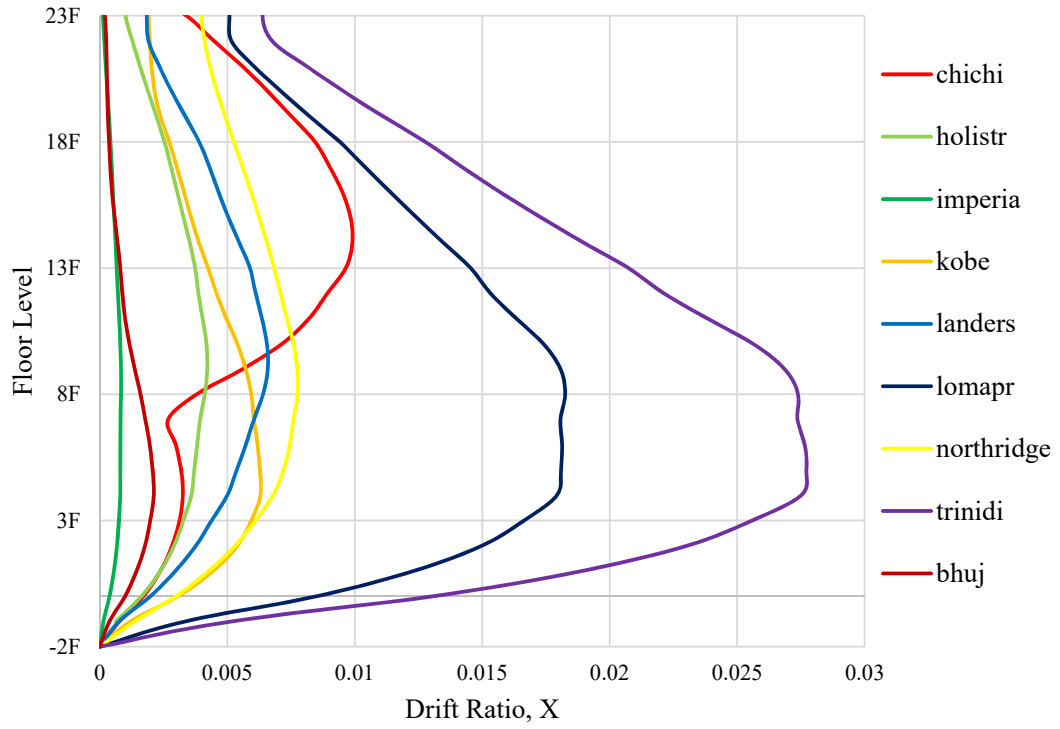


Fig 5.27: Storey drift ratio for different GMs (post-fire MCE condition).

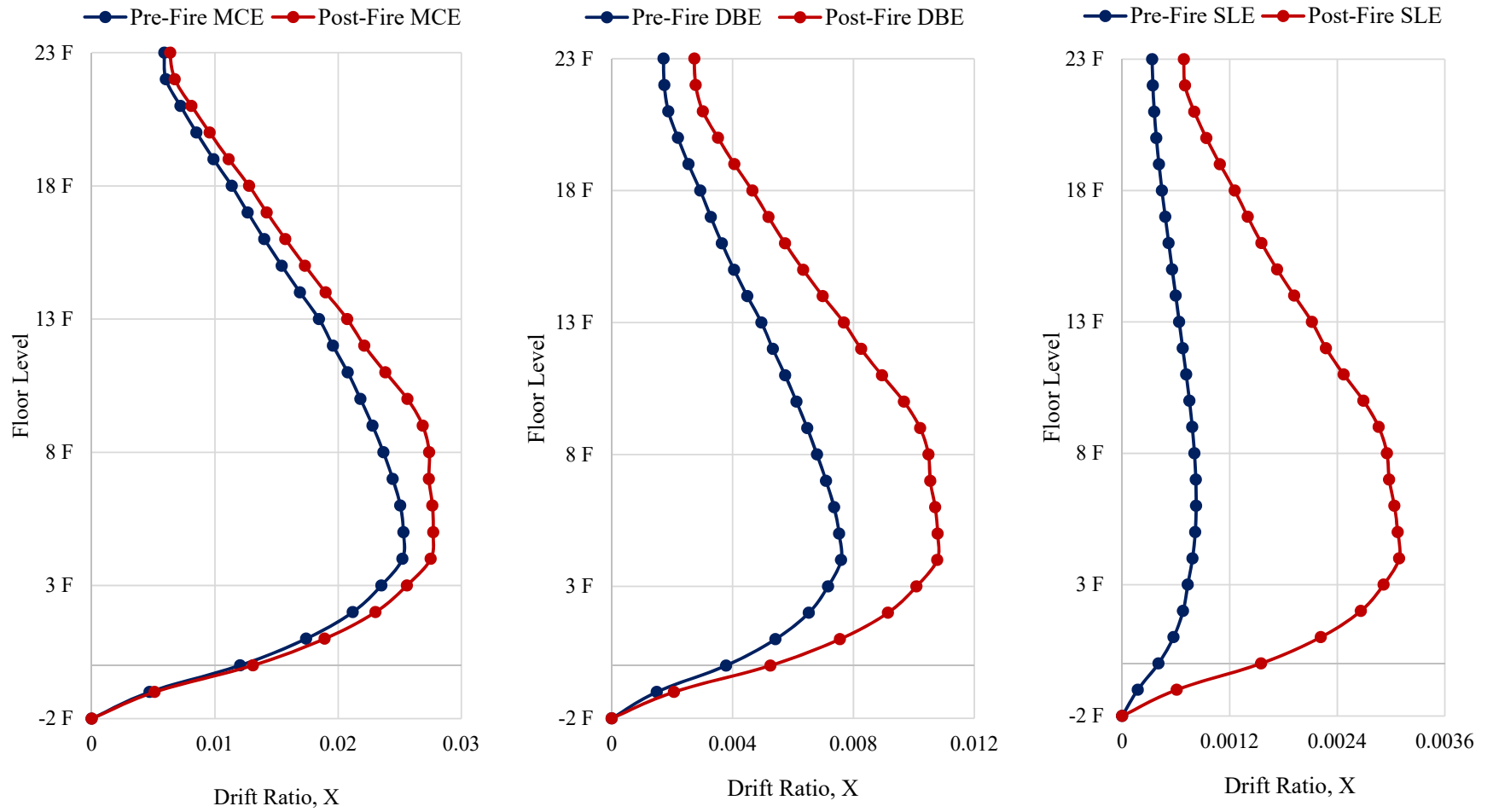


Fig 5.28: Maximum storey drift ratio in the X direction for MCE, DBE & SLE condition (for Trinidad GMs).

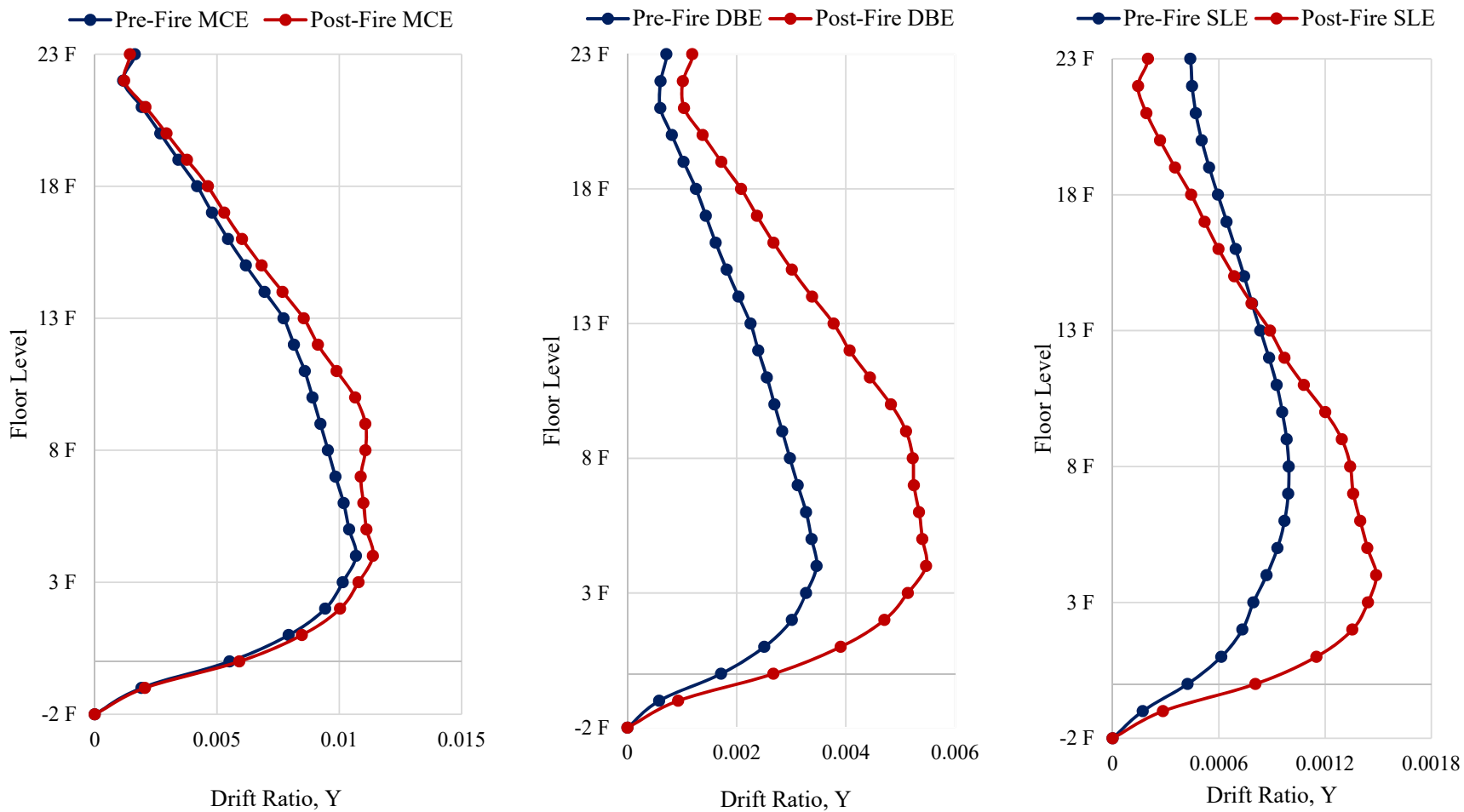


Fig 5.29: Maximum storey drift ratio in the Y direction for MCE, DBE & SLE condition (for Trinidad GMs).

5.10.3 Concrete and Rebar Stress-Strain Curve

As per the philosophy of the performance-based design approach, concrete and rebar strain is one of the key parameters to determine the internal stress-strain features of the structure. Detailed comparative fiber stress, strain, and states of fibers of a wall at the 7th-floor level are presented in Table 5-10 & Fig 5.40. For fiber hinge states of the shear wall, all hinges are in the range of A to IO state. Maximum fiber strain of shear wall concrete for pre and post-fire conditions is 0.0009 & 0.001 (SLE); 0.0022 & 0.0024 (DBE) and 0.0037 & 0.0043(MCE), respectively. Maximum fiber strain of shear wall rebar for pre and post-fire conditions is 0.00076 & 0.00083(SLE); 0.0015 & 0.0018(DBE) and 0.0036 & 0.0042(MCE), respectively. According to ASCE 41-13, these strain values are also acceptable ($\epsilon_c < 0.005$, $\epsilon_t < 0.05$). Moreover, the strain results of other hinges are also shown in Fig 5.30~Fig 5.35

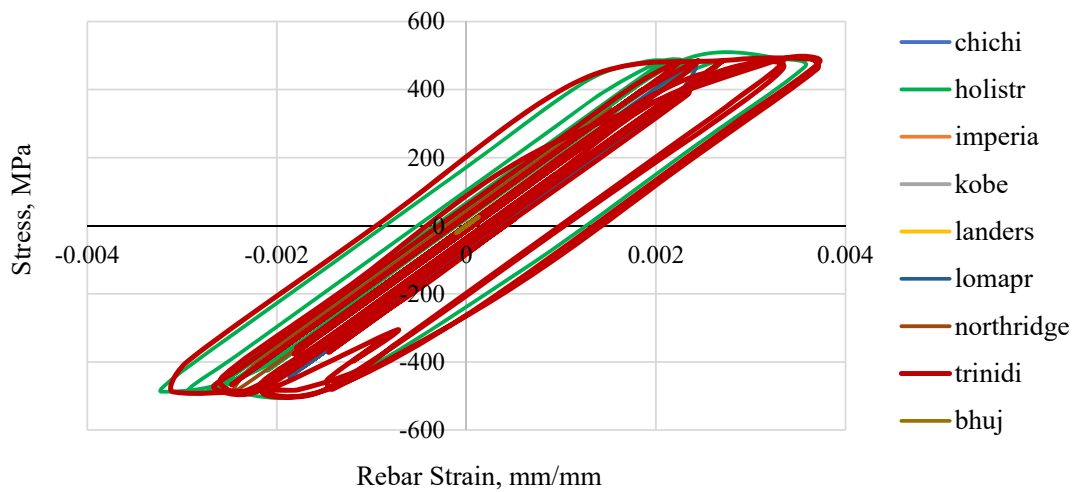


Fig 5.30: Rebar stress-strain curve for hinge W8H19 (7F), fiber-19.

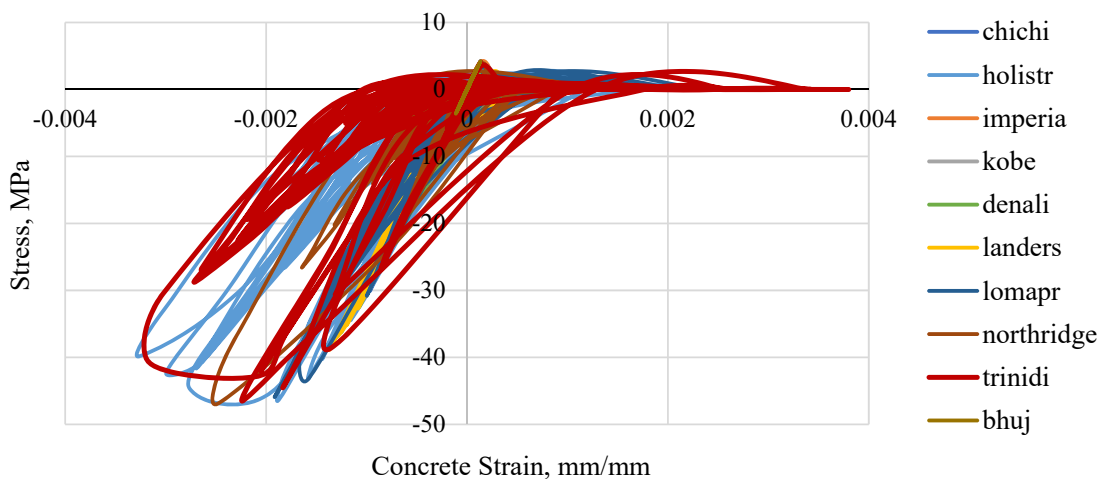


Fig 5.31: Concrete stress-strain curve for hinge W8H19 (8F), fiber-17.

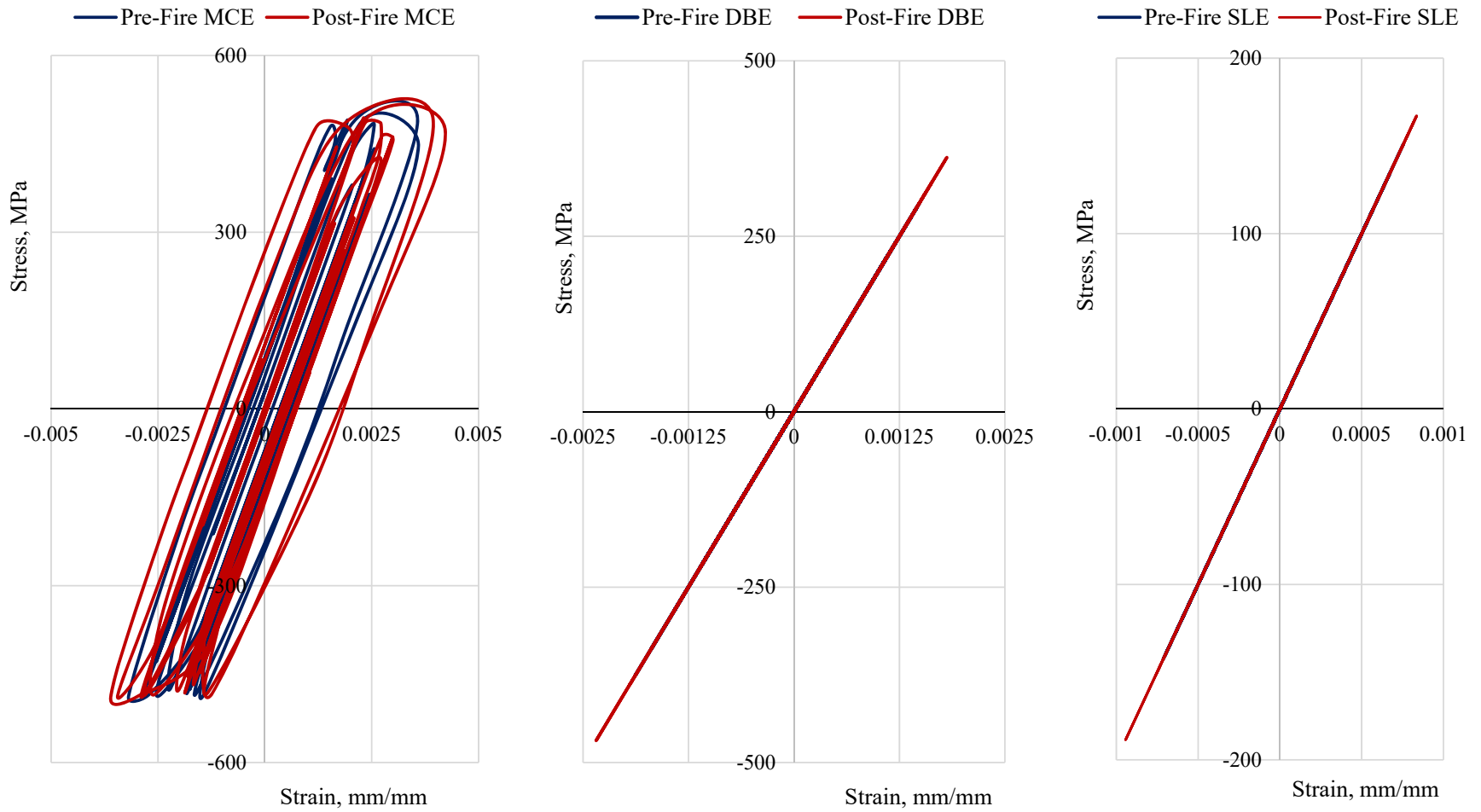


Fig 5.32: Rebar stress-strain curve for hinge W2H18 (8F), fiber-19 for MCE, DBE & SLE condition.

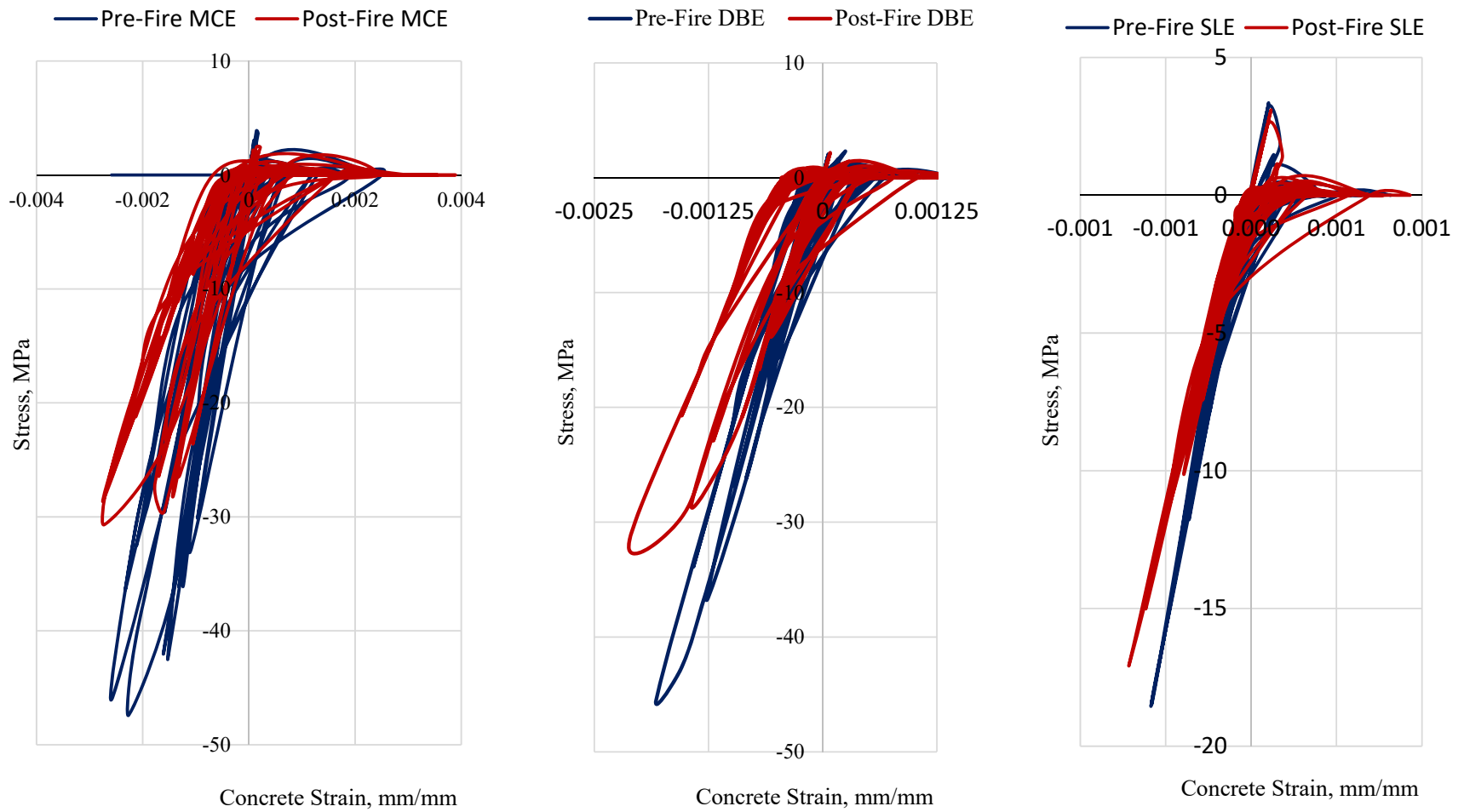


Fig 5.33: Concrete stress-strain curve for hinge W8H19 (7F), fiber-4 for MCE, DBE & SLE condition.

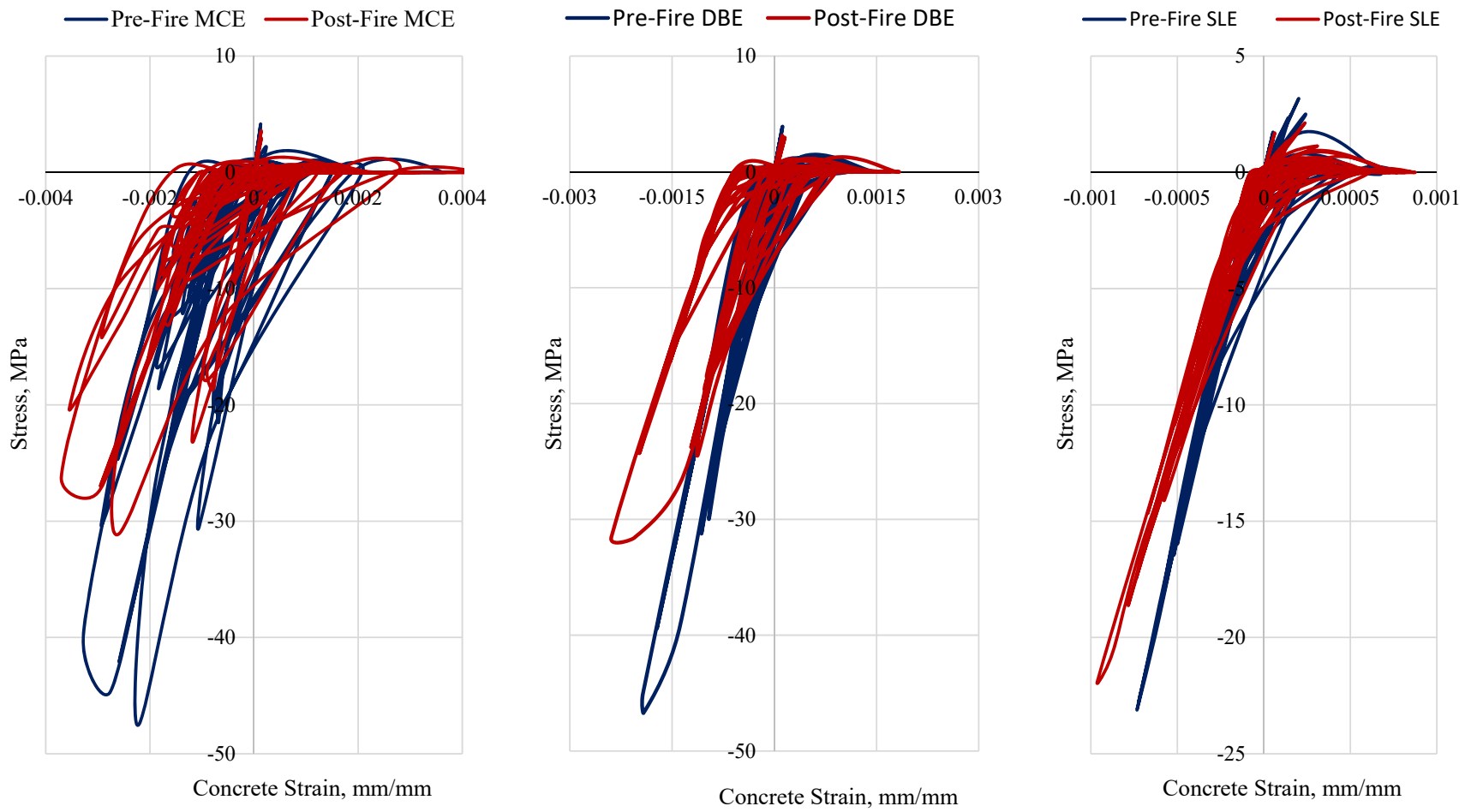


Fig 5.34: Concrete stress-strain curve for hinge W2H18 (8F), fiber-17 for MCE, DBE & SLE condition.

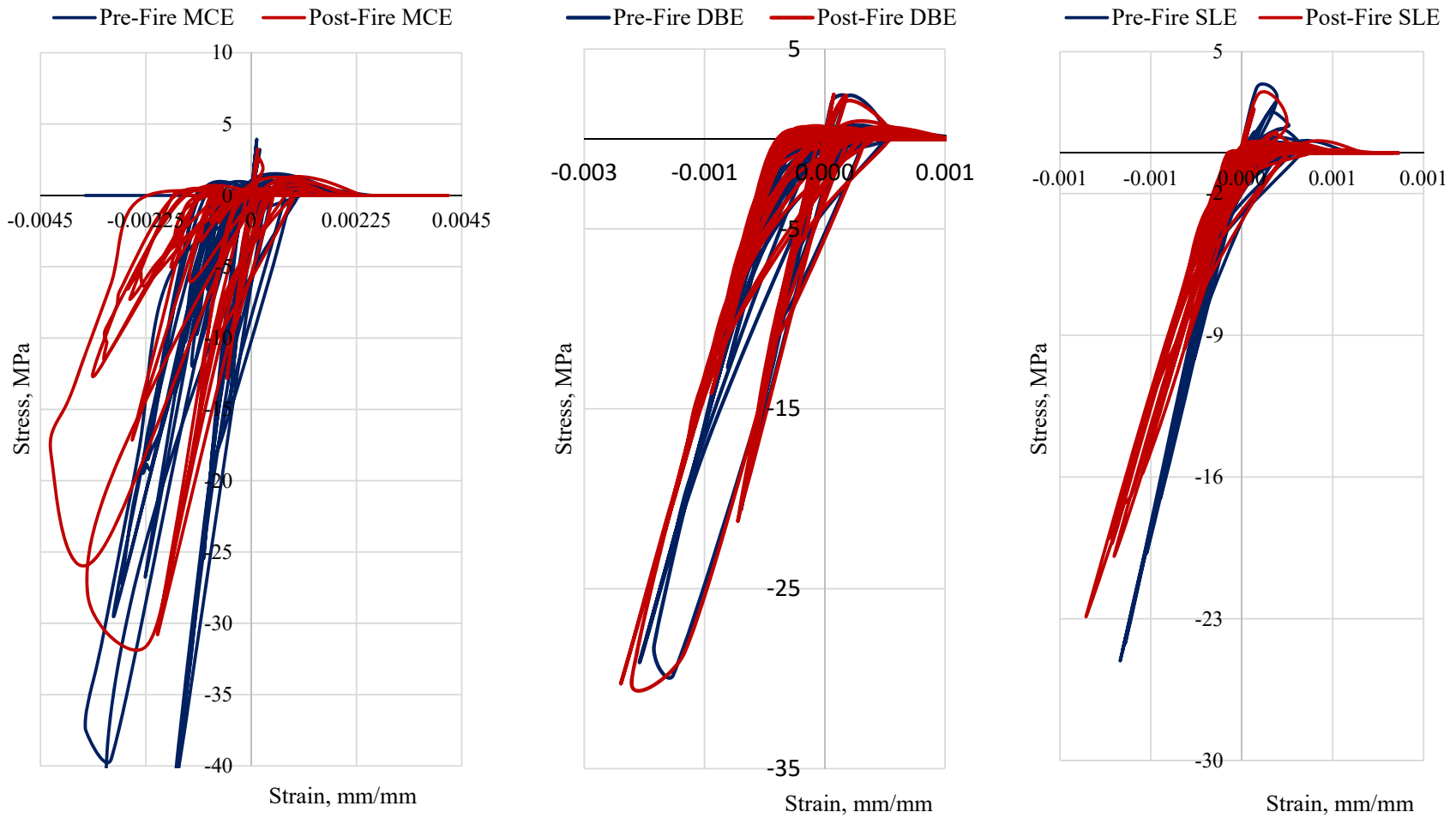


Fig 5.35: Concrete stress-strain curve for hinge W278H16 (9F), fiber-1 for MCE, DBE & SLE condition.

5.10.4 Moment Rotation Curve of Hinges

Hysteretic responses of wall hinges at the seventh, eighth, and ninth-floor levels are presented in Fig 5.37 to Fig 5.39. The colors of different ground motions highlight their hysteretic response regarding moment rotation responses. Maximum hinge rotation of shear wall for pre and post-fire condition is 0.0017 rad & 0.0018 rad (SLE); 0.0041 rad & 0.0045 rad (DBE) and 0.0064 rad & 0.0079 rad (MCE), respectively. The amount of moment carrying capacity of the wall also depends on the size of the wall and its direction to the ground motions.

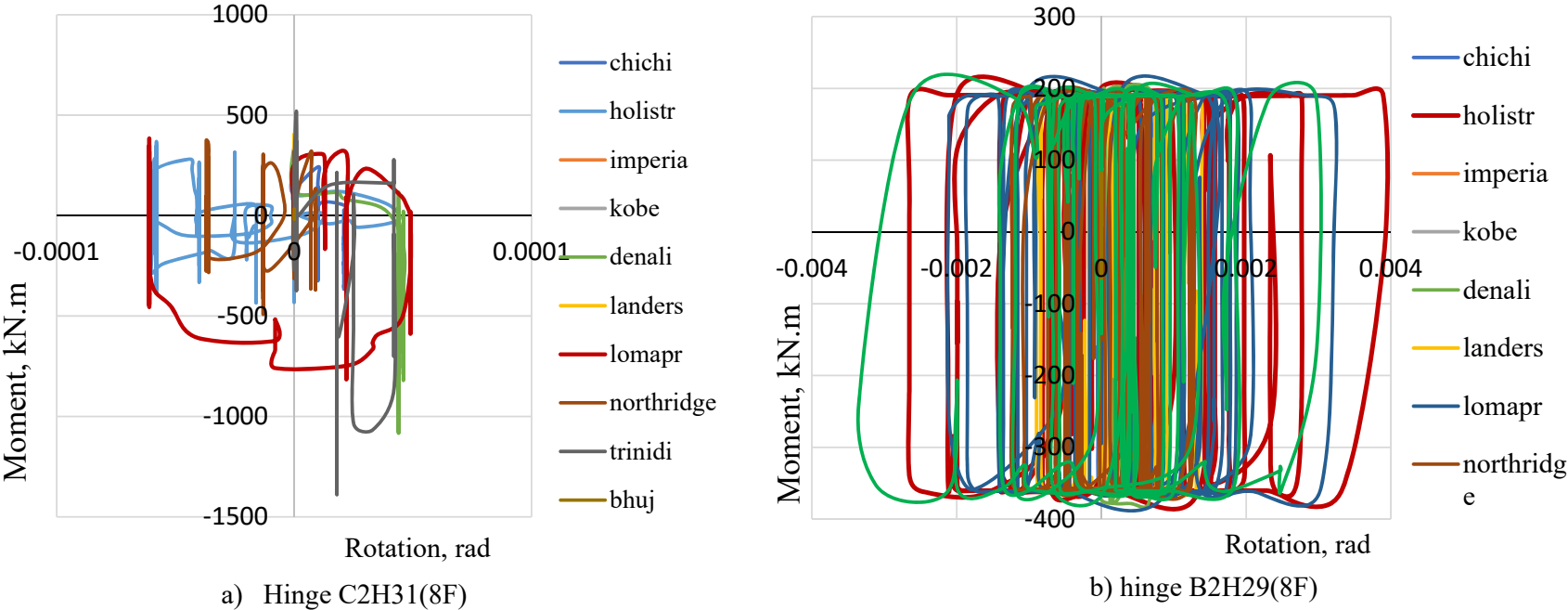


Fig 5.36: Hysteretic Response of Hinge for different GMs.

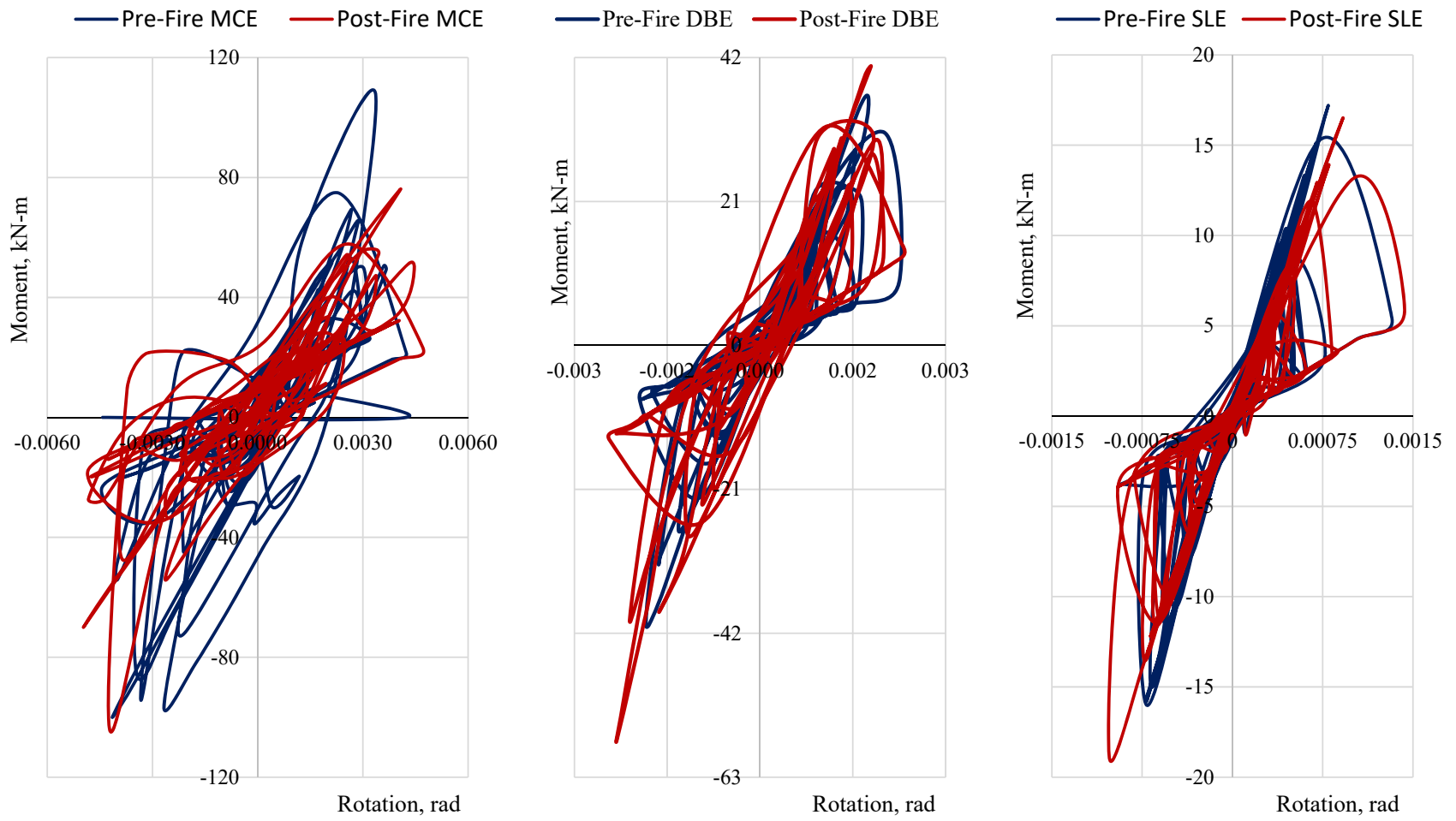


Fig 5.37: Shear wall moment rotation curve for hinge W8H19 (7F), for MCE, DBE & SLE condition.

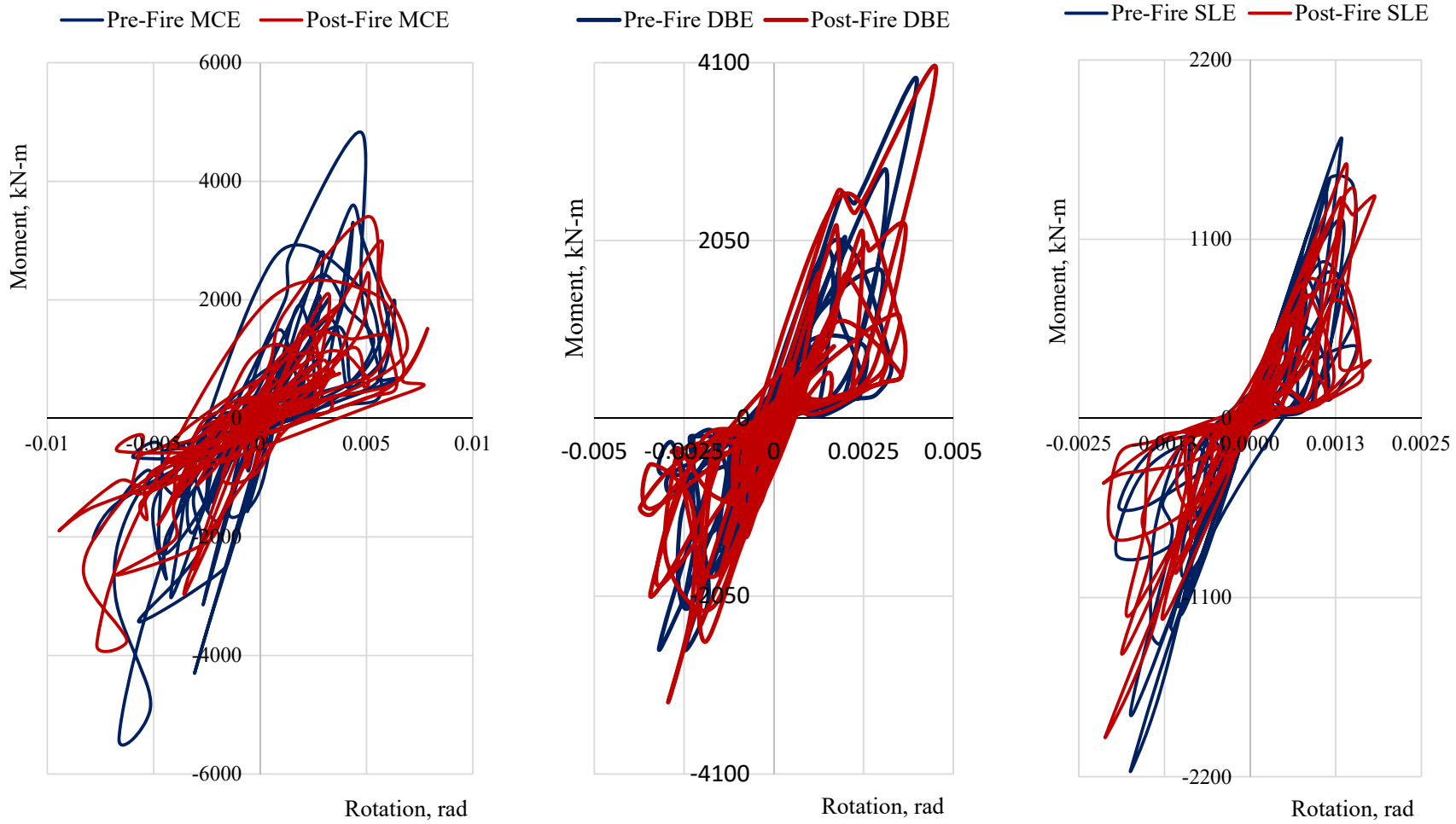


Fig 5.38: Shear wall moment rotation curve for hinge W2H18 (8F), for MCE, DBE & SLE condition.

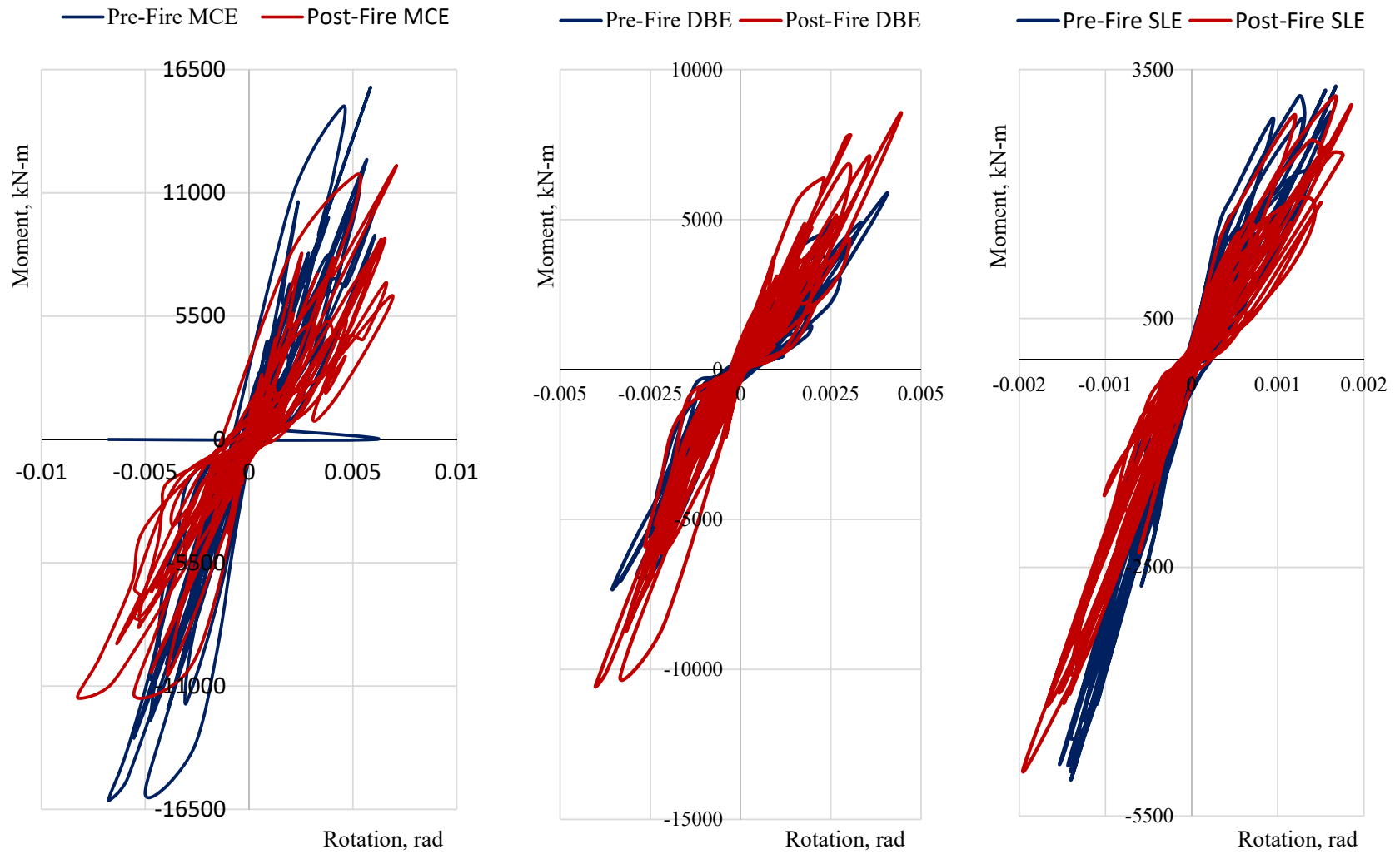


Fig 5.39: Shear wall moment rotation curve for hinge W278H16 (9F), for MCE, DBE & SLE condition.

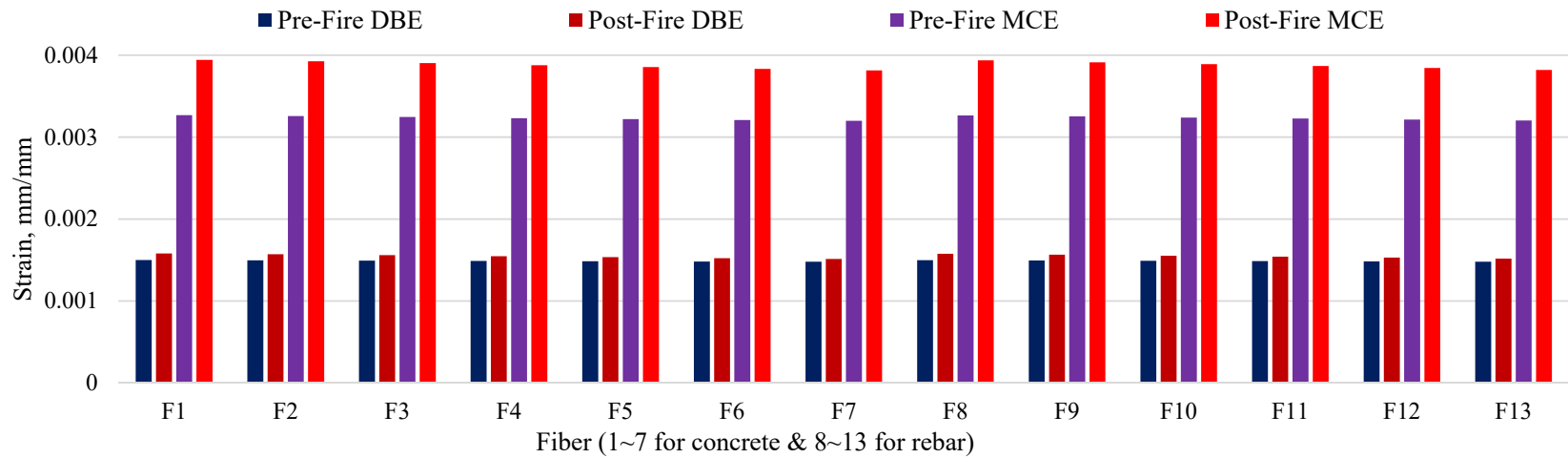


Fig 5.40: Comparative strain for various fibers of concrete and rebar for W8H19 (7F) hinge at MCE & DBE condition.

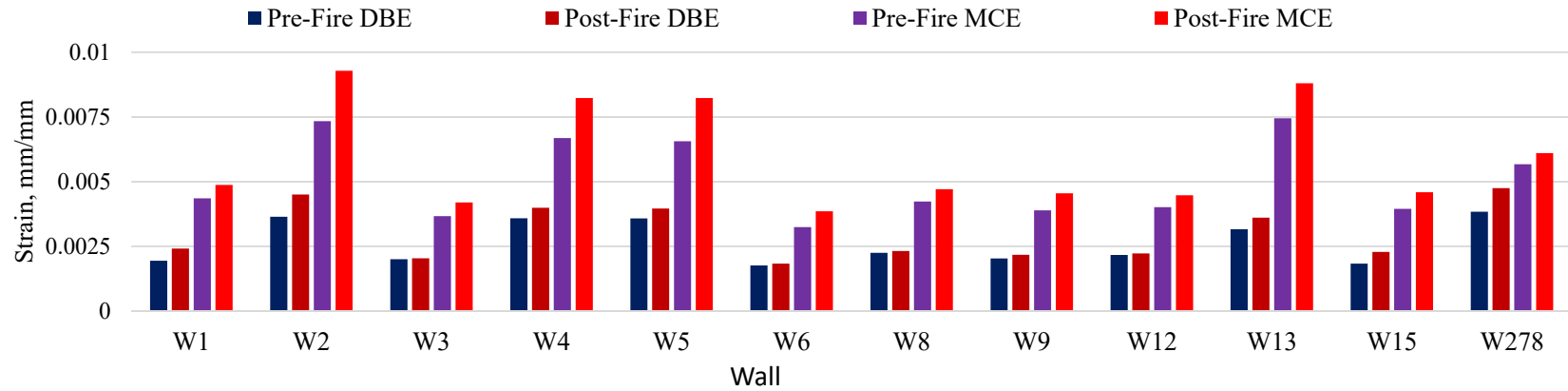


Fig 5.41: Comparative rotation of various wall hinges of 7th floor at MCE & DBE condition.

Table 5-10: Fiber stress and status of hinge-W8H19 (7F)

Fiber No.	Fiber Area	Pre-Fire DBE Condition			Post-Fire DBE Condition			Fiber Strain Increase (%)	Pre-Fire MCE Condition			Post-Fire MCE Condition			Fiber Strain Increase (%)
		Fiber Stress	Fiber Strain	Fiber Status	Fiber Stress	Fiber Strain	Fiber Status		Fiber Stress	Fiber Strain	Fiber State	Fiber Stress	Fiber Strain	Fiber Status	
1	112	2.66	0.00150	A to IO	2.31	0.00158	A to IO	5.4	3.86	0.00327	A to IO	3.12	0.00394	A to IO	20.7
2	224	2.56	0.00150	A to IO	2.27	0.00157	A to IO	5.0	3.94	0.00326	A to IO	2.99	0.00393	A to IO	20.5
3	224	2.42	0.00149	A to IO	2.21	0.00156	A to IO	4.4	4.04	0.00325	A to IO	2.75	0.00390	A to IO	20.2
4	224	2.28	0.00149	A to IO	2.16	0.00155	A to IO	3.9	3.86	0.00323	A to IO	2.42	0.00388	A to IO	20.0
5	224	2.13	0.00149	A to IO	2.1	0.00154	A to IO	3.3	3.67	0.00322	A to IO	2.44	0.00386	A to IO	19.7
6	224	2.01	0.00148	A to IO	2.05	0.00152	A to IO	2.8	3.71	0.00321	A to IO	2.48	0.00383	A to IO	19.5
7	112	2.06	0.00148	A to IO	2.03	0.00151	A to IO	2.4	3.74	0.00320	A to IO	2.51	0.00381	A to IO	19.2
8	8.4	299.56	0.00150	A to IO	315.26	0.00158	A to IO	5.3	487.83	0.00326	A to IO	489.7	0.00394	A to IO	20.6
9	8.4	298.83	0.00150	A to IO	312.87	0.00157	A to IO	4.7	487.77	0.00325	A to IO	489.61	0.00391	A to IO	20.4
10	8.4	298.11	0.00149	A to IO	310.48	0.00155	A to IO	4.2	487.72	0.00324	A to IO	489.53	0.00389	A to IO	20.1
11	8.4	297.39	0.00149	A to IO	308.08	0.00154	A to IO	3.6	487.67	0.00323	A to IO	489.44	0.00387	A to IO	19.9
12	8.4	296.66	0.00148	A to IO	305.69	0.00153	A to IO	3.0	487.61	0.00321	A to IO	489.36	0.00384	A to IO	19.6
13	8.4	295.94	0.00148	A to IO	303.3	0.00152	A to IO	2.5	487.56	0.00320	A to IO	489.27	0.00382	A to IO	19.3

Table 5-11: Hinge state and status of 7th floor wall

Wall	Fiber No.	Fiber Area	Pre-Fire DBE Condition			Post-Fire DBE Condition			Fiber Rotation Increase (%)	Pre-Fire DBE MCE Condition			Post-Fire MCE Condition			Fiber Rotation Increase (%)
			Moment (kN-m)	Rotation (rad)	Fiber Status	Moment (kN-m)	Rotation (rad)	Fiber Status		Moment (kN-m)	Rotation (rad)	Fiber Status	Moment (kN-m)	Rotation (rad)	Fiber Status	
W1	1	112	43	0.0019	A to IO	49	0.0024	A to IO	24.6	71	0.0044	A to IO	67	0.0049	A to IO	12.0
W2	2	224	4645	0.0036	A to IO	3572	0.0045	A to IO	23.5	3154	0.0073	A to IO	3085	0.0093	A to IO	26.6
W3	3	224	2239	0.0020	A to IO	1526	0.0020	A to IO	1.9	1786	0.0037	A to IO	1632	0.0042	A to IO	14.4
W4	4	224	5016	0.0036	A to IO	3793	0.0040	A to IO	11.3	4622	0.0067	A to IO	4795	0.0082	A to IO	23.2
W5	5	224	289	0.0036	A to IO	279	0.0040	A to IO	10.6	708	0.0066	A to IO	769	0.0082	A to IO	25.5
W6	6	224	13643	0.0018	A to IO	8192	0.0018	A to IO	4.1	10372	0.0032	A to IO	10696	0.0039	A to IO	19.0
W8	7	112	48	0.0023	A to IO	41	0.0023	A to IO	3.3	80	0.0042	A to IO	76	0.0047	A to IO	11.2
W9	8	8.4	105	0.0020	A to IO	115	0.0022	A to IO	7.1	135	0.0039	A to IO	169	0.0045	A to IO	16.9
W12	9	8.4	109	0.0022	A to IO	107	0.0022	A to IO	2.3	136	0.0040	A to IO	106	0.0045	A to IO	11.4
W13	10	8.4	10973	0.0032	A to IO	8203	0.0036	A to IO	14.1	9316	0.0074	A to IO	8613	0.0088	A to IO	18.2
W15	11	8.4	159	0.0018	A to IO	118	0.0023	A to IO	24.8	132	0.0040	A to IO	231	0.0046	A to IO	16.3
W278	12	8.4	10169	0.0038	A to IO	9105	0.0047	A to IO	23.5	12016	0.0057	A to IO	12600	0.0061	A to IO	7.6

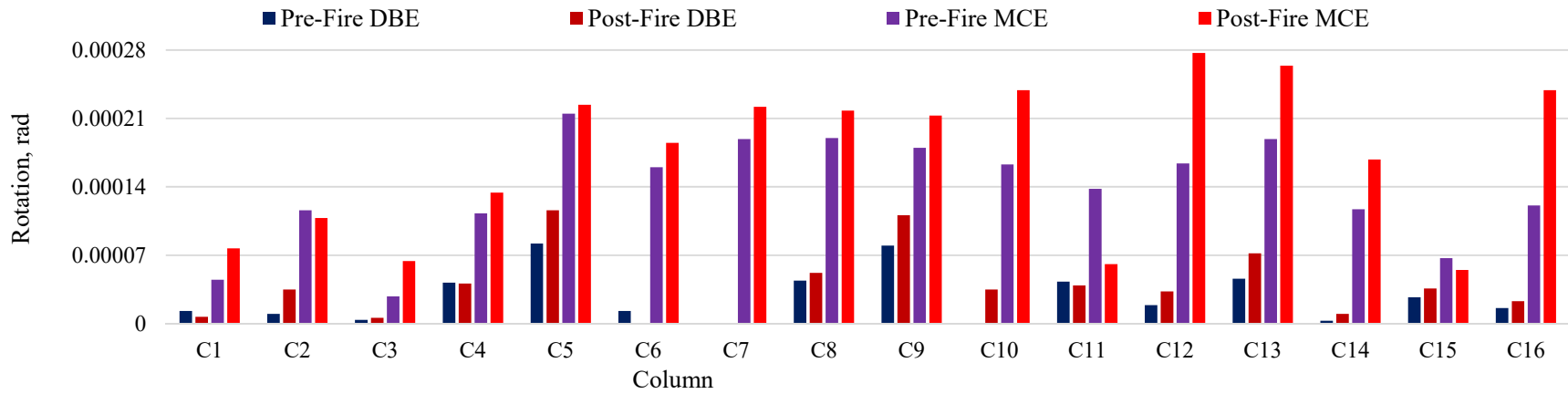


Fig 5.42: Comparatives of column hinge (W8H19-8F) rotation for MCE & DBE condition.

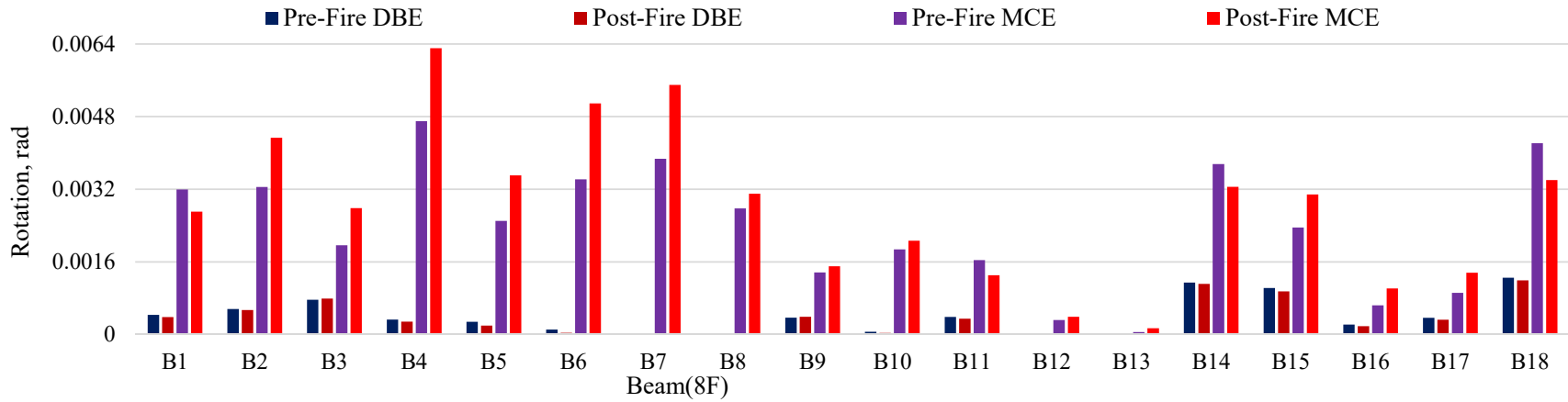


Fig 5.43: Comparatives of beam (8F) hinge rotation for MCE & DBE condition.

5.11 Summary

Full three-dimensional modeling of 23 storied with 02 basement FR tower has been performed by structural analysis software. Forced based design (FBD) has been conducted by the elastic linear analysis for the return periods of 43, 475, and 2475 years, and the corresponding PGA values are 0.13g, 0.2g, and 0.30g. Linear analysis has been performed and the deflection and drift and column PMM ratio for the post-fire condition found as 10-20%, 20-37% and 39-46% increase respectively than the pre-fire condition. Moreover, the global stiffness of the structure has been reduced by 28%.

For the determinations of the structure's nonlinear dynamic response Non Linear Time History analysis have been performed. Mander's hysteresis model for the confined and unconfined concrete, park strain hardening hysteresis model have been applied for NLTHA. The ten devastating earthquake time function has been scaled to the target seismic accelerations. NLTH results have been examined to check the displacement, drift ratio, strain and moment-rotation responses. The strain values compared for the 43 years, 475 years and 2475 years return periods. The maximum concrete strain in the fiber of the shear wall was found 0.0001, 0.0024, and 0.0043 for the 43 years, 475 years, and 2475 years return periods post fire condition. Maximum fiber strain of shear wall rebar for pre and post fire condition is 0.00076 & 0.00083(SLE); 0.0015 & 0.0018(DBE) and 0.0036 & 0.0042(MCE) respectively. The concrete and rebar strain of shearwall were evaluated for the three return periods of the earthquake and found 10-17% strain increase for post-fire condition. Moreover, the drift curve of fire affected floor has been deflected slightly (slope changes from straight line to curve) from the regular floor. Maximum hinge rotation occurred at beam-18 for DBE and beam-4 for MCE condition which indicates 20-34% increase due to fire effect. Moreover, hinge rotation of column and shearwall fiber has been increased noticeably.

CHAPTER 6

CONCLUSIONS AND RECOMMENDATIONS

6.1 Conclusions

In this study, post fire seismic responses of a fire damaged 23 storied commercial building with 2 basements has been evaluated. All identifiable influencing parameters must be taken into consideration for such damage assessment Post-fire structural capacity in terms of strength and serviceability is very crucial for a building as it decides the restoration and rehabilitation of the building. A comprehensive methodology has been presented for the assessment of the residual load-bearing capacity after exposure to fire. The damage states of different component for 7th, 8th and 9th floor of the studied building is determined using on-site visual inspection, non-destructive testing and the removal of concrete core and testing of reinforcement samples for engineering judgment.

Several on-site and laboratory-based techniques are used to aid in the diagnosis of the RCC component's condition. The most direct method of estimating the compressive strength of in situ concrete is performed by testing cores cutting from the structure. ACI 562 has been used to calculate the equivalent concrete core strength. The UPV test is for the estimation of concrete strength based on the relationship between pulse velocity and compressive strength. Carbonation depth is found by spraying a freshly broken/drilled surface with a phenolphthalein indicator.

Inspection of fire-burnt material helps to predict the maximum gas temperature. Finite element analysis has been performed to calculate the fire temperature in association with the visual inspection. The maximum gas temperature has been used to calculate the stress of structural members, developed by the fire effect. Based on the fire stress developed on structural member, material's residual capacity has been calculated and compared. Subsequently, the FBD design has been performed by conducting a linear static analysis following Bangladesh National Building Code 2020.

Linear static analysis has been performed using commercially available finite element analysis software to predict the global displacement, storey drift, and the demand-capacity ratio of concrete columns for the return period of 43, 475, & 2475 years. A series non-linear time

history analysis has been conducted for ten different seismic ground motions that also helped to estimate the base shear, drift ratio, material strain, and hinge rotations for 43, 475, and 2475 years return periods. The limiting value of acceptance criteria was evaluated following the ASCE/SEI 41. The base shear, displacement capacity, and concrete & rebar strain moment rotation have also been evaluated following the acceptance criteria. The performance parameters satisfied the requirements as per the ASCE/SEI 41-13 guide specification. Based on those investigations, the following conclusions can be made:

- a) As per visual inspection, the beam and column capital of slabs are the most significantly damaged structural elements. The concrete cover from several parts of the slabs has split out. The concrete clear covers of the slab and its reinforcement were exposed and visible in many places on the fire-damaged floors. Structural members like columns, walls, beams, and slabs were cracked because of the thermal expansion and some explosions that occurred during the fire. Also, the plaster of the building was damaged slightly because of the temperature rise. Thermal expansion of the materials caused visible vertical deformation to iron or aluminum expansion joints.
- b) The damage classification chart presents the damage intensity or damage level in the different fire-affected areas of the building. The damage intensity shows that the entire area of the floors is affected by the fire as there is no zero damage zone, nearly 72% of the 7th-floor roof, 80% of the 8th-floor roof, and 75% of the 9th-floor roof are burnt moderately (damage rating 0 to 2) and 28% of the 7th-floor roof, 20% of the 8th-floor roof, and 25% of the 9th-floor roof are damaged at different intensities (damage rating 3 to 5) for both structural and non-structural components. Moreover, severe damages on the structural components have been observed at 5% on the 7th and the 9th-floor roofs, which is nearly 8% for the 8th-floor roof.
- c) The average concrete compressive strength of the damaged columns was reduced by as high as 33% of the actual strength (lower on the surface, higher towards the center). In the damaged section of the vertical member, the compressive strength of the concrete was found 24.5 MPa which is less than the undamaged section of strength of 36.6 MPa. In addition, the compressive strength of several samples taken from the damaged sections of horizontal members (beam and slab) is found 23.5 MPa

which is also lower than the undamaged strength of 30.3 Mpa. Moreover, the rebar tensile strength testing shows that the strength is reduced by 15 % approximately. This may indicate that the quality of the concrete is lower than that stated for the pre-fire condition . Furthermore, the maximum carbonation depth was 38 mm, indicating the concrete damage by fire.

- d) The parametric method has been used to estimate the maximum gas temperature numerically using the computer program FIN EC software. The maximum gas temperature is 1047.4°C, and the fire is ventilation controlled. A heat transfer analysis is performed to determine the temperature distribution across the cross-section (i.e., the thermal gradient in the element). Using the developed temperature across the cross-section, residual concrete compressive strength has been calculated using the Euro code. The residual concrete compressive strength of the fire-damaged column has been calculated as 24.7 MPa, which is close to concrete core equivalent compressive strength for damage condition.
- e) A decrease in the cross-section area of the beams and column capitals is observed. The bond between longitudinal reinforcement and concrete decreases because of the spalling and removal of concrete cover. Considering the bond loss between concrete and reinforcement with the decrease in the material strength, the load-carrying capacities of the beams and slabs decreased. Capacity reductions of 11-12% and 26-27% are observed from the moment-curvature and column interaction diagram, respectively.
- f) The deflection and inter-storey drift ratio of the fire-affected stories of the building has been increased by 10-20% and 26-37 %, respectively. Ultimate displacements were achieved at around a 2.7 % drift ratio at the fire-exposed floor. The global stiffness of the building has been reduced by up to 26% in post-fire conditions. The stiffness of the structure decreased with fire exposure due to the decrease in elastic modulus and tensile strength of concrete after fire exposure. The fire event causes the stability loss of the structure.
- g) The demand capacity ratio of column and shear wall has been found beyond the allowable limit (>1) in some cases. This may be occurred due to loss of stiffness and strength of concrete and reinforcements.
- h) The maximum base shear of different GMs for pre and the post-fire condition is 60599 KN & 62532 (SLE); 144156 KN & 145426 KN (DBE), and 184393 KN &

187944 KN (MCE), respectively. The base shear obtained from nonlinear time-history analysis based on ten pairs of ground motions under the MCE earthquake level was found to 3 times and 1.3 times higher than SLE and DBE earthquake levels, respectively. Moreover, it has been found that the base shear obtained from Trinidi & Holistr ground motion is considerably higher than all other GMs.

- i) Based on the performance-based design approach, the concrete and rebar strains are key parameters that indicate the hinge states of the structural elements in the range of A to IO state. Maximum fiber strain of shear wall concrete for pre and post-fire conditions is 0.0009 & 0.001 (SLE); 0.0022 & 0.0024 (DBE) and 0.0037 & 0.0043(MCE), respectively. Maximum fiber strain of shear wall rebar for pre and post-fire conditions is 0.00076 & 0.00083(SLE); 0.0015 & 0.0018(DBE) and 0.0036 & 0.0042(MCE), respectively. According to ASCE 41-13, these strain values are also within the acceptable ($\epsilon_c < 0.005$, $\epsilon_t < 0.05$) limit.
- j) Hysteretic responses of wall hinges affect the hinge rotation. Maximum hinge rotations of shear wall for pre and post-fire conditions are 0.0017 rad & 0.0018 rad (SLE); 0.0041 rad & 0.0045 rad (DBE) and 0.0064 rad & 0.0079 rad (MCE), respectively.

This study is an effort to illustrate an standard procedure to assess the fire damaged buiding in a seismic zone. The outcomes of the study may helps the stakeholders to understand the structural performance level at difference seismic levels and hence take strategic decisions as per their requirement and applications.

6.2 Limitation

The effects of a fire on a building may not be immediately apparent, and some damage may be hidden from view. For example, the fire may have weakened the structural elements of the building, but this damage may not be visible without extensive testing or examination. In some cases, the data used for the analysis may be incomplete or inaccurate. The extent of the fire and the resulting damage may not be fully known, which can make it difficult to accurately assess the structural integrity of the building. The severity and duration of the fire can vary widely depending on a number of factors, including the fuel source, the

location of the fire, and the response time of the fire department. These variables can make it difficult to predict the impact of the fire on the building. The properties of building materials, such as concrete and steel, can be affected by high temperatures. However, the exact extent of this effect may not be known, and there may be variability in how different materials respond to fire. The analytical methods used for post-fire seismic analysis may have limitations, particularly when it comes to predicting the behavior of complex structures or systems. Additionally, the accuracy of the analysis may be influenced by the assumptions made about the building's geometry, material properties, and other factors.

6.3 Recommendations for Future Research

This presented study proposed a systematic way for analyzing structure in a post-fire earthquake (PFE) scenario. It developed appropriate schemes of analysis for the post-fire seismic (PFS) performance of an RC high-rise commercial building. However, the study presented here is limited and needs to be expanded to estimate a more realistic fire temperature. The study included 2D fire analysis for two types of structural members, i.e., column & beam. The 3D modeling of such structures would be the more appropriate way to extend this study to understand the behavior of fully developed fire.

Moreover, using the performance-based framework, it is possible to determine the structure's potential repair and retrofitting cost under a potentially seismic event. The research can be extended to the collapse fragility and repair cost using the performance-based framework. Regional data has to be made available to estimate the repair cost and construction time properly.

REFERENCES

- ACI 318-08, (2008). Building code requirements for structural concrete (ACI 318-08) and commentary. American Concrete Institute. Farmington Hills, Michigan, USA
- Ada, M., Yüzer, N. and Ayvaz, Y. (2019). Postfire damage assessment of a rc factory building. *Journal of performance of constructed facilities*, 33(5), p.04019047.
- Agrawal, A. and Kodur, V. (2020). A novel experimental approach for evaluating residual capacity of fire damaged concrete members. *Fire Technology*, 56, pp. 715-735.
- Al-Rousan, R. (2020). Optimum endurance time of reinforced concrete one way slab subjected to fire. *Procedia Manufacturing*, 44, pp. 520-527.
- Arioz, O. (2007). Effects of elevated temperatures on properties of concrete. *Fire Safety Journal*, 42(8), pp. 516-522.
- Aseem, A., Latif, B. W., Khushnood, R. A. and Mushtaq, A. (2019). Structural health assessment of fire damaged building using non-destructive testing and micrographical forensic analysis: A case study. *Case Studies in Construction Materials*, 11, p. e00258.
- Bamonte, P. and Gambarova, P. (2014). Properties of concrete subjected to extreme thermal conditions. *Journal of structural fire engineering*, 5(1), pp. 47-62.
- Bangladesh National Building Code (2020). Provisions for structural analysis. Part-VI, Chapter-2, pp. 3093-3185.
- Bangladesh National Building Code (2020). Provisions for structural design. Part-VI, Chapter-6, pp. 3449-3576.
- Bazant, Z. P., Kaplan, M. F. and Bazant, Z. P. (1996). *Concrete at high temperatures: Material properties and mathematical models*. 2nd ed. London: Addison-Wesley.
- Beck, K., Janvier-Badosa, S., Brunetaud, X., Török, Á. and Al-Mukhtar, M. (2016). Non-destructive diagnosis by colorimetry of building stone subjected to high temperatures. *European Journal of Environmental and Civil Engineering*, 20(6), pp.643-655.
- Birely, A. C. and Ni, S. (2016). On the effect of design parameters and boundary conditions on the post-earthquake fire performance of RC structural walls. *Journal of structural fire engineering*, 15(2), pp.803-810.
- Bisby, L. and Stratford, T. (2013). Design for fire of concrete elements strengthened or reinforced with fibre-reinforced polymer: State of the art and opportunities from performance-based approaches. *Canadian journal of civil engineering*, 40(11), pp.1034-1043.
- Bocchini, P., Frangopol, D. M., Ummenhofer, T. and Zinke, T. (2014). Resilience and sustainability of civil infrastructure: Toward a unified approach. *Journal of Infrastructure Systems*, 20(2), pp. 04014004.

- Bratina, S., Saje, M. and Planinc, I. (2007). The effects of different strain contributions on the response of rc beams in fire. *Engineering Structures*, 29(3), pp. 418-430.
- Butler, B. W. (2010). Characterization of convective heating in full scale wildland fires. 6th International Conference on Forest Fire Research, pp. 15-18.
- Cadorin, J. F. and Franssen, J. M. (2003). A tool to design steel elements submitted to compartment fires—ozone v2. Part 1: Pre-and post-flashover compartment fire model. *Fire Safety Journal*, 38(5), pp. 395-427.
- Cadorin, J. F., Pintea, D., Dotreppe, J.C. and Franssen, J.M. (2003). A tool to design steel elements submitted to compartment fires ozone v2. Part 2: Methodology and application. *Fire safety journal*, 38(5), pp. 429-451.
- California Seismic Safety Commission, (1996). Applied Technology Council. Seismic evaluation and retrofit of concrete buildings, Report ATC-40, Redwood City, USA.
- Charleston, J. (1997). NEHRP guidelines for the seismic rehabilitation of buildings (FEMA 273). Building Seismic Safety Council: Washington, DC, USA.
- Chiang, C. H. and Tsai, C. L. (2003). Time–temperature analysis of bond strength of a rebar after fire exposure. *Cement and Concrete Research*, 33, pp. 1651-1654.
- Dahal, P. and Mullen, C. (2021). Incorporation of post-earthquake fire (pef) and subsequent aftershock for performance analysis of steel buildings. *Elsevier in structures*, 33, pp. 3810-3821.
- Desnerck, P., Lees, J. M. and Morley, C. T. (2017). The effect of local reinforcing bar reductions and anchorage zone cracking on the load capacity of rc half-joints. *Engineering Structures*, 152, pp. 865-877.
- Dwaikat, M. B. (2009). Flexural response of reinforced concrete beams exposed to fire. 1st ed. Michigan: ProQuest LLC.
- Elghazouli, A. Y., Cashell, K. A. and Izzuddin, B. A. (2009). Experimental evaluation of the mechanical properties of steel reinforcement at elevated temperature. *Fire Safety Journal*, 44(6), pp. 909-919.
- EN (2002). Eurocode 1991-1-2: Actions on structures. Part 1–2: General actions—actions on structures exposed to fire. European Standards, London.
- EN (2004). Eurocode 1991-1-2: Design of concrete structures-part 1-2: General rules-structural fire design. European Standards, London.
- EN (2010). Eurocode 1991-1-2: Actions on structures–part 1-2: General actions–actions on structures exposed to fire. European Standards, London.
- Felicetti, R. (2014). Assessment of fire damage in concrete structures: New inspection tools and combined interpretation of results. *Proceedings International Conference “Structures in Fire”-SIF14*, pp. 1111-1120.

- FEMA-356, (2000). Pre-standard and Commentary for the Seismic Rehabilitation of Buildings. US Federal Emergency Management Agency Washington, DC, report no. FEMA-356.
- FEMA-450, (2003). Recommended provisions for seismic regulations for new buildings and other structures, part 1: Provisions, federal emergency management agency, Washington, DC, report no. FEMA-450.
- Fletcher, I. A., Welch, S., Torero, J. L., Carvel, R. O. and Usmani, A. (2007). Behaviour of concrete structures in fire. *Thermal science*, 11(2), pp. 37-52.
- Gao, W. Y., Dai, J. G. and Teng, J. G. (2016). Fire resistance of rc beams under design fire exposure. *Magazine of Concrete Research*, 69(8), pp. 402-423.
- Goel, S. C., Liao, W. C., Reza Bayat, M. and Chao, S. H. (2010). Performance-based plastic design (PBD) method for earthquake-resistant structures: An overview. *The structural design of tall and special buildings*, 19(1-2), pp. 115-137.
- Gulvanessian, H., Calgaro, J. A. and Holický, M. (2002). Designer's guide to EN 1990: Eurocode: Basis of structural design. Thomas Telford.
- Gunalan, S. and Mahendran, M. (2014). Experimental investigation of post-fire mechanical properties of cold-formed steels. *Thin-Walled Structures*, 84, pp. 241-254.
- Guo, H., Dong, Y. and Gu, X. (2020). Durability assessment of reinforced concrete structures considering global warming: A performance-based engineering and experimental approach. *Construction and Building Materials*, 233, pp. 117251.
- Hager, I. (2013). Behaviour of cement concrete at high temperature. *Archives of Civil Engineering*, 68(2), pp. 79-91
- Hager, I. and Tracz, T. (2010). The impact of the amount and length of fibrillated polypropylene fibres on the properties of hpc exposed to high temperature. *Archives of Civil Engineering*, 56(1), pp. 57-68.
- Han, Y., Xie, Y., Wang, W., Jiang, R. and Yin, K. (2012). Determining the fire-damage temperature of concrete by inclusion decrepitation. *Fire Safety Journal*, 47, pp. 40-45.
- Helmy, A. I. (2003). Fire protection of reinforced concrete columns retrofitted using advanced composite materials. 10th international colloquium on structural and geotechnical engineering, 10th ICSGE, Ain Shams University, Cairo.
- Hertz, K. (1982). The anchorage capacity of reinforcing bars at normal and high temperatures. *Magazine of Concrete Research*, 34(121), pp. 213-220.
- Hertz, K. D. (1998). Limits of spalling of fire exposed concrete: Supporting document for Danish code of practise DS411 chapter 9.
- Hertz, K. D. (2005). Concrete strength for fire safety design. *Magazine of Concrete Research*, 57(8), pp. 445-453.

- Hobbs, B. and Tchoketch, K. M. (2007). Non-destructive testing techniques for the forensic engineering investigation of reinforced concrete buildings. *Forensic Science International*, 167(2-3), pp. 167-172.
- Hsu, T. T., Slate, F. O., Sterman, G. M. and Winter, G. (1963). Microcracking of plain concrete and the shape of the stress-strain curve. *ACI Journal Proceedings*, 60.
- Hsu, T. T., Slate, F. O., Sturman, G. M. and Winter, G. (1963). Microcracking of plain concrete and the shape of the stress-strain curve. *Construction and Building Materials*, 60(2), pp. 209-224
- Huang, Z. (2010). The behaviour of reinforced concrete slabs in fire. *Fire Safety Journal*, 45(5), pp. 271-282.
- IBC (2012a). International Building Code. International Code Council: Washington DC, United States.
- IBC (2012b). International Building Code. International Code Council: Washington DC, United States.
- IBC (2012c). International Building Code. International Code Council: Washington DC, United States.
- Ichinose, T., Kanayama, Y., Inoue, Y. and Bolander, J. E. (2004). Size effect on bond strength of deformed bars. *Construction and Building Materials*, 18(7), pp. 549-558.
- Ioannou, I., Aspinall, W., Rush, D., Bisby, L. and Rossetto, T. (2017). Expert judgment-based fragility assessment of reinforced concrete buildings exposed to fire. *Reliability Engineering & System Safety*, 167, pp. 105-127.
- ISO 834 (1999a). Fire resistance tests-elements of building construction. International Organization for Standardization, Geneva, Switzerland.
- ISO 834 (1999b). Fire resistance tests-elements of building construction. International Organization for Standardization, Geneva, Switzerland.
- Jiang, J., Chen, L., Jiang, S., Li, G. Q. and Usmani, A. (2015). Fire safety assessment of super tall buildings: A case study on shanghai tower. *Case Studies in Fire Safety*, 4, pp. 28-38.
- Julio, R. M. (2001). Linear static seismic lateral force procedures. *The seismic design handbook*, pp. 247-273.
- Kam, W. Y., Pampanin, S. and Elwood, K. (2011). Seismic performance of reinforced concrete buildings in the 22 february christchurch (lyttleton) earthquake (Doctoral dissertation, University of Canterbury).
- Kankanamge, N. D. and Mahendran, M. (2011). Mechanical properties of cold-formed steels at elevated temperatures. *Thin-Walled Structures*, 49, pp. 26-44.
- Khaksefidi, S., Ghalehnovi, M. and Brito, J. D. (2021). Bond behaviour of high-strength steel rebars in normal (nsc) and ultra-high performance concrete (UHPC). *Journal of Building Engineering*, 33, pp. 101592.

- Khoury, G. A. (2000). Effect of fire on concrete and concrete structures. *Progress in structural engineering and materials*, 2, pp. 429-447.
- Kizilkanat, A. B., Yüzer, N. and Kabay, N. (2013). Thermo-physical properties of concrete exposed to high temperature. *Construction and Building Materials*, 45, pp. 157-161.
- Klersfeld, N. and Nordenson, G. (2003). World trade center emergency damage assessment of buildings: Structural engineers association of new york inspections of september and october 2001, Structural Engineers Association of New York.
- Knyziak, P., Kowalski, R. and Krentowski, J. R. (2019). Fire damage of rc slab structure of a shopping center. *Engineering Failure Analysis*, 97, pp. 53-60.
- Kodur, V. (2014). Properties of concrete at elevated temperatures. *International Scholarly Research Notices*, 2014.
- Kodur, V. and Agrawal, A. (2016). An approach for evaluating residual capacity of reinforced concrete beams exposed to fire. *Engineering Structures*, 110, pp. 293-306.
- Kodur, V. K. R. and Agrawal, A. (2017). Effect of temperature induced bond degradation on fire response of reinforced concrete beams. *Engineering Structures*, 142, pp. 98-109.
- Kodur, V. K. R. and Dwaikat, M. (2008). Flexural response of reinforced concrete beams exposed to fire. *Structural Concrete*, 9, pp. 45-54.
- Lange, D., Devaney, S. and Usmani, A. (2014). An application of the peer performance based earthquake engineering framework to structures in fire. *Engineering Structures*, 66, pp. 100-115.
- Lee, J., Choi, K. and Hong, K. (2010). The effect of high temperature on color and residual compressive strength of concrete. *Proceedings of the 7th International Conference on Fracture Mechanics of Concrete and Concrete Structures. High Performance, Fiber Reinforced Concrete, Special Loadings and Structural Applications*, Jeju, South Korea, pp.23-28.
- Lin, W. M., Lin, T. D. and Powers-Couche, L. J. (1996). Microstructures of fire-damaged concrete. *ACI Materials Journal*, 93(3), pp. 199-205.
- Luo, X., Sun, W. and Chan, S. Y. N. (2000). Effect of heating and cooling regimes on residual strength and microstructure of normal strength and high-performance concrete. *Cement and Concrete Research*, 30(3), pp. 379-383.
- Ma, Q., Guo, R., Zhao, Z., Lin, Z. and He, K. (2015). Mechanical properties of concrete at high temperature—a review. *Construction and Building Materials*, 93, pp. 371-383.
- Maio, A., Giaccio, G. and Zerbino, R. (2002). Non-destructive tests for the evaluation of concrete exposed to high temperatures. *Cement, Concrete, and Aggregates*, 24(2), pp. 58-67.
- Malhotra, H. L. (1956). The effect of temperature on the compressive strength of concrete. *Magazine of Concrete Research*, 8(23), pp. 85-94.

- Mostafaei, H., Kashef, A., Sultan, M., McCartney, C., Leroux, P. and Cowalchuk, R. (2014). Resilience of critical infrastructure to extreme fires-gaps and challenges. National Research Council Ottawa, Ontario Canada.
- Mousavi, S., Bagchi, A. and Kodur, V. K. (2008). Review of post-earthquake fire hazard to building structures. *Canadian Journal of Civil Engineering*, 35(7), pp. 689-698.
- Naoshin, N., Alam, D., Medha, N. J. and Akhtar, S. (2020). A study on fire preparedness in kurmitola bihari camp slum, mirpur, dhaka, bangladesh. *IOSR Journal of Humanities and Social Sciences*, 25, pp. 56-60.
- Naser, M. and Kodur, V. (2018). Cognitive infrastructure-a modern concept for resilient performance under extreme events. *Automation in Construction*, 90, pp. 253-264.
- Neves, I. C., Rodrigues, J. P. C. and Loureiro, A. D. P. (1996). Mechanical properties of reinforcing and prestressing steels after heating. *Journal of Materials in Civil Engineering*, 8(4), pp. 189-194.
- Ni, S. (2018). Performance of flexure-controlled reinforced concrete structural walls under sequential fire-earthquake loads, Ph.D. Thesis, Div. of structural engineering, University of Maryland, USA.
- Ni, S. and Gernay, T. (2020). Predicting residual deformations in a reinforced concrete building structure after a fire event. *Engineering Structures*, 202, pp. 109853.
- Ning, F., Mickleborough, N. C. and Chan, C. M. (1999). The effective stiffness of reinforced concrete flexural members under service load conditions. *Australian Journal of Structural Engineering*, 2, pp. 135.
- Okba, S., Helmy, A. I. and Morsy, K. M. (2003). Retrofitting of reinforced concrete columns subjected to fire using advanced composite materials. *Proceedings of International Conference on Performance of Construction Materials in The New Millennium, ICPCM, 18-22 Feb 2003, Cairo, Egypt.* pp. 685-694.
- Osman, M. H., Sarbini, N. N., Ibrahim, I. S., Ma, C. K., Ismail, M. and Mohd, M. F. (2017). A case study on the structural assessment of fire damaged building. *IOP Conference Series: Materials Science and Engineering*, 271, pp. 012100.
- Ozawa, M., Uchida, S., Kamada, T. and Morimoto, H. (2012). Study of mechanisms of explosive spalling in high-strength concrete at high temperatures using acoustic emission. *Construction and Building Materials*, 37, pp. 621-628.
- Pekelnicky, R., Engineers, S., Chris Poland, S. and Engineers, N. (2012). Seismic evaluation and retrofit rehabilitation of existing buildings. *Proceedings of the SEAOC (report ASCE 41-13)*.
- Poliakova, T. and Grigoryan, M. (2018). Fire safety issues in the design and construction of high-rise buildings. *MATEC Web Conf.*, 196.
- Purkiss, J. A. and Li, L. Y. (2013). *Fire safety engineering design of structures*, 3rd ed. Boca Raton: CRC press.

- Qin, D., Gao, P., Aslam, F., Sufian, M. and Al-abdul-jabbar, H. (2021). A comprehensive review on fire damage assessment of reinforced concrete structures. *Case Studies in Construction Materials*, pp. e00843.
- Reifenstein, A. P., Kahraman, H., Coin, C. D. A., Calos, N. J., Miller, G. and Uwins, P. (1999). Behaviour of selected minerals in an improved ash fusion test: Quartz, potassium feldspar, sodium feldspar, kaolinite, illite, calcite, dolomite, siderite, pyrite and apatite. *Fuel*, 78(12), pp. 1449-1461.
- Rodriguez, J., Ortega, L. and Casal, J. (1997). Load carrying capacity of concrete structures with corroded reinforcement. *Construction and building materials*, 11(4), pp. 239-248.
- Ryu, E., Shin, Y. and Kim, H. (2018). Effect of loading and beam sizes on the structural behaviors of reinforced concrete beams under and after fire. *International Journal of Concrete Structures and Materials*, 12(1), pp. 54.
- Schwab, K. and Sala-I-Martin, X. (2010). The global competitiveness report 2010-2011. World Economic Forum, Geneva.
- Shang, X. and Lu, Z. (2014). Impact of high temperature on the compressive strength of ecc. *Advances in Materials Science and Engineering*, 2014, pp. 919078.
- Sharma, A., Bošnjak, J. and Bessert, S. (2019). Experimental investigations on residual bond performance in concrete subjected to elevated temperature. *Engineering Structures*, 187, pp. 384-395.
- Shi, X., Tan, T.-H., Tan, K.-H. and Guo, Z. (2004). Influence of concrete cover on fire resistance of reinforced concrete flexural members. *Journal of Structural Engineering*, 130, pp. 1225-1232.
- Shoukry, S. N., William, G. W., Downie, B. and Riad, M. Y. (2011). Effect of moisture and temperature on the mechanical properties of concrete. *Construction and Building Materials*, 25, pp. 688-696.
- Singh, T. G. and Singh, K. D. (2019). Post-fire mechanical properties of YSt-310 cold-formed steel tubular sections. *Journal of Constructional Steel Research*, 153, pp. 654-666.
- Spinardi, G., Bisby, L. and Torero, J. (2017). A review of sociological issues in fire safety regulation. *Fire Technology*, 53, pp. 1011-1037.
- Subramanian, N. and Geetha, K. (1997). Concrete cover for durable rc structures. *ratio*, 5, pp. 10.
- Tanyildizi, H. and Coskun, A. (2008). Performance of lightweight concrete with silica fume after high temperature. *Construction and Building Materials*, 22(10), pp. 2124-2129.
- Tao, Z., Wang, X.-Q. and Uy, B. (2013). Stress-strain curves of structural steel and reinforcing steel after exposure to elevated temperatures. *Journal of Materials in Civil Engineering*, 25(9), pp. 1306-1316.

- Themelis, S. (2008). Pushover analysis for seismic assessment and design of structures. Ph.D. Thesis, Div. of structural engineering, Heriot-Watt University.
- Topçu, İ. B. and Karakurt, C. (2008). Properties of reinforced concrete steel rebars exposed to high temperatures. *Research Letters in Materials Science*, 2008, p. 814137.
- Topcu, I. B., Boğa, A. R. and Demir, A. (2011). Influence of cover thickness on the mechanical properties of steel bar in mortar exposed to high temperatures. *Fire and Materials*, 35(2), pp. 93-103.
- Torić, N., Boko, I. and Peroš, B. (2013). Reduction of postfire properties of high-strength concrete. *Advances in Materials Science and Engineering*, 2013, p. 712953.
- UBC (1997). Uniform building code. International Conference of Building Officials, Whittier, CA.
- Ünlüoğlu, E., Topçu, İ. B. and Yalaman, B. (2007). Concrete cover effect on reinforced concrete bars exposed to high temperatures. *Construction and Building Materials*, 21, pp. 1155-1160.
- Van-Coile, R. (2015). Reliability-based decision making for concrete elements exposed to fire. Ph.D. Thesis, Div. of structural engineering, Ghent University.
- Van-Coile, R., Caspeele, R. and Taerwe, L. (2015). Reliability-based methodology for determining an equivalent standard fire duration. *International Fire Safety Symposium (IFireSS-2015)*. pp.1-10.
- Varela, J., Tanner, J. and Klingner, R. (2004). Development of response modification coefficient and deflection amplification factors for design of aac structural systems. *Proceedings of 13th World Conference on Earthquake Engineering-12WCEE*, Vancouver, Canada.
- Wakelyn, P., Thompson, D. and Nevius, C. (2006). National fire and building codes and cotton bale storage. *Beltwide Cotton Conferences*, San Antonio, Texas - January 3 - 6, 2006, pp. 689-693.
- Wang, Y. C., Marsden, J. and Kelly, M. (2011). Challenges of fire fighting in fire engineered built environment. *Procedia Engineering*, 11, pp. 583-592.
- Wei, L. and Qing-Ning, L. (2012). Performance-based seismic design of complicated tall building structures beyond the code specification. *The Structural Design of Tall and Special Buildings*, 21(8), pp. 578-591.
- Wickström, U. (1986). A very simple method for estimating temperature in fire exposed concrete structures. *SP Fire Research*.
- Wróblewska, J. and Kowalski, R. (2020). Assessing concrete strength in fire-damaged structures. *Construction and Building Materials*, 254, p. 119122.
- Wróblewski, R. and Stawiski, B. (2020). Ultrasonic assessment of the concrete residual strength after a real fire exposure. *Buildings*, 10(9), p.154.

- Xiao, J., Xie, Q., Li, Z. and Wang, W. (2017). Fire resistance and post-fire seismic behavior of high strength concrete shear walls. *Fire technology*, 53, pp. 65-86.
- Yin, K. F., Han, Y. and Liu, Y. (2011). Experimental research on bond strength between rebar and concrete after high temperature. *Applied mechanics and materials*, 2011. Trans Tech Publications Ltd., pp. 1057-1061.
- Yüzer, N., Akbaş, B. and Kızılkant, A. B. (2007). Predicting the compressive strength of concrete exposed to high temperatures with a neural network model. *TÇMB*, 3rd International Symposium Sustainability in Cement and Concrete, İstanbul.
- Zandi H. K., Kettil, P. and Lundgren, K. (2011). Analysis of mechanical behavior of corroded reinforced concrete structures. *ACI Structural Journal*, 108, pp. 532-541.
- Zhang, Q., Xiong, E., Liang, X. and Miao, X. (2017). Performance-based plastic design method of high-rise steel frames. *Journal of Vibroengineering*, 19, pp. 2003-2018.
- Zhu, H., Wu, G., Zhang, L., Zhang, J. and Hui, D. (2014). Experimental study on the fire resistance of rc beams strengthened with near-surface-mounted high-Tg BFRP bars. *Composites Part B: Engineering*, 60, pp. 680-687.